Using Remote Sensing to Understand Urban Air Quality Exposures and Inequities

Matthew Bechle

A dissertation

submitted in partial fulfillment of the

requirements for the degree of

Doctor of Philosophy

University of Washington

2021

Reading Committee:

Julian D. Marshall, Chair

Timothy V. Larson

Dylan B. Millet

Program Authorized to Offer Degree:

Civil and Environmental Engineering

University of Washington

Abstract

Using Remote Sensing to Understand Urban Air Quality Exposures and Inequities

Matthew Bechle

Chair of the Supervisory Committee:

Julian D. Marshall

Department of Civil and Environmental Engineering

Outdoor air pollution is one of the leading causes of morbidity and mortality in the United States and around the world, but these impacts are not distributed equally. Countries, communities, and households that are socially and economically deprived often experience higher levels of air pollution. Yet too often these locations remain unmonitored or insufficiently monitored by traditional ground-based measurements. In this dissertation I employ satellite-based remote sensing of nitrogen dioxide (NO_2), a major contributor to urban air pollution and a proxy for a toxic mix of pollutants associated with traffic and combustion emissions, to explore air pollution levels globally and within the US. Within the last two decades, satellite air pollution measurements have considerably expanded the capability to measure air pollution in previously unmonitored locations and across administrative boundaries.

Cities serve as focal points, concentrating social and economic opportunities, but may also concentrate hazards, including air pollution. Strategic, compact urban design may be a way to improve a cities air quality, yet global empirical evidence has historically been limited by data availability and consistency. Here I use satellite-based measurements of NO_2 and built-up land area to explore the relationship between city-wide NO_2 levels and urban form characteristics (i.e., contiguity, circularity, percent impervious surfaces, percent vegetation coverage) for a global sample of 1,274 cities. Three of the urban form metrics (contiguity, circularity, and vegetation) have a small, but statistically significant relationship with city NO_2 levels; however, the combined effect of these three attributes could be sizeable. For example, a city at the 75^{th} percentile for all three metrics could accommodate, on average, twice the population as a city at the 25^{th} percentile, while maintaining similar air quality. This work also shows that country level factors such as economic conditions and environmental policies may impact the urban form – air pollution relationships. Moreover, the impact of urban form on air quality may be larger for small cities, an important finding given the large portion of current and projected future population that lives in small cities.

Satellite air pollution measurements are limited by their spatial resolution. For example, they are well suited for exploring NO_2 levels between cities, as described above; however, alone they typically cannot capture the fine-scale spatial variability needed to characterize population exposure to air pollution. Satellite-based empirical models combine the regional concentrations from satellite measurements with ground-based measurements and local land use and land cover information to predict air pollution concentrations with high spatial resolution (typically 1 km or less). These models have become ubiquitous, yet few studies have investigated how satellite and

other regional air pollution covariates impact these models. In this dissertation, I address this gap by exploring the effect of several regional NO_2 covariates in an empirical model for annual average NO_2 over the contiguous US and find that inclusion of a regional covariate improves model predictive power, yet choice of covariate has limited impact.

Additionally, empirical models can be data and computationally intensive, and are often limited to long-term averages and a small number of years. Here, I address these issues by developing a straightforward and easy to implement spatiotemporal scaling technique to extend the temporal coverage of a year-2006 annual NO_2 model to over a decade (2000-2010) of monthly NO_2 estimates. The resulting estimates are data publicly available online. The spatiotemporal scaling technique and these data have since been used in several publications exploring health effects and residential exposure disparities associated with outdoor NO_2 levels.

Residential air pollution disparities in the contiguous US have become a topic of recent interest. Children are a particularly vulnerable population and disparities in their air pollution exposure could have lasting impacts. Despite this, little has been done to track outdoor air pollution levels at schools throughout the US. In this dissertation, I add to this body of work by exploring a criteria pollutant, NO_2, and by considering home and school locations to better understand the role of public schools in students' total exposure. I find that, on average, racial and ethnic minority students live in and attend schools in areas with higher NO_2 levels than their non-Hispanic, white peers, and that impoverished students (defined here as those eligible for school lunch programs) attend, on average, schools with higher NO_2 levels than their non-impoverished peers. Minority students are much more likely than their white peers to live in

areas above the World Health Organization's annual outdoor NO_2 guideline, and this likelihood is larger at schools than at home locations, particularly when comparing predominately minority schools to predominately white schools. This finding -- that public schools may exacerbate disparities -- has important implications for addressing childhood inequities. Notably, strategies that do not address school exposure inequities may fail to address overall exposure inequities. Moreover, strategies to reduce school segregation or to identify and mitigate NO_2 levels at the most at-risk schools could have a significant impact on children's overall NO_2 inequities. This work also shows that race and income are intertwined; independently, more impoverished schools and schools with more minority students tend to be in areas with higher NO_2 levels than more well-off schools and schools with fewer minority students. Schools in large urban areas exhibit disparities by race/ethnicity alone, even when controlling for school-level income. This work highlights NO_2 disparities at public schools throughout the contiguous US. Those national disparities are driven largely by disparities in the 50 largest urban areas, which provides motivation for additional exploration and tracking of air pollution levels at these locations.

In summary, in this dissertation I have demonstrated how satellite measurements and empirical models that incorporate satellite measurements vastly improve the capability of uncovering and monitoring air pollution exposure disparities for a global and US-wide analysis. Recently launched and soon to be launched satellite-borne sensors promise higher spatial and temporal resolution air pollution measurements. Those measurements will allow for better understanding of concentrations and emission sources, as well as improve satellite-based empirical models, facilitating further tracking and characterization of exposures and exposure disparities from global to local scales.

List of tables

List of figures

Table of Contents

Chapter 1

Introduction

Outdoor air pollution is a leading cause of morbidity and mortality in the United States and around the world.[1] Health effects from air pollution impact nearly every system of the body, and at all ages, from childhood development to the onset of dementia.[2] Additionally, air pollution exposures are distributed unequally, often with socioeconomic disadvantaged countries, communities, and households exposed to higher levels of air pollution.[1,3] These air pollution disparities exist from the global scale (e.g., stronger emission controls in developed versus developing countries) to the local scale (e.g., siting of sources near disadvantaged communities without the political capital to resist) and even household scale (e.g., families that can afford home filtration and clean fuel for heating and cooking versus those who cannot).

An important step towards addressing disparities is to quantify and characterize these exposures and disparities, with an aim towards uncovering potentially modifiable factors that impact them. In the last two decades, satellite measurements of air pollution have dramatically increased the ability to explore air pollution in unmonitored locations and across administrative boundaries.[4–6] Remote sensing has given researchers the ability to explore new air pollution issues, for example, emissions from Canadian oil sands mining[7] or the impact of armed conflict on emissions[8]. Moreover, the availability of global air pollution measurements with consistent methodology from remote sensing has allowed for analyses with broad geographic coverage.

In this dissertation I focus on nitrogen dioxide (NO_2), a key component of urban air pollution, and a marker for a toxic mix of pollutants linked to traffic and other combustion related emissions.[9] For example, highway and non-highway (e.g., planes, trains, watercraft, construction) vehicles account for 76% of urban NO_x ($NO + NO_2$) emissions.[10] NO_2 is well suited for remote sensing owing in part to its relatively short lifetime (~hours) that makes it indicative of localized emissions and ground level concentrations. NO_2 is also associated with several adverse health outcomes[9,11–20] and a criteria air pollutant regulated by the US Environmental Protection Agency (US EPA). I employ estimates of NO_2 from several satellite borne sensors for this work. All of the sensors rely on solar backscatter to detect wavelengths corresponding to NO_2 absorption in the atmosphere, allowing for the estimation of tropospheric NO_2 column abundance with near global coverage.[4,5] More information is provided in Chapters 2 and 3 on the satellite NO_2 data sets employed here.

Cities concentrate social and economic activities, but may also concentrate environmental hazards such as air pollution.[21,22] Moreover, the majority of the world population lives in cities,[23] making cities a key component of addressing environmental health issues. Evidence suggests that density and other aspects of urban form (the size, shape, and layout of a city) may impact a city's air pollution levels. [24–30] Prior to the availability of satellite air pollution measurements, empirical studies on this topic were limited by data availability and consistency. Recent studies have used satellite air pollution estimates to find urban form – air pollution relationships for 830 cities in East Asia[30] and 83 global cities.[26] My work builds on the prior research by employing a large sample of global cities (1,274), allowing for the exploration of factors (i.e., city population, country-level income, environmental performance and policy) that may influence the

relationship between urban form and air quality. This work highlights the utility of the broad geographic coverage of satellite air pollution measurements.

Studies employing satellite measurements of air pollution are often limited by the spatial resolution of the satellite data. Air pollution measurements from satellites detect spatial averages and are typically incapable of capturing fine-scale spatial variability (< 1 km).[5] As a result, satellite air pollution measurements may not be the best tool for exploring within-city and neighborhood level exposures and disparities. Within the last decade, satellite measurements have been incorporated into empirical modeling frameworks to predict concentrations with high spatial resolution (typically 1 km or less) in unmonitored locations and over broad geographic scales. These models usually rely on ground-based monitoring data for training and a myriad of geographic covariates that may predict sources and concentrations. The addition of globally available satellite air pollution measurements, as well as other satellite-based geographic covariates, has led to the expansion of empirical prediction models from city- and regional-scales to national- and global-scales without sacrificing spatial resolution.[31–39] Despite extensive efforts to develop satellite-based empirical models, few studies have explored the choice of satellite and other regional air pollution covariates in model building.[37] I aim to address this gap by exploring the effect of various regional NO_2 covariates in an empirical model for the contiguous US. Additionally, these models require extensive data collection and processing, can be computationally intensive, and are often restricted to long-term averages or a small number of years. In this dissertation I attempt to address some of these limitations by developing a simple yet effective spatiotemporal scaling technique to extend temporal coverage of an annual average NO_2 model to additional years and to monthly estimates.

Fine spatial scale estimates from empirical prediction models with national coverage have been used to explore health effects of air pollution and to explore residential exposure disparities.[40–42] Children are a vulnerable population group; disparities in their air pollution exposure could lead to disparities in cognition, education, economic attainment, and health that may have lasting effects into adulthood and future generations.[43–45] Moreover, children have less agency over their personal exposures, putting a greater burden on addressing exposures in public settings like school. Understanding exposure and disparities for school-aged children at home and at school may be an important aspect of addressing greater societal disparities. To my knowledge, only one peer reviewed study has attempted to characterize air pollution at schools in the contiguous US, but that prior study focuses on a small subset of emissions (neurotoxicants) and only at school locations.[46] In this dissertation I explore students' home and school air pollution levels and consider NO_2, a common criteria air pollutant.

This dissertation contains three original studies, employing satellite NO_2 estimates to explore air quality exposures and disparities globally and for the US. Chapter 2, which has been published in a peer-reviewed journal article,[47] employs satellite-based air pollution and built-up area measurements for more than 1,200 global cities to explore impacts of urban form on air pollution, as well as how factors such as country economics and policy or city population size may effect these relationships. Chapter 3, also previously published in a peer-reviewed article,[48] extends the spatial resolution and temporal coverage of satellite-based NO_2 observations using a two-stage empirical modeling approach. In Chapter 4, I use the model from Chapter 3 to estimate NO_2 levels at public school and home locations for students in the contiguous US, exploring

effects of urbanicity, race/ethnicity, and income. Finally, Chapter 5 discusses the broader implications of this dissertation and areas for future research.

Chapter 2

Urban NO_2 and urban form: Satellite-based evidence for more than 1,200 cities

2.1 Summary

Modifying urban form may be a strategy to mitigate urban air pollution. For example, evidence suggests that urban form can affect motor vehicle usage, a major contributor to urban air pollution. I use satellite-based measurements of urban form and nitrogen dioxide (NO_2) to explore relationships between urban form and air pollution for a global data set of 1,274 cities. Three of the urban form metrics studied (contiguity, circularity, and vegetation) have a statistically significant relationship with urban NO_2; their combined effect could be substantial. As illustration, if findings presented here are causal, that would suggest that if Christchurch, New Zealand (a city at the 75th percentile for all three urban-form metrics, and with a network of buses, trams, and bicycle facilities) was transformed to match the urban form of Indio - Cathedral City, California, United States (a city at the 25th percentile for those same metrics, and exhibiting sprawl-like suburban development), the models suggest that Christchurch's NO_2 concentrations would be ~60% higher than its current level. I also find that the combined effect of urban form on NO_2 is larger for small cities ($\beta \times IQR = -0.46$ for cities < ~300,000 people, versus −0.22 for all cities), an important finding given that cities less than 500,000 people contain a majority of the urban population and are where much of the future urban growth is expected to occur. This work highlights the need for future study of how changes in urban

form and related land use and transportation policies impact urban air pollution, especially for small cities.

2.2 Introduction

More than half of the world population, 3.9 billion people (54%) in 2014, live in urban areas, with an additional 2.5 billion urban dwellers expected by 2050.[23] Cities serve as economic and social centers, concentrating people, activities, ideas, and industries. Cities may also concentrate environmental hazards such as air pollution, and potentially health inequities.[21,22] As such, cities are a focal point for understanding and addressing environmental health issues. Urban air pollution is responsible for millions of deaths each year globally, and is one of the top ten causes of death in the United States.[49] Mortality estimates from the Global Burden of Disease are predominately attributed to fine particles. On the other hand, the International Agency for Research on Cancer classifies outdoor air pollution (i.e., as a mixture, rather than a single pollutant) as the leading environmental carcinogen.[50] Urban air quality has generally improved for most developed countries, but worsened in most developing countries owing to rapid urban growth, increased automobile usage and congestion, and often lax environmental regulations.[51–54]

Transportation is one of the largest contributors to urban air pollution for pollutants such as carbon monoxide, nitrogen oxides, benzene, ozone, and fine particulate matter ($PM_{2.5}$).[55,56] For example, recent estimates suggest that globally, approximately 25% of ambient urban $PM_{2.5}$ is attributable to motor vehicles.[57] Strategies to reduce motor vehicle use may play a role in improving urban air quality. Evidence suggests that changes in urban form can impact

travel behavior such as travel distance, trip frequency, and mode choice.[58–64] For example, increasing population density is associated with a decrease in per capita daily vehicle-miles traveled (VMT) and an increase in walking and biking trips. [61–66] Dense neighborhoods with mixed land uses may be more accommodating to shorter trips and alternative modes of transportation (e.g., walking, biking, mass-transit) while also presenting barriers or disincentives to driving (e.g., limited parking, higher parking costs, congestion).[62,66] Similarly, the development of alternative transportation infrastructure may increase demand for nearby residential and retail property and consequently increase density.[67–69]

The existing literature suggests that increased density and other built environment characteristics (e.g., compactness, contiguity, centrality) are associated with lower air pollutant concentrations.[24–30] Empirical investigations of the relationship between urban form and air pollution are mostly limited to cities in developed countries (primarily in the United States) and tend to focus on large cities. Yet the majority of the worlds urban population lives in small cities (less than 500,000 people) and most of the future urban growth is expected to occur in small cities and developing countries.[23] A study of 83 global cities found that all else equal, more-contiguous urban form is associated with lower concentrations,[26] a similar finding to U.S.-only studies.[29] More recently, Larkin et al. investigated 830 cities in East Asia during 2000 – 2010 and found that changes in urban form (determined, e.g., via lights at night, impervious surfaces, population density) were associated with changes in air quality.[30] They reported that the urban form - air quality relationship varies with city population; increasing population while limiting urban land growth may attenuate or decrease per capita emissions.[30] These studies are few in number, yet illustrate the potential importance of urban form as a tool for improving air quality.

The existing literature encourages further exploration of these relationships and how they may vary globally. To date, most studies of urban form and air pollution in developing countries have focused on East Asia, it is still unknown whether urban form - air quality relationships hold for low income countries globally, and to what degree differences in national policy may impact these relationships. Additionally, in their analysis of East Asian cities, Larkin et al. found evidence that ideal urban form typologies vary by city population size, this may be true in other regions, but to my knowledge, it has not been previously studied.

Here I employ satellite-based measurements of nitrogen dioxide (NO_2, a proxy for traffic-related air pollution and a major constituent of urban air pollution)[51] and a global data set of 1,274 urban areas[70] to explore the relationship between urban form and air quality. My work builds on prior research by employing a much larger sample of global cities, allowing for the exploration of factors (i.e., city population, country-level income, environmental performance and policy) that may influence the relationship between urban form and air quality. In this work I can explore how urban form - air quality relationships vary for a consistent set of cities in low- and high-income countries, giving insight into the impacts of urban form in developing countries where existing literature is limited. Additionally, more than half of the cities in the data set (n = 675 cities; 53% of all cities) are small cities (100,000–500,000 people), allowing for exploration of the relationship of urban form and air pollution for a large global sample of small cities.

2.3 Methodology

I study NO_2, a major constituent of urban air pollution. NO_2 also serves as a marker for a suite of pollutants linked to traffic and other combustion related emissions,[9] and as a useful

proxy for urban air pollution owing to its relatively short lifetime (~hours) that makes it indicative of localized emissions. NO_2 is associated with several adverse health outcomes, including aggravation of respiratory diseases,[11,12] increased hospitalization and emergency room visits[13], incidence of asthma,[14] mortality,[9,15–17] and lung cancer.[18] NO_2 is a criteria air pollutant regulated by the U.S. Environmental Protection Agency (U.S. EPA), as well as a precursor to secondary particle formation, photochemical ozone production, and acid rain. Therefore, NO_2 is well suited for the exploration of urban form and urban air pollution undertaken here.

I employ publicly available global estimates of gridded (0.1°×0.1° [~11×11 km^2 at the equator]) annual surface NO_2 concentrations. A detailed description of these data are provided elsewhere.[51] Briefly, tropospheric column NO_2 measurements from three satellite-based instruments (GOME, SCHIAMACHY, and GOME-2) are combined with a global chemical transport model to estimate annual surface NO_2 concentration over a 17 year period (1996-2012).[51] This method of estimating surface NO_2 from satellite measurements has been shown to capture within-urban variability and has been previously used to explore global aspects of urban NO_2 concentrations.[26,71,72] To reduce effects of inter-annual variability I average three years of surface NO_2 estimates (2000-2002; corresponding to the three years nearest to the built-up area measurements). Satellite measurements of air pollution offer global coverage, and consistent data quality with uniform methodology across cities and regions, and have proven to be a useful tool for exploring urban air pollution globally.[26,30,52,54,72] Estimates of NO_2 surface concentrations derived via satellite measurements are typically lower than 24-hour average in situ measurements for several reasons, including: satellite measurements occur during daytime hours when NO_2 concentrations can be comparatively low; satellite measurements represent spatially averaged

concentrations whereas point-based measurements may capture nearby sources; chemical interferences from most in situ monitors may positively bias those estimates; and, potential underestimation of NO_2 surface-to-column ratios in urban areas due to model spatial resolution.[71] Nevertheless, satellite-based estimates of NO_2 have been shown to capture the spatial variability of surface concentrations,[71] and are well suited for exploring the relative differences in concentration between urban areas.[26,30,72]

I previously explored the relationship between urban form and air pollution for a globally stratified sample of 83 cities.[26] To my knowledge, that was the first global exploration of this relationship. This prior study employed built-up area estimates (derived from 30 m Landsat imagery) provided by the World Bank Dynamics of Global Urban Expansion Study.[73] The number of cities provided by the World Bank Study was limited, owing to the time and cost of processing additional cities. The small sample size in the earlier study prevented me from exploring several underlying factors that may influence the urban form - air pollution relationship.

Here, I investigate the urban form - air pollution relationship in greater depth using published estimates of built-up urban area for 3,646 global cities.[74] Built-up area was determined by supervised classification of 500 m Moderate Resolution Imaging Spectroradiometer (MODIS) satellite data for years 2001-2002.[75] Potere et al. recently compared ten global maps of urban land cover circa year-2000 and found the MODIS 500 m (MOD500) data employed here to be the most accurate.[76] I therefore trade spatial fidelity of built-up area estimates (30 m previously versus 500 m here) for a much larger sample of cities (83 previously, 3,646 cites here). Angel et

al. clustered built-up areas if the distance between centroids of nearest-neighbor pixels was less than a maximum distance threshold, and resulting urban clusters were paired with a database of named large cities (at least 100,000 people) to create the final data set of 3,646 global cities I employ here.[70] The dataset also includes year-2000 population for each urban cluster, total built-up urban area, and a measure of the circularity of each city's built-up area.

The four urban form metrics considered here, and described next, are circularity, contiguity, percent vegetation, and percent impervious surfaces. Angel et al. calculated circularity via the proximity index (hereinafter referred to as "circularity"), a measure of urban compactness (value range: 0 to 1; value for perfect circle: 1) quantifying the relative closeness of the entire built-up area within a city to its geographic center.[70] The proximity index is the ratio of the average distance from all points in an equal-area circle to its center (two-thirds of the radius of the equal-area circle) and the average distance to the centroid of each urban cluster from all built-up pixels in the cluster.[77] Assuming a monocentric city, a circular footprint offers the shortest average distance to the city center and closer proximity of people in the periphery and activities in the urban core. A city exhibiting this type of compactness may indicate a more efficient use of urban area, and may induce fewer and shorter vehicle trips. In addition to the provided circularity index, I derive a contiguity index (value range: 0 to 1), calculated as the ratio of the largest contiguous polygon of built-up area pixels to the total built-up area for a given city. Large amounts of leapfrog or exurban development, and polycentricism (particularly with satellite cities) would result in a low contiguity index. This type of development could increase the average distance between origins and destinations, as well as create multiple destination

centers that may not be centrally located. Therefore, less contiguous cities may be less easily served by public transit, and could induce more automobile traffic and longer travel distances.

Figure 2.1 shows built-up urban area estimates for three of the 3,646 cities, contrasting the MOD500 built-up estimates employed in this analysis (shown left) with built-up estimates from finer resolution (30 m) Landsat imagery (shown right) employed in my prior work. This figure illustrates that the MOD500 built-up area generally captures the geometric form of the primary built-up area, yet the Landsat imagery clearly captures roadways, small patches of urban discontinuity, and small pockets of suburban and exurban developments that the MOD500 data set cannot. The coarse features of MOD500 data set are the result of its large pixel size (~500 m), as evidenced by better representation for the larger cities in Figure 2.1. The MOD500 also suffers from apparent generalization (i.e., the reduction in detail of mapping features) from converting the built-up features to a Google Earth platform. Nevertheless, the MOD500 is, to my knowledge, the largest collection of built-up area estimates for a global database of cities, providing information for ~40× more cities than the Landsat data set employed in my previous study (3,636 cites [MOD500] versus 83 cities [Landsat]).[74] One aspect of this tradeoff is that the interpretation of the urban form metrics may change when the resolution of the underlying built-up area estimates change. For example, the maximum distance threshold Angel et al. used to cluster urban pixels in the MOD500 data set is a function of total built-up area:

$$\textit{(Eq. 2.1)} \qquad D = 649.21\, Ln(A) - 5234.6$$

where *D* is the distance threshold (units: meters) and *A* is the cluster size (hectares). From this equation I determine that cities with less than ~50 km^2 of total built-up area are only comprised of a single cluster.[70]

Consequently, analyses here only include cities larger than 50 km^2, where there is less concern about the contiguity metric being impacted by pixel size. This approach leaves 1,303 cities of the 3,624 cities. An additional 29 cities were removed owing to missing air pollution data, resulting in 1,274 cities for this analysis: ~35% of cities comprising ~72% of the total population in the MOD500 database, yet still an order of magnitude more cities than the higher resolution Landsat database.

The circularity metric was calculated differently for the Landsat versus the MOD500 cities. (The Landsat database calculated the ratio of built-up area to total buildable area in a circle circumscribing the main built-up area of the city.) There is low correlation between metrics derived from the MOD500 and 30 m Landsat built-up area estimates (r = 0.35 and 0.31 for circularity and contiguity, respectively) for the 63 common cities in each data set, illustrating that the MOD500 and Landsat based metrics capture different urban spatial characteristics. Therefore, for questions considered here, direct comparisons between analyses employing MOD500 versus Landsat[26] cannot be made. Figure 2.2 shows built-up urban area and the urban form metrics for four similarly-sized (~200 km^2) cities from the database of the 1,274 cities analyzed.

I also employ satellite-based estimates of impervious surfaces[78] and vegetative cover[79] in order to quantify the average percentage of built-up area occupied by impervious surfaces and vegetative cover within each city. These data provide continuous estimates of the percentage of impervious surfaces and vegetative cover at 1 km and 500 m resolution, respectively. For each city, I calculate the average percent coverage for grid cells overlapping the built-up area. The impervious surfaces data employs population and satellite-based lights at night to estimate impervious surfaces.[78] The impervious surface data and underlying lights at night data are associated with density (e.g., population, residential, business) and economic activity.[80] Increased impervious surface estimates are also associated with increased land surface temperature, a phenomenon known as the urban heat island effect.[81] Vegetative cover may capture several different urban aspects including (1) fewer land uses with sources, (2) vegetative attenuation of the heat island, and (3) suburban land uses. For the cities in this study, impervious surface and vegetative cover exhibit modest correlation (r = -0.20), suggesting that these two metrics capture different aspects of urban form

I employ country-level gross domestic product (GDP) per capita (hereinafter referred to as "income") using a three-year mean for the years corresponding to the air quality data (2000-2002; reported in 2005 USD),[82] to account for differences in economic development. Finally, I include several meteorological metrics: (1) harmonic mean of dilution rate (product of wind-speed and mixing height)[83] to account for differences in atmospheric dilution, (2) annual solar insolation[84] to account for differences in the chemical lifetime of NO_2 (primarily chemical loss of NO_2 is to nitric acid, which is sensitive to sunlight and temperature)[85,86], and (3) the percent of

days with significant rainfall ($\geq$ 0.1 mm)[87] to account for potential differences in wet deposition. Summary statistics for all variables are provided in Table 2.1.

I create linear regression models for the logarithm of arithmetic mean NO_2 concentration in each city to determine the dependence of urban NO_2 concentration on the urban characteristics described above. The population and income metrics were found to be logarithmically distributed, I therefore employ logarithm of population and logarithm of income in the model as the population and income metrics. In addition to the core model, I create several sub-models, using the same variables as the full model, with subsets of cities based on tertiles of income, city population, and environmental performance (see below) in order to explore how these factors may impact the effect of urban form on urban NO_2. I employ the GDP per capita metric from above for income tertiles (cut points: $1,980; $22,000), and urban population for city size tertiles (cut points: 289,000 people; 788,000 people). I employ the Yale 2008 Environmental Performance Index (EPI)[88] as a quantitative indicator of environmental policies and outcomes[89] (tertile cut points: 72.5; 81.0). The EPI is a country-level index based on 25 performance indicators whose value ranges from 39.5 (Angola) to 95.5 (Switzerland), with increasing values associated with better environmental performance. The 2008 EPI is the earliest edition of the EPI, and based on data covering several years (~2000-2010).[88] As a sensitivity analysis of the sub-models, I also explore models with interaction terms between the three factors (log[income], log[population], EPI) and the urban form metrics.

I employ Monte-Carlo coefficient/*p*-value/sample-size (CPS) charts as both a sensitivity analysis to explore the strength of the predictors included in the core model, and to aid in

interpretation of sub-sample modeling results. Monte-Carlo CPS charts summarize coefficients and *p*-values for sub-models created from Monte-Carlo random sampling at a range of sample sizes.[90] Here, I employ Monte-Carlo random sampling (500 iterations) for n = 100 to 1,200 cities at intervals of 100 cities, and report the CPS charts for all of the predictors included in the core model.

2.4 Results

The core model, including all 1,274 cities, captures 59% of the variation in the dependent variable (logarithm of satellite-derived NO_2 concentration). This simple yet powerful model offers useful insights into the relationship between urban form and air pollution, and offers a basis of comparison for sub-model explorations. Table 2.2 summarizes model parameters for this core model. Table 2.3 shows pairwise correlations between model parameters. I employ variance inflation factor as a test of multicollinearity (VIF < 1.9 for all parameters). The coefficient plots (shown as $\beta \times$ IQR) and *p*-value plots shown in Figure 2.3 illustrate the strength of the predictors included in the core model. As sample size increases, the coefficients converge on the final model coefficient. Moreover, for all significant predictors (all but impervious surfaces) the *p*-value decreases with increasing sample size, indicating a clear signal from these variables. The large number of cities needed in the model for the urban form metrics to be statistically significant (n > ~1,000) illustrates the utility of this large data base of cities, as well as the utility of high resolution built-up area data sets that have indicated significant urban form effects with smaller sample sizes.[26,30]

Of the urban characteristics (i.e., log[population] and urban form metrics), log[population] had the largest effect ($\beta \times$ IQR = 0.45) with higher population associated with worsened air quality. Increased urban contiguity, circularity and vegetation metrics are significantly ($p < 0.008$) associated with lower urban NO_2 concentrations. The impervious surface metric has a non-significant effect ($p = 0.19$) on urban NO_2. The magnitude of the effect size of the three significant urban form metrics are small relative to log[population] ($\beta \times$ IQR: -0.06 to -0.09), however, their combined effect could be large. For example, a city with circularity, contiguity and vegetation metrics at the 75th percentile could, on average, accommodate approximately twice the population of a city with these metrics at the 25th percentile while maintaining similar air quality.

Tables 2.4-2.6 provide details for the income, city-size, and EPI tertile submodels. Figure 2.4 summarizes standardized coefficients for the urban form metrics for all of the sub-models. I use the Monte-Carlo sub-sample simulations from the CPS plot analyses to determine statistically significant changes in standardized coefficients for the sub-models (n = 391 - 434): the blue shaded region in Figure 2.4 shows the 5th and 95th percentile range in $\beta \times$ IQR from the coefficient CPS plots in Figure 2.3 for a sample size of 400 (i.e., approximately one-third of the overall sample size, because these analyses divide the dataset into tertiles). Figure 2.4 illustrates that contiguity may have a larger effect size for small cities and cities in countries with high environmental performance, and an attenuation of the contiguity - urban NO_2 relationship for large cities. Attenuation of the circularity - urban NO_2 relationship is exhibited for cities in countries with high income or high environmental performance. The impervious surface metric is sensitive to country-level income: cities in low-income countries exhibit a positive relationship

between impervious surfaces and log-NO_2 ($p = 0.11$), whereas cities in high-income countries exhibit a significant negative relationship ($p < 0.001$). Aside from an increase in the effect for small cities, vegetation appears mostly unaffected by the factors considered here. Sensitivity models with interaction terms are presented in Tables 2.7-2.10. The effect modification from the interaction models strongly agree with most of the significant sub-model findings ($p < 0.001$ for interaction terms), however, agreement is modest for the attenuation of circularity with increasing income and increasing EPI ($p = 0.11$ and 0.07 for income and EPI interaction terms, respectively) and the effect modification for population on vegetation is the opposite direction of the sub-model results ($p = 0.15$). Additionally, the interaction models illustrate a small, yet statistically significant, attenuation of vegetation with increasing income ($p = 0.001$) and increasing EPI ($p < 0.0001$).

Meteorology and country-level income play an important role in describing differences in urban NO_2 concentrations among cities; income, solar insolation, and precipitation together describe 52% of the variation in urban NO_2 concentration. Considering standardized coefficients, solar insolation and income have comparable effect sizes ($\beta \times$ IQR = -1.09 and 1.02 for insolation and log[income], respectively), and more than twice the effect size as the next largest predictors ($\beta \times$ IQR = -0.50 and 0.45 for precipitation and log[population], respectively). Of the three meteorological metrics, dilution rate has the smallest effect on concentrations ($\beta \times$ IQR = -0.03).

2.5 Discussion

I find that three of the four urban form metrics considered in this study (contiguity, circularity and vegetation) have a statistically significant ($p < 0.008$) negative association with urban NO_2 concentrations, illustrating the potential for urban form to impact urban air pollution. The magnitude of the effect size of the three significant urban form metrics (β × IQR: −0.06 to −0.09) is similar to that of dilution, a consistent finding with previous work on this topic.[26] Despite the small effect size of these metrics, their combined effect could be large. In other words, if one hypothetically considers the results in Table 2.2 to be causal, a city that enhances their urban form may see improvement in urban air quality, or the offset of worsening air quality associated with population growth. For example, a city with circularity, contiguity and vegetation metrics at the 75th percentile could, on average, accommodate approximately twice the population of a city with these metrics at the 25th percentile while maintaining similar air quality. These findings illustrate the potential utility of urban form as part of a comprehensive strategy for addressing urban air pollution.

Subsample Models

The sub-sample models, exploring changes in urban form metrics by income, city population size, and environmental performance tertiles, provide insight into factors that may alter the core urban form–urban NO_2 relationships. For low-income countries, increasing impervious surfaces is associated with worsened NO_2 air pollution, possibly indicating increased emissions from a higher level of developed land (or more specifically, car-centric developed land) within the built-up pixels defining a city. Impervious surfaces may also be capturing within-country differences in economic activity, and the resulting increase in emissions from

those activities. On the other hand, for high-income countries the findings are seemingly counterintuitive: increasing impervious surfaces is associated with reduced NO_2 air pollution. One possible explanation is that in high income countries, the impervious surfaces metric is capturing differences in density (e.g., population, business), resulting in lower per capita VMT. As a sensitivity analysis I include logarithm of net population density (the total population divided by the total built-up area) as an explanatory variable, however, the population density coefficient is highly insignificant ($p = 0.96$) and does not change the other explanatory variable coefficients. It is possible that density characteristics not captured by net population density could be at play here, however, it is unclear. Interpretation of the impervious surfaces coefficient is complicated by the fact that it is associated with urban heat island effect, which could alter NO_2 concentrations in myriad ways (e.g., increased emissions from air conditioning usage, more NO_x as NO rather than NO_2, higher levels of daytime dilution owing to larger mixing area). Income also appears to impact the effect size of the circularity and vegetation metrics (cities in high-income countries exhibit an attenuation of the circularity and vegetation coefficients). These findings support further research on the differences in urban form - urban NO_2 relationships for cities in high- and low-income countries.

The magnitude of the contiguity coefficient appears to decrease with increasing city size: small cities exhibit a larger negative relationship with urban NO_2 compared to the full model, whereas in large cities contiguity appears to have no effect. A possible explanation for this finding is that, all else equal, a more contiguous city may have higher per-area NO_x emissions even if per capita emissions decrease because the emissions occur on a smaller footprint. In a larger city, this could result in higher concentrations for some parts of the city owing to (1)

insufficient dilution relative to the increased local emissions, or (2) longer NO_x lifetime as a result of OH suppression from more spatially focused NO_x emissions. City size also impacts the magnitude of the vegetation parameter, with small cities exhibiting a larger vegetation coefficient. It is unclear why this would be the case, but the effect may arise from some convolution of vegetation's role as a depositional surface, and its role as a source of biogenic hydrocarbons that change the chemical regime for NO_2 oxidation. The fact that contiguity and vegetation both have larger impacts on urban NO_2 for small cities is an important finding, given that more than half of the global urban population live in smaller cities (<500,000 people).[23] The collective effect of the four urban form metrics is greater for smaller cities (combined $\beta \times IQR = -0.46$, versus -0.22 for all cities), consistent with findings from Larkin et al. for East Asia[30] and further highlighting the importance of well-planned development and urban growth for smaller cities. This finding also highlights the need for further understanding of urban form and air pollution relationships in small urban areas; much of the current research has focused on large urban areas and megacities.

The magnitude of the circularity coefficient decreases with improved environmental performance, suggesting that circularity effects on urban NO_2 may be less important in countries with stronger environmental policy and performance. On the other hand, the magnitude of the contiguity coefficient is higher in countries with high environmental performance. These findings illustrate that environmental policy alters the relationship between urban form and air pollution, and suggests that the efficacy of urban form strategies may be dependent on existing environmental policies.[89]

Meteorology

Meteorological variables explain a large portion of the variability in urban NO_2 concentrations between cities. The effect size for precipitation is on par with that of population ($\beta \times IQR = -0.50$ versus 0.45 for precipitation and log[population], respectively). Wet deposition is not a major sink for NO_2, so the large effect for precipitation seen here is somewhat surprising, however, it is consistent with published findings for urban NO_2 in East Asia.[30] Relative to solar insolation and precipitation, the effect size for dilution rate was small, possibly owing to the relatively short chemical lifetime of NO_2 in the atmosphere (daytime NO_x e-folding lifetimes estimated from airplane and satellite measurements for urban locations are ~4–6 h)[91,92]. It is also possible that the solar insolation and precipitation variables are in fact capturing other, correlating, aspects of meteorologically driven urban NO_2 variation; excluding them from the model results in a more than doubling of the dilution rate effect size ($\beta \times IQR = -0.08$).

Limitations of the Study

A major limitation of this study is that it is cross-sectional, owing to the lack of built-up area estimates over time. That aspect hinders the ability to draw conclusions regarding causality. The analysis is also limited by the characteristics of the data sets employed and their data quality. For example, the built-up area estimates include only cities with at least 100,000 people, yet many people live in (and much of the future growth of cities will be in) urban areas with fewer than 100,000 people. Similarly, the analysis excludes cities smaller than 50 km^2 because of the coarseness of the built-up area estimates and the need to avoid issues with calculating the contiguity index (see Methods). I cannot confidently extend claims from this analysis to cities

below those thresholds (<100,000 people or 50 km^2). Another potential limitation of the analysis is the measure of urban air pollution: satellite-based NO_2 concentration. Measurements occur in the mid- to late morning, during satellite overpass, when NO_2 concentrations may be lower than 24-h average concentrations. I therefore may be underestimating concentrations for cities with large diurnal patterns that cannot be captured via this type of measurement. Another limitation of this study is that the air pollution metric employs ambient concentration rather than exposure. Urban form changes such as increased density may reduce net emissions and average concentrations, but exposures may be higher in dense neighborhoods and cities because sources and people are closer together.[93] For example, Schweitzer & Zhou employed a composite measure of regional compactness for U.S. Metropolitan Statistical Areas (i.e., Smart Growth America's sprawl index) and found that compact regions had lower concentrations of ozone, yet higher levels of exposure to ozone and fine particles (two important air pollutants).[25] In contrast, Clark et al. employed several regional urban form indicators for U.S. Urbanized Areas and found that while density was associated with higher ozone and fine particle exposure, another urban form metric (population-centrality) was associated with lower exposures.[27] Given the resolution of the air pollution data, I chose not to consider population exposure. It is potentially possible that increasing contiguity and compactness could worsen exposure, on average, despite the findings here indicating improved ambient concentrations.

Implications of Findings

Overall, these findings demonstrate that urban form has a statistically significant relationship with urban NO_2 concentrations. Our cross-sectional investigation highlights the need for further study of urban design and planning as a potential strategy to address air quality. While

meteorology (aside from dilution rate), country-level income, and city population size all had a larger effect on urban NO_2 than the urban form metrics, the combined impact of the three statistically significant metrics (contiguity, circularity, and vegetation) could have large consequences for concentrations. While these findings are generally consistent with my prior work, in this study I find that certain factors may alter the relationship between urban form and air pollution. For example, I find that urban form may have a greater impact on urban NO_2 for small cities than for large cities. This is an important finding given that more than half of the world's urban population lives in small urban areas, and because changes to urban form may be easier for small urban areas (owing to less existing infrastructure and the potential for greater relative impact from future growth). I also find that direction of effect for impervious surfaces differs between cities in high- and low-income countries, suggesting that urban form strategies may differ at various stages of growth and development.

Table 2.1. Summary statistics among the 1,274 cities

Parameter	Unit	Mean	Std Dev	P25	P50	P75
NO_2 concentration	ppb	2.11	2.17	0.52	1.37	2.99
Income	year-2005 US$	$13,100	$14,600	$1,000	$3,600	$26,800
Population	million people	1.12	2.26	0.23	0.45	1.08
Built-up area	km^2	219	423	69.3	105	191
Population density	1,000 people / km^2	5.7	5.4	2.2	4.0	7.3
Contiguity	unitless (0-1)	0.86	0.15	0.82	0.92	0.97
Circularity	unitless (0-1)	0.80	0.10	0.75	0.82	0.88
Vegetation	%	6.4	8.8	0.4	2.9	8.8
Impervious	%	36.3	15.9	24.6	33.3	46.0
Dilution rate	m^2 / s	536	441	374	458	561
Days of rain	%	33.8	14.4	23.1	33.4	44.0
Annual insolation	W / m^2	190	37	162	189	219
EPI*	unitless (0-100)	75.1	10.0	65.1	80.5	82.7

*Only 1255 cities are in countries with an EPI value.

Table 2.2. Linear regression model for logarithm of mean urban NO_2

Parameter*	Units	β	SE	P > *t*	β × IQR	partial-R^2
annual insolation	W / m^2	-1.9E-02	7.4E-04	< 0.001	-1.09	0.34
log[income]	log[Y2005 US$]	0.31	0.02	< 0.001	1.02	0.45
% days of rain	%	-2.4E-02	1.7E-03	< 0.001	-0.50	0.52
log[pop]	Log[person]	0.67	0.06	< 0.001	0.45	0.58
dilution rate	m^2 / s	-1.7E-04	5.0E-05	< 0.001	-0.03	0.58
contiguity	unitless (0-1)	-0.48	0.15	0.001	-0.07	0.59
circularity	unitless (0-1)	-0.67	0.22	0.003	-0.09	0.59
% vegetation	%	-7.1E-03	2.6E-03	0.007	-0.06	0.59
% impervious	%	-2.4E-03	1.8E-03	0.19	-0.05	0.59
_constant	log[ppb]	-0.71	0.49	0.15		

*Variables listed by order selected into a forward stepwise ($p > 0.05$) model.

Table 2.3. Pairwise correlation matrix for model parameters

	log[NO_2]	Annual insolation	Rainfall	log[pop]	log[income]	Dilution rate	Contiguity	Circularity	Vegetation	Impervious
log[NO_2]	1									
Annual insolation	-0.58	1								
Rainfall	0.09	-0.52	1							
log[pop]	0.11	0.12	-0.08	1.00						
log[income]	0.51	-0.34	0.23	-0.22	1.00					
Dilution rate	-0.10	0.12	0.05	0.06	0.06	1.00				
Contiguity	-0.16	0.09	-0.06	-0.01	-0.10	0.01	1.00			
Circularity	-0.16	0.08	-0.07	0.01	-0.21	-0.14	0.15	1.00		
Vegetation	0.07	-0.11	0.20	-0.17	0.33	-0.04	-0.05	-0.22	1.00	
Impervious	-0.09	0.30	-0.18	0.62	-0.20	0.03	0.18	0.14	-0.20	1.00

Table 2.4. Income sub-sample linear regression models for logarithm of mean urban NO_2

	Low-income (< $1,980)				**Medium-income ($1,980 - $22,000)**				**High-income (> $22,000)**			
	n = 425				n = 428				n = 421			
	R^2 = 0.57				R^2 = 0.53				R^2 = 0.40			
	Adj-R^2 = 0.56				Adj-R^2 = 0.52				Adj-R^2 = 0.39			
	β	**SE**	**P > *t***	***β* × IQR**	***β***	**SE**	**P > *t***	***β* × IQR**	***β***	**SE**	**P > *t***	***β* × IQR**
annual insolation	-2.6E-02	1.7E-03	< 0.001	-1.26	-1.7E-02	1.1E-03	< 0.001	-1.10	-1.4E-02	1.7E-03	< 0.001	-0.71
% days of rain	-3.1E-02	3.3E-03	< 0.001	-0.52	-9.1E-03	2.8E-03	0.001	-0.19	-2.6E-02	3.6E-03	< 0.001	-0.45
log[pop]	0.60	0.11	< 0.001	0.37	0.64	0.11	< 0.001	0.39	0.64	0.08	< 0.001	0.36
log[income]	0.39	0.08	< 0.001	0.31	0.51	0.06	< 0.001	0.50	-0.30	0.21	0.16	-0.10
dilution rate	-1.7E-04	1.4E-04	0.22	-0.02	-1.6E-04	6.2E-05	0.01	-0.03	-2.1E-04	9.2E-05	0.02	-0.04
contiguity	-0.89	0.26	0.001	-0.13	-0.35	0.27	0.21	-0.05	-0.22	0.21	0.29	-0.03
circularity	-1.52	0.45	0.001	-0.17	-0.61	0.40	0.12	-0.08	-0.20	0.32	0.53	0.03
% vegetation	-1.1E-02	9.5E-03	0.26	-0.03	-1.4E-02	4.3E-03	0.001	-0.12	8.5E-04	3.4E-03	0.80	0.01
% impervious	5.6E-03	3.4E-03	0.11	0.15	-1.4E-03	3.0E-03	0.65	0.03	-1.7E-02	3.1E-03	< 0.001	-0.23
_constant	1.59	1.24	0.2		-3.58	0.93	< 0.001		4.61	2.20	0.04	

Table 2.5. City-size sub-sample linear regression models for logarithm of mean urban NO_2

	Small cities (< 289,000) n = 425 R^2 = 0.59 Adj-R^2 = 0.58				**Medium cities (289,000 - 788,000)** n = 425 R^2 = 0.56 Adj-R^2 = 0.56				**Large cities (> 788,000)** n = 424 R^2 = 0.69 Adj-R^2 = 0.68			
	β	**SE**	**P > *t***	***β* × IQR**	***β***	**SE**	**P > *t***	***β* × IQR**	***β***	**SE**	**P > *t***	***β* × IQR**
annual insolation	-1.7E-02	1.3E-03	< 0.001	-0.94	-1.8E-02	1.2E-03	< 0.001	-1.09	-2.2E-02	1.2E-03	< 0.001	-1.24
% days of rain	-1.7E-02	3.2E-03	< 0.001	-0.32	-2.0E-02	3.0E-03	< 0.001	-0.43	-3.3E-02	2.8E-03	< 0.001	-0.71
log[pop]	0.07	0.29	0.81	0.02	0.75	0.30	0.02	0.17	1.1	0.11	< 0.001	0.45
log[income]	0.39	0.03	< 0.001	1.13	0.29	0.03	< 0.001	0.95	0.27	0.03	< 0.001	0.80
dilution rate	-5.3E-04	1.4E-05	< 0.001	-0.10	-3.6E-04	1.2E-04	0.004	-0.07	-9.2E-06	5.7E-05	0.87	0.00
contiguity	-0.96	0.24	< 0.001	-0.17	-0.32	0.27	0.24	-0.04	0.08	0.25	0.75	0.01
circularity	-0.91	0.38	0.02	-0.13	-0.26	0.37	0.49	-0.03	-0.78	0.40	0.05	-0.09
% vegetation	-1.4E-02	3.9E-03	< 0.001	-0.16	-4.1E-03	5.0E-03	0.38	-0.03	-7.7E-03	6.0E-03	0.20	-0.05
% impervious	-1.2E-02	4.2E-03	0.006	-0.14	2.6E-03	3.3E-03	0.43	0.04	-3.3E-03	2.7E-03	0.21	-0.07
_constant	2.39	1.63	0.14		-1.94	1.82	0.29		-2.78	0.90	0.002	

Table 2.6. Environmental Performance Index sub-sample linear regression models for logarithm of mean urban NO_2

	Low EPI (< 72.5) n = 430 R^2 = 0.58 Adj-R^2 = 0.57				**Medium EPI (72.5 - 81.0)** n = 434 R^2 = 0.66 Adj-R^2 = 0.65				**High EPI (> 81.0)** n = 391 R^2 = 0.61 Adj-R^2 = 0.60			
	β	**SE**	**P > *t***	***β* × IQR**	***β***	**SE**	**P > *t***	***β* × IQR**	***β***	**SE**	**P > *t***	***β* × IQR**
annual insolation	-2.5E-02	1.7E-03	< 0.001	-1.21	-2.0E-02	1.5E-03	< 0.001	-1.24	-1.6E-02	1.1E-03	< 0.001	-0.93
% days of rain	-3.0E-02	3.8E-03	< 0.001	-0.51	-2.2E-02	4.6E-03	< 0.001	-0.34	-1.3E-02	3.0E-03	< 0.001	-0.24
log[pop]	0.67	0.11	< 0.001	0.41	0.70	0.08	< 0.001	0.47	0.42	0.12	0.001	0.22
log[income]	0.27	0.04	< 0.001	0.45	0.37	0.02	< 0.001	0.76	0.37	0.03	< 0.001	0.89
dilution rate	-1.6E-04	1.3E-04	0.21	-0.03	-4.2E-04	8.9E-05	< 0.001	-0.07	-6.5E-05	6.5E-05	0.32	-0.02
contiguity	-0.40	0.27	0.14	-0.06	-0.08	0.22	0.71	-0.01	-1.1	0.26	< 0.001	-0.15
circularity	-1.4	0.43	0.001	-0.17	-0.69	0.35	0.05	-0.09	0.17	0.38	0.64	0.03
% vegetation	-2.6E-02	7.1E-03	0.001	-0.10	-6.9E-03	3.6E-03	0.06	-0.08	-3.0E-03	4.6E-03	0.52	-0.03
% impervious	-3.1E-03	3.1E-03	0.33	-0.08	-3.6E-03	2.7E-03	0.18	-0.06	3.3E-03	4.3E-03	0.45	0.06
_constant	1.56	0.99	0.12		-1.40	0.74	0.06		-1.44	0.91	0.11	

Table 2.7. Linear regression model for logarithm of mean urban NO_2 with interaction terms for contiguity metric*

	β	**SE**	**P > *t***	***β***	**SE**	**P > *t***	***β***	**SE**	**P > *t***	***β***	**SE**	**P > *t***
insolation	-1.9E-02	7.3E-04	< 0.001	-1.9E-02	7.4E-04	< 0.001	-1.9E-02	7.3E-04	< 0.001	-1.9E-02	7.4E-04	< 0.001
log[income]	0.31	0.02	< 0.001	0.31	0.02	< 0.001	0.32	0.02	< 0.001	0.31	0.02	< 0.001
% days of rain	-2.4E-02	1.8E-03	< 0.001	-2.4E-02	1.8E-03	< 0.001	-2.4E-02	1.8E-03	< 0.001	-2.3E-02	1.8E-03	< 0.001
log[pop]	0.67	0.06	< 0.001	0.67	0.06	< 0.001	0.70	0.06	< 0.001	0.67	0.06	< 0.001
dilution rate	-1.7E-04	5.0E-05	< 0.001	-1.7E-04	5.0E-05	< 0.001	-1.8E-04	5.0E-05	< 0.001	-1.8E-04	5.0E-05	< 0.001
contiguity	-0.48	0.15	0.001	-0.48	0.15	0.001	-0.44	0.15	0.003	-0.49	0.15	0.001
circularity	-0.67	0.22	0.003	-0.67	0.22	0.003	-0.66	0.22	0.003	-0.61	0.23	0.008
% vegetation	-7.1E-03	2.6E-03	0.007	-6.8E-03	2.7E-03	0.01	-7.2E-03	2.6E-03	0.006	-7.9E-03	2.7E-03	0.003
% impervious	-2.4E-03	1.8E-03	0.19	-2.3E-03	1.8E-03	0.199	-3.1E-03	1.8E-03	0.09	-3.1E-03	1.9E-03	0.09
contiguity × log[income]	--	--	--	0.07	0.09	0.40	--	--	--	--	--	--
× log[pop]	--	--	--	--	--	--	0.82	0.27	< 0.001	--	--	--
× EPI	--	--	--	--	--	--	--	--	--	-0.01	0.01	0.61
constant	4.69	0.17	< 0.001	4.70	0.17	< 0.001	4.71	0.17	< 0.001	4.63	0.17	< 0.001

*In order to make results more interpretable, variables are centered (by subtracting the mean from all values) so that the main effects represent average conditions. For example, in the model with contiguity × log[income], the main effect for contiguity (β = -0.48) is the effect at the average value of log[income].

Table 2.8. Linear regression model for logarithm of mean urban NO_2 with interaction terms for circularity metric

	β	**SE**	**P > *t***	***β***	**SE**	**P > *t***	***β***	**SE**	**P > *t***	***β***	**SE**	**P > *t***
insolation	-1.9E-02	7.3E-04	< 0.001	-1.9E-02	7.4E-04	< 0.001	-1.9E-02	7.4E-04	< 0.001	-1.9E-02	7.4E-04	< 0.001
log[income]	0.31	0.02	< 0.001	0.31	0.02	< 0.001	0.31	0.02	< 0.001	0.31	0.02	< 0.001
% days of rain	-2.4E-02	1.8E-03	< 0.001	-2.4E-02	1.8E-03	< 0.001	-2.4E-02	1.8E-03	< 0.001	-2.4E-02	1.8E-03	< 0.001
log[pop]	0.67	0.06	< 0.001	0.66	0.06	< 0.001	0.67	0.06	< 0.001	0.66	0.06	< 0.001
dilution rate	-1.7E-04	5.0E-05	< 0.001	-1.7E-04	5.0E-05	< 0.001	-1.7E-04	5.0E-05	< 0.001	-1.8E-04	5.0E-05	< 0.001
contiguity	-0.48	0.15	0.001	-0.49	0.15	0.001	-0.48	0.15	0.001	-0.51	0.15	0.001
circularity	-0.67	0.22	0.003	-0.73	0.23	0.001	-0.66	0.23	0.004	-0.66	0.23	0.004
% vegetation	-7.1E-03	2.6E-03	0.007	-6.3E-03	2.7E-03	0.02	-7.1E-03	2.6E-03	0.007	-7.4E-03	2.7E-03	0.005
% impervious	-2.4E-03	1.8E-03	0.19	-2.2E-03	1.8E-03	0.24	-2.5E-03	1.8E-03	0.18	-2.8E-03	1.9E-03	0.14
circularity × log[income]	--	--	--	0.22	0.14	0.11	--	--	--	--	--	--
× log[pop]	--	--	--	--	--	--	0.10	0.45	0.82	--	--	--
× EPI	--	--	--	--	--	--	--	--	--	0.04	0.02	0.07
constant	4.69	0.17	< 0.001	4.68	0.17	< 0.001	4.69	0.17	< 0.001	4.65	0.17	< 0.001

*In order to make results more interpretable, variables are centered (by subtracting the mean from all values) so that the main effects represent average conditions. For example, in the model with circularity × log[income], the main effect for circularity (β = -0.73) is the effect at the average value of log[income].

Table 2.9. Linear regression model for logarithm of mean urban NO_2 with interaction terms for vegetation metric

	β	**SE**	**P > *t***	***β***	**SE**	**P > *t***	***β***	**SE**	**P > *t***	***β***	**SE**	**P > *t***
insolation	-1.9E-02	7.3E-04	< 0.001	-1.9E-02	7.4E-04	< 0.001	-1.9E-02	7.3E-04	< 0.001	-1.9E-02	7.3E-04	< 0.001
log[income]	0.31	0.02	< 0.001	0.32	0.02	< 0.001	0.32	0.02	< 0.001	0.32	0.02	< 0.001
% days of rain	-2.4E-02	1.8E-03	< 0.001	-2.3E-02	1.8E-03	< 0.001	-2.4E-02	1.8E-03	< 0.001	-2.3E-02	1.8E-03	< 0.001
log[pop]	0.67	0.06	< 0.001	0.66	0.06	< 0.001	0.67	0.06	< 0.001	0.66	0.06	< 0.001
dilution rate	-1.7E-04	5.0E-05	< 0.001	-1.7E-04	5.0E-05	0.001	-1.8E-04	5.0E-05	< 0.001	-1.7E-04	5.0E-05	0.001
contiguity	-0.48	0.15	0.001	-0.46	0.15	0.002	-0.48	0.15	0.001	-0.47	0.15	0.001
circularity	-0.67	0.22	0.003	-0.60	0.23	0.008	-0.65	0.23	0.004	-0.58	0.23	0.01
% vegetation	-7.1E-03	2.6E-03	0.007	-1.1E-02	3.1E-03	< 0.001	-8.8E-03	2.9E-03	0.002	-1.2E-02	2.8E-03	< 0.001
% impervious	-2.4E-03	1.8E-03	0.19	-2.1E-03	1.8E-03	0.26	-2.7E-03	1.8E-03	0.14	-3.0E-03	1.8E-03	0.11
% vegetation × log[income]	--	--	--	4.6E-03	1.9E-03	0.01	--	--	--	--	--	--
× log[pop]	--	--	--	--	--	--	-8.0E-03	5.6E-03	0.15	--	--	--
× EPI	--	--	--	--	--	--	--	--	--	1.4E-03	3.0E-04	< 0.001
constant	4.69	0.17	< 0.001	4.61	0.18	< 0.001	4.68	0.17	< 0.001	4.61	0.17	< 0.001

*In order to make results more interpretable, variables are centered (by subtracting the mean from all values) so that the main effects represent average conditions. For example, in the model with % vegetation × log[income], the main effect for vegetation (β = -1.1E-02) is the effect at the average value of log[income].

Table 2.10. Linear regression model for logarithm of mean urban NO_2 with interaction terms for impervious metric

	β	**SE**	**P > *t***	***β***	**SE**	**P > *t***	***β***	**SE**	**P > *t***	***β***	**SE**	**P > *t***
insolation	-1.9E-02	7.3E-04	< 0.001	-1.9E-02	7.3E-04	< 0.001	-1.9E-02	7.3E-04	< 0.001	-1.9E-02	7.4E-04	< 0.001
log[income]	0.31	0.02	< 0.001	0.32	0.02	< 0.001	0.32	0.02	< 0.001	0.31	0.02	< 0.001
% days of rain	-2.4E-02	1.8E-03	< 0.001	-2.4E-02	1.8E-03	< 0.001	-2.4E-02	1.8E-03	< 0.001	-2.4E-02	1.8E-03	< 0.001
log[pop]	0.67	0.06	< 0.001	0.66	0.06	< 0.001	0.65	0.06	< 0.001	0.67	0.06	< 0.001
dilution rate	-1.7E-04	5.0E-05	< 0.001	-1.7E-04	5.0E-05	< 0.001	-1.7E-04	5.0E-05	0.001	-1.8E-04	5.0E-05	< 0.001
contiguity	-0.48	0.15	0.001	-0.50	0.15	0.001	-0.47	0.15	0.001	-0.49	0.15	0.001
circularity	-0.67	0.22	0.003	-0.69	0.22	0.002	-0.63	0.22	0.005	-0.61	0.23	0.007
% vegetation	-7.1E-03	2.6E-03	0.007	-8.7E-03	2.7E-03	0.001	-7.6E-03	2.6E-03	0.004	-7.5E-03	2.7E-03	0.005
% impervious	-2.4E-03	1.8E-03	0.19	-3.2E-03	1.8E-03	0.08	-3.6E-03	1.8E-03	0.05	-2.7E-03	1.9E-03	0.17
% impervious × log[income]	--	--	--	-2.6E-03	8.8E-04	< 0.001	--	--	--	--	--	--
× log[pop]	--	--	--	--	--	--	1.0E-02	2.6E-03	< 0.001	--	--	--
× EPI	--	--	--	--	--	--	--	--	--	1.2E-04	1.4E-04	0.39
constant	4.69	0.17	< 0.001	4.68	0.17	< 0.001	4.66	0.17	< 0.001	4.66	0.18	< 0.001

*In order to make results more interpretable, variables are centered (by subtracting the mean from all values) so that the main effects represent average conditions. For example, in the model with % impervious × log[income], the main effect for impervious (β = -3.2E-02) is the effect at the average value of log[income].

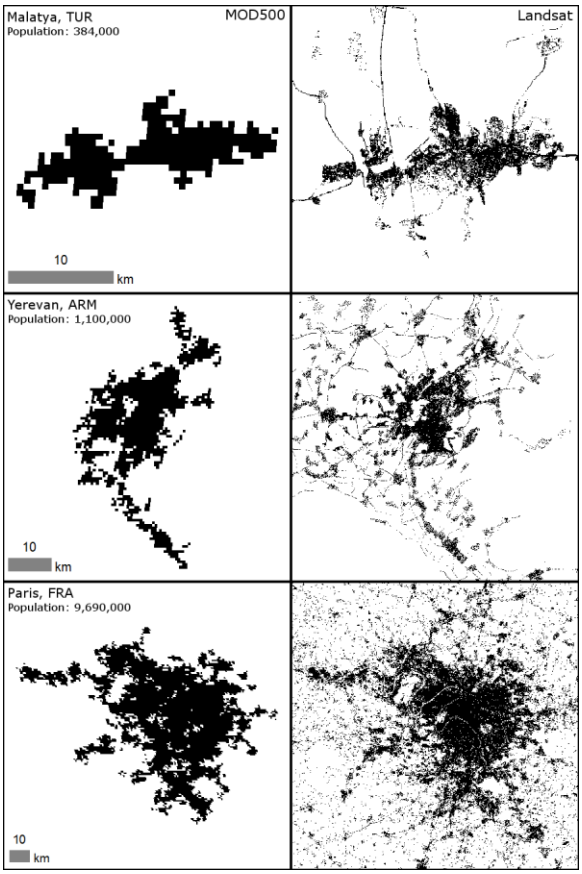

Figure 2.1. Urban extents for three cities (small, medium, and large), illustrating built-up urban area estimates from the 500 m MODIS data (left) employed here and the 30 m Landsat data (right) employed in Bechle et al. 2011.[26]

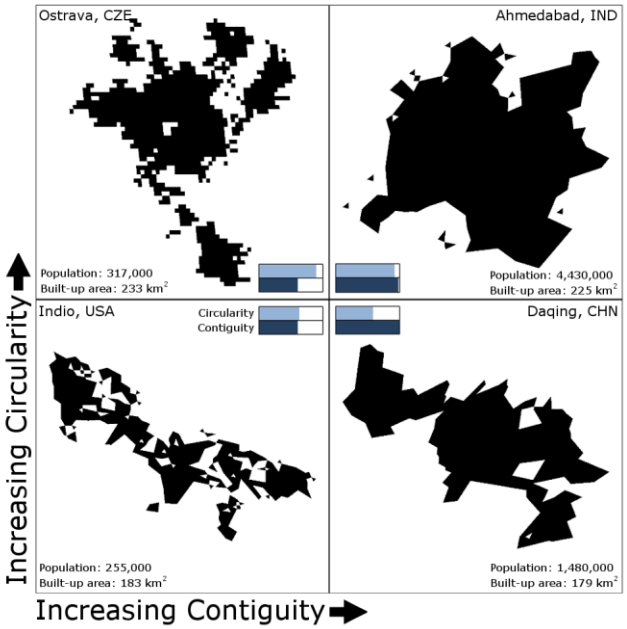

Figure 2.2. Characteristic cities illustrating contiguity (urban patchiness) and circularity based on 500 m MODIS built-up area (shown in black). Bar charts illustrate actual contiguity and circularity indices (range: 0-1) for each city.

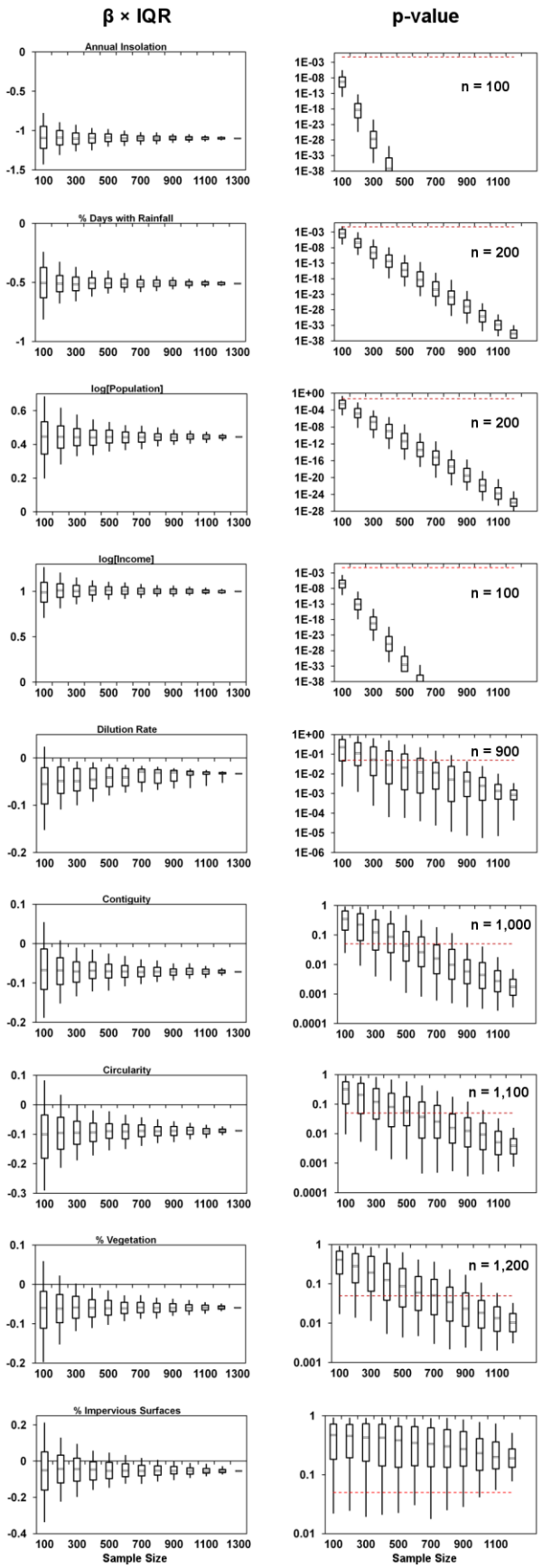

Figure 2.3. Summary of β×IQR (left) and p-value (right) for each variable based on Monte-Carlo random sampling (500 iterations) for indicated sub-sample size. Boxes indicate 25th and 75th percentile values, lines indicate 5th and 95th percentile values, and bars indicates median values. For p-value plots, horizontal red-line indicates p = 0.05 value. For all panels except the bottom panel (impervious surfaces), the p-value decreases for larger sample sizes. Number in p-value plot (e.g., "n=100" in top row) is an estimate of the minimum sample size for which the 95th percentile p-value is 0.05 or smaller.

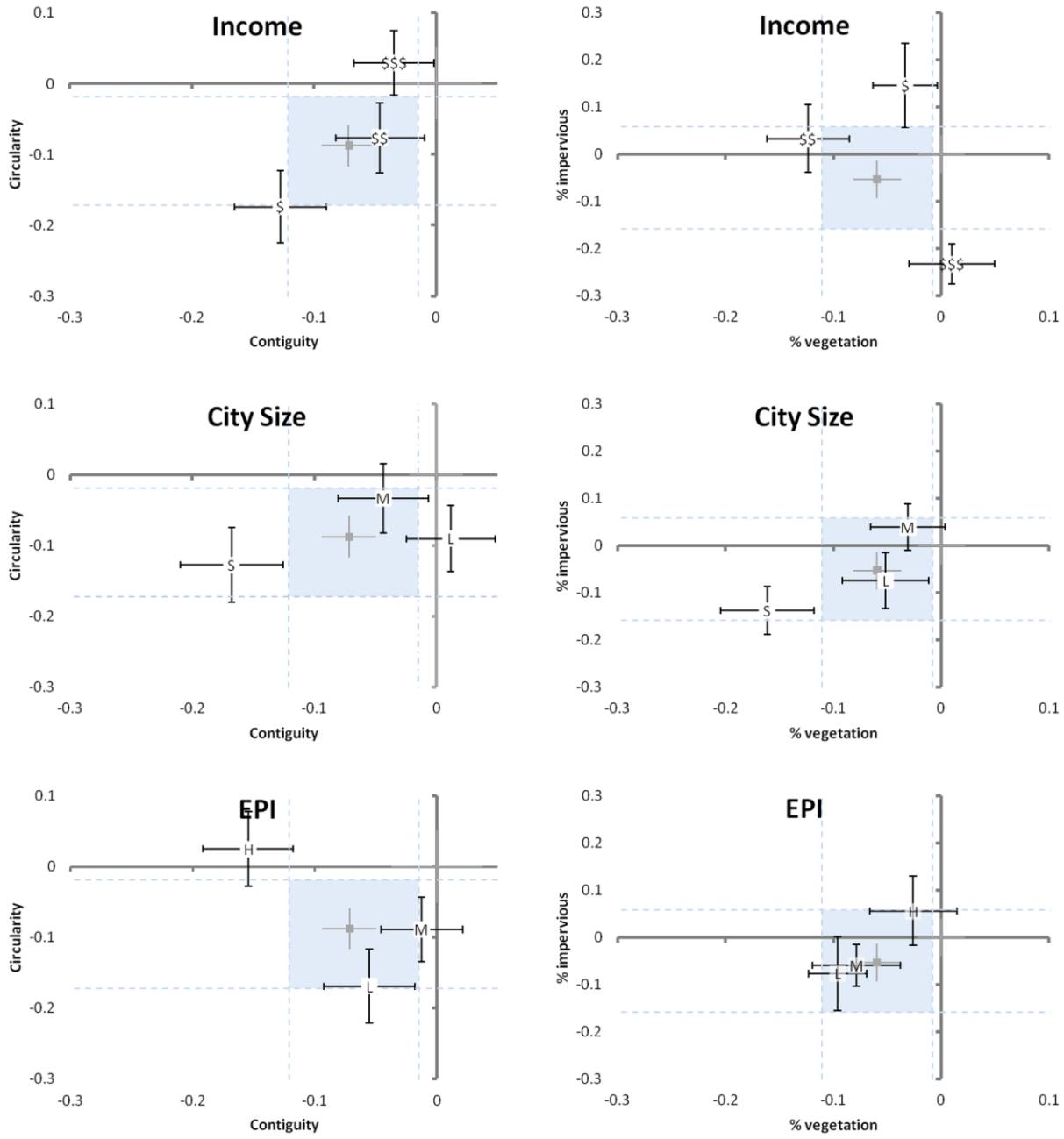

Figure 2.4. Summary of urban form coefficients for sub-sample models by tertile of income (top), city population (middle), and environmental performance index (bottom). Black symbols show β × IQR and lines indicate SE × IQR for the corresponding sub-models, grey squares and lines show β × IQR and SE × IQR for the full model. Blue dashed lines show the 5th and 95th percentile values for β × IQR based on Monte-Carlo random sampling at sample sizes approximating the tertiles (n=400). Values outside of the blue shaded box are considered statistically significant (i.e., outside the 90% confidence interval of the value for the base, based on the sample size of the tertile).

Chapter 3

National Spatiotemporal Exposure Surface for NO_2

3.1 Summary

Land-use regression (LUR) is widely used for estimating within-urban variability in air pollution. While LUR has recently been extended to national and continental scales, these models are typically for long-term averages. Here I present NO_2 surfaces for the continental United States with excellent spatial resolution (~100 m) and monthly average concentrations for one decade. I investigate multiple potential data sources (e.g., satellite column and surface estimates, high- and standard-resolution satellite data, and a mechanistic model [WRF-Chem]), approaches to model building (e.g., one model for the whole country versus having separate models for urban and rural areas, monthly LURs versus temporal scaling of a spatial LUR), and spatial interpolation methods for temporal scaling factors (e.g., kriging versus inverse distance weighted). The core approach uses NO_2 measurements from U.S. EPA monitors (2000–2010) to build a spatial LUR and to calculate spatially varying temporal scaling factors. The model captures 82% of the spatial and 76% of the temporal variability (population-weighted average) of monthly mean NO_2 concentrations from U.S. EPA monitors with low average bias (21%) and error (2.4 ppb). Model performance in absolute terms is similar near versus far from monitors, and in urban, suburban, and rural locations (mean absolute error 2–3 ppb); since low-density locations generally experience lower concentrations, model performance in relative terms is better near monitors than far from monitors (mean bias 3% versus 40%) and is better for urban and suburban locations (1–6%) than for rural locations (78%, reflecting the relatively clean

conditions in many rural areas). During 2000–2010, population-weighted mean NO_2 exposure decreased 42% (1.0 ppb [~5.2%] per year), from 23.2 ppb (year 2000) to 13.5 ppb (year 2010). I apply the approach to all U.S. Census blocks in the contiguous United States to provide 132 months of publicly available, high-resolution NO_2 concentration estimates.

3.2 Introduction

Nitrogen dioxide (NO_2) is a key component of urban air pollution generally associated with traffic-related emissions. Epidemiological studies have linked NO_2 to several adverse health outcomes including premature mortality[9,15,16], lung cancer[19], and asthma exacerbations[14,20]. Predicting spatial and temporal variability in outdoor air pollution over large geographical areas has become an important goal for population exposure assessment, health studies, environmental justice, and public policy research. Regulatory monitors, which provide the basis for many investigations, can provide good temporal resolution, but generally are unable to capture within-urban variability in pollutant concentration owing to the limited number of monitors and their proximity.[71,94]

Land use regression (LUR) has emerged as a useful tool for exploring within-urban variability in outdoor air pollution.[95] LUR is an empirical-statistical modeling approach that employs in situ measurements and geographic variables to predict concentrations at non-measurement locations. The technique has been used extensively to assess within-city variability in outdoor air pollution at the urban level.[94,96,97] More recently, LUR and similar geostatistical techniques have been employed to model fine-scale air pollution concentrations over large geographic regions. With an increasing amount of geographic data available with national and

global coverage, including land use and pollutant measurements from satellite instruments, LUR has been successfully applied over broad geographic regions for many locations, including the United States[31–33], Canada[34], Europe[35,36], Australia[37], and China[38,39]. Such models are useful for broad scale cross-sectional exploration of air pollution concentrations and exposures.

Nevertheless, while small scale LUR techniques have been studied extensively[95], continental scale LUR modeling requires further examination. Several studies have suggested 40 - 100 monitoring locations are necessary to obtain a robust LUR model, however, these results are based on LUR for urban areas and small countries rather than continental LUR.[95,98–100] Here I seek to test several aspects of continental LUR, with the goal of improving a prior national-scale spatial LUR model of annual-mean NO_2 for the United States.[32]

While the primary objective of LUR has generally been to improve the spatial resolution of air pollution estimates, spatiotemporal LUR models have become more prevalent at both local[101–111] and regional or national scales.[33,112–119] Here I seek to develop an ex post facto approach, employing regulatory monitoring data to temporally scale estimates from an improved version of the prior national-scale spatial LUR model. This general approach has been used to extend the temporal coverage of urban-scale LUR[120–122] and national-scale satellite-based estimates,[123] but to my knowledge has not been employed for national-scale LUR models. An advantage to this approach is its low computational requirements and ease of extending temporal coverage to other similar long-term LUR models.

I seek to create spatial NO_2 surfaces in the continental United States that provide the excellent spatial resolution typical for urban-scale LURs (~100 m scale), cover 100% of U.S. Census blocks, and provide monthly average concentrations for one decade. I focus on NO_2 because it has been shown to be a useful indicator of fresh combustion emissions, likely representing a mix of toxic species[9,15], and because NO_2 concentrations have been shown to correlate with land use, making it a good candidate pollutant for new LUR models. Contributions of this paper to the literature include advancing LUR as a method by (1) testing model robustness to the number of training sites used for building a continental LUR, (2) comparing model sensitivity to inclusion of various regional NO_2 predictor variables (e.g., satellite column, satellite surface, high-resolution satellite, model surfaces from a mechanistic model), and (3) by presenting a large-scale ex post facto approach to obtain temporal estimates from an existing national-scale LUR.

3.3 Methodology

3.3.1 Spatial LUR Model

Existing LUR Model

I build on a previously-developed year-2006 LUR for ground-level NO_2 for the contiguous United States.[32] Distinct features of the model relative to typical LURs included (1) broad geographic coverage, (2) inclusion of satellite-derived estimates of ground-level NO_2 and of regulatory monitoring data rather than de novo measurements, and, (3) greater temporal coverage and precision. Model-building incorporated six land-use characteristics (impervious surface, tree canopy, population, and major/minor/total road length) evaluated for 22 buffers

(100 m - 10 km) and three point-based values (elevation, distance to coast, and satellite NO_2), model details are available in Table 3.1. Model formulation employed conventional stepwise forward regression.[124] This year-2006 annual-mean model explained 78% of the spatial variability, with low mean bias (22% [overall], 5% [urban & suburban]). Model R^2 and internal leave-one-out validation may over-estimate LUR performance; holdout cross validation may provide better evaluation.[98,99] The base model is robust to holdout cross validation (90% of monitoring data for model-building, 10% for model-testing; Monte Carlo random sampling (n=500; median R^2 = 0.76)). Additional details for the prior LUR are available elsewhere.[32]

Regional NO_2 Covariates

Novotny et al. report a ~0.1 increase in model R^2 when including satellite-based NO_2 as a predictor; other continental LURs report similar improvements (R^2 increase ~0.02-0.15) .[34,36,37] Recent work suggests that satellite column abundance (total concentration within a vertical column) may be sufficient to track spatial patterns in ground level NO_2,[71] in which case converting column abundance to surface concentrations may be unnecessary for LUR. Knibbs et al. reported LUR R^2 values of 0.81 when using column abundance, versus 0.79 with satellite-based surface estimates.[37]

Here, I compare model performance for LUR employing various regional NO_2 covariates. I consider column abundance and surface concentrations from two NO_2 algorithms for the Ozone Monitoring Instrument (OMI): (1) a global product (DOMINO, version 1.0.2, collection 3; http://www.temis.nl), and (2) a higher-resolution U.S.-only product (BEHR, version 2.0A; http://behr.cchem.berkeley.edu/TheBEHRProduct.aspx).[125] For California and Nevada,

NO_2 estimates were 30% lower for BEHR than for DOMINO over remote regions, but 8% higher (BERH vs DOMINO) over polluted regions.[125] Surface concentrations are estimated from GEOS-Chem surface-to-column ratios, as in Novotny et al.[32]

I also include modeled NO_2 from a 12 km WRF-Chem chemical transport model simulation for North America.[126] Finally, I include linear combinations of satellite + WRF-Chem NO_2 surfaces, calculated as the sum of standardized surfaces. I do this because when satellite and WRF-Chem NO_2 covariates are offered together during model building, both are selected into the final models. Standardized surfaces are obtained by dividing each gridded estimated by the U.S. spatial mean concentration.

Addressing model artifacts

Using relative measures (e.g., bias), the Novotny et al. model exhibits better model performance in urban and suburban (mean bias: 5%) locations than rural (71%) locations.[32] Moreover, Figure 3.1 shows the Novotny et al. LUR NO_2 surface for the continental U.S. compared to WRF-Chem and DOMINO NO_2 surfaces. This figure indicates broad agreement among methods, but marked by regional differences between the methods, including over-estimation by the LUR of the low concentrations in rural and remote mountain West. Potential causes of the discrepancies include differences in the association between land use and NO_2 for urban/suburban versus for rural locations or monitor locations that do not adequately span the (independent) variable space. Regional discrepancies in Figure 3.1 generally correspond to elevation (e.g., the Rocky Mountains, California's Central Valley) and tree canopy (e.g., Northern Minnesota, Pacific Northwest, Southeast; see Figure 3.2).

Monitor locations are not representative of elevations in the continental U.S.; the inter-quartile range (IQR) of monitors' elevation is 0-300 m, yet 65% of the continental U.S. land area is >300 m. Additionally, the capacity of tree canopy as a sink for NO_2 is likely small,[127,128] however, tree canopy has a negative coefficient and the magnitude of its effect (β×IQR = -0.91) is similar to that of major roadways (β×IQR = 0.97).[32] In the model, tree canopy likely represents a land use with little or no combustion sources in urban/suburban areas, but in rural areas this variable is effectively acting (incorrectly in the model) as a large sink for NO_2. Here, I address these discrepancies by (1) truncating elevation to the IQR (all values over 300 m are set to 300 m), and (2) removing tree canopy as a potential independent variable.

I attempt to further address poor model performance in rural areas by testing two alternative modeling approaches: (1) I employ the natural logarithm of NO_2 concentration as the dependent variable. Here, model building is as above, but with the dependent variable changed to the natural logarithm of year 2006 annual average NO_2 concentration. (2) I develop separate models for urban versus rural areas, by first subdividing EPA monitoring data into urban (plus suburban) versus rural.

Spatial Model Evaluation

I evaluate all spatial models based on R^2, adjusted- R^2, mean error, absolute error, mean bias, and absolute bias, given by the following equations:

$$MB = \frac{1}{N}\sum_{i=1}^{N}\left(\frac{C_m - C_o}{C_o}\right) \qquad \textit{(Eq. 3.1)}$$

$$AB = \frac{1}{N}\sum_{i=1}^{N}\left(\frac{|C_m - C_o|}{C_o}\right) \qquad \textit{(Eq. 3.2)}$$

$$E = \frac{1}{N}\sum_{i=1}^{N}(C_m - C_o) \qquad \textit{(Eq. 3.3)}$$

$$AE = \frac{1}{N}\sum_{i=1}^{N}|C_m - C_o| \qquad \textit{(Eq. 3.4)}$$

where C_m is the modeled average concentration for station i; C_o is the average observed concentration for station i; and N is the number of monitoring stations. After selecting a final base spatial LUR model, as an additional sensitivity analysis, I use a Monte Carlo random sampling approach to explore model stability as a function of the number of training locations used for model building. Briefly, I conduct model building using random subsets of monitoring data (5%, 10%, 20%, 30%, 40%, 50%, 60%, 70%, 80%, 90%), and evaluate the model's ability to predict concentrations at the remaining locations. For each subset size, performance metrics are calculated for 500 iterations.

3.3.2 Monthly NO_2 Surfaces

Overview of Temporal Scaling

I also expand on my prior work by incorporating an order of magnitude more data for the dependent variable (11 years instead of 1 year) and by developing an approach that reflects spatiotemporal variability. I start with eleven years (2000 - 2010) of hourly in situ NO_2 measurements for all U.S. EPA regulatory monitoring stations in the contiguous United States.[129] I calculate monthly-mean concentrations for each monitor for months meeting the EPA reliability criterion of at least 75% of hourly values.

I calculate monthly scaling factors, which account for monthly deviations relative to the reference year, at each monitoring location using the following equation:

$$(Eq.\ 3.5) \qquad SF_{im} = \frac{C_{im}}{LUR_{2006}(x_i)}.$$

Here, SF_{im} is the scaling factor for monitor i and month m, C_{im} is the monthly-mean monitor concentration, and $LUR_{2006}(x_i)$ is the year-2006 LUR model estimate at the location (x_i) of monitor i.

I then create a scaling surface for each month (for a total of 132 months) by spatially interpolating the monthly scaling factors; I tested three interpolation techniques: (1) kriging (Bayesian kriging; ArcGIS 10.2), (2) inverse-distance weighting (IDW), and (3) nearest-neighbor (NN). Kriging is a geostatistical interpolation technique for which a model of the spatial surface of a parameter (the scaling factor for this application) is determined from the spatial dependence of the underlying data. Classical ordinary kriging assumes an unknown constant trend, which is determined via ad hoc fitting of the spatial dependence. Here I employ Bayesian kriging using ArcGIS 10.2 software to create kriging surfaces. Bayesian kriging differs from classical kriging by accounting for the error associated with estimating the spatial dependence, relying on iterative maximum likelihood fitting of the spatial dependence. This method is desirable for this application because it automates the trend fitting process, allowing for easier estimation of a large number of scaling surfaces.

The other two interpolation techniques (IDW and NN) are less sophisticated, deterministic methods. The simplest method, NN, assigns the nearest measured value as an estimate at the prediction location. For IDW, I consider the weighted-mean of values from the three nearest monitor locations, given by the following equations:

$$(Eq.\ 3.6) \qquad SS(x)_m = \sum_{i=1}^{3} \frac{w_i\, SF_{im}}{\sum_{j=0}^{3} w_j}$$

$$\textit{(Eq. 3.7)} \qquad w_i = \frac{1}{d(x,x_i)}$$

Here, $SS(x)_m$ is the (spatially-varying) scaling surface estimate at interpolated point x for month m; w_i is the IDW weighting factor; $d(x,x_i)$ is the distance from the interpolated point, x, to the location (x_i) of monitor i.

The monthly scaling surfaces are applied to the year-2006 LUR to create monthly NO_2 surfaces:

$$\textit{(Eq. 3.8)} \qquad LUR(x)_m = LUR(x)_{2006} \times SS(x)_m$$

where $LUR(x)_m$ is the LUR model estimate at point x for month m, $LUR(x)_{2006}$ is the year-2006 LUR model estimate at point x, and $SS(x)_m$ is the (spatially-varying) scaling surface interpolated from the Scaling Factor (SF_{im}) values at monitor locations.

Monthly NO_2 Surface Evaluation

To determine the goodness of fit of the monthly NO_2 surfaces, I estimate concentrations at each monitor location (i.e., excluding the monitor where the estimate is being made and using the remaining data to predict at this location) and compare these estimates with observed monitor concentrations. I evaluate model performance via spatial-only, temporal-only, and combined spatiotemporal comparisons. To determine spatial-only performance, I calculate R^2 statistics for each month (132 months) using monthly-mean concentrations, and for each year (11 years) using annual-mean concentrations. To determine annual and long-term temporal-only performance, I calculate R^2 statistics of monthly-mean concentrations for each monitor location with at least 75% of months (at least 9 months for annual and 98 months for 11 years) of measurements. I determine long-term (132 months) and annual spatiotemporal performance using all monitor-

months. I report mean error, absolute error, mean bias and absolute bias. I also investigate summary statistics by distance to the nearest monitor (<10 km, <25 km, 25-50 km and >50 km), and by U.S. EPA-designated location type (urban, suburban, rural). To assess the performance of the model where there are people, I present population-weighted evaluations of model performance, based on U.S. Census population within a 1-km buffer of monitor location. I assess within-city performance by calculating the above performance metrics for all monitors located within a single urban area, for the ten urban areas with the most monitors. Monthly residuals were tested for Moran's *I* spatial autocorrelation using ArcGIS 10.2. Finally, as a sensitivity analysis, I compare the monthly NO_2 surface approach described above to (1) monthly LUR models for year-2006, (2) estimates from satellite-based measurements, and (3) a standard non-LUR approach: IDW interpolation of the monthly mean monitor values.

3.4 Results

3.4.1 Spatial LUR Model

Regional NO_2 Covariates

I tested seven approaches for estimating regional NO_2 (DOMINO satellite column and surface estimates; BEHR satellite column and surface estimates; 12 km WRF-Chem model; linear combinations of DOMINO and WRF-Chem; linear combinations of BEHR and WRF-Chem). I find that the continental LUR employed here is relatively insensitive to the choice of regional NO_2 covariate, but including no regional NO_2 covariate degrades performance (R^2 = 0.77 - 0.81 among models with regional NO_2, versus R^2 = 0.66 if no regional-NO_2 variable is included). Models using satellite column NO_2 perform slightly better than those employing

satellite-based surface estimates (see Table 3.2); this finding is consistent with a previous LUR of NO_2 for Australia[37] and suggests that the extra steps needed to estimate surface concentrations from satellite column measurements may be unnecessary for LUR models. I find that a model using a linear combination of satellite + WRF-Chem provides the best predictive power (R^2 = 0.81); I employ that regional NO_2 covariate (DOMINO + WRF-Chem) for analyses below.

Addressing model artifacts and final annual model selection

As mentioned above, I attempted to addresses the prior over-estimation of low concentrations in rural and remote mountain West by truncating the elevation variable at the IQR of monitor locations and by removing tree canopy as a land use variable. Table 3.3 shows the resulting model and Table 3.4 shows model performance. With these changes, overall model performance diminishes slightly (R^2 = 0.79, mean absolute error = 2.3 ppb, mean bias = 18%; mean absolute bias = 34%) and performance at rural monitors is largely unchanged, however, Figure 3.1 shows that the resulting model better captures the regional NO_2 patterns exhibited by the WRF-Chem and DOMINO estimates.

Tables 3.5 and 3.6 show the two alternative LUR models (natural logarithm, urban + rural). Table 3.7 shows the model performance for the same two models and for the core LUR. Model performance is worse when using the natural logarithm of NO_2 (overall R^2 = 0.64 vs 0.79 for the traditional model), and similar (0.80) for the urban + rural model. Model performance is slightly better for the urban + rural model when considering only urban (R^2 = 0.79 [urban+rural] vs. 0.76 [traditional]) and rural (0.60 vs. 0.50) monitors. Mean absolute error is similar for the urban + rural model when considering all monitors (2.3 ppb vs. 2.3 ppb) and only urban monitors

(2.3 ppb vs. 2.4 ppb) and moderately better when considering only rural monitors (2.0 ppb vs. 2.4 ppb). Population-weighted mean metrics (based on 2000 US Census population within 1 km) are similar for the urban + rural and traditional models (R^2: 0.83 vs. 0.81; mean abs. error: 2.30 ppb vs. 2.43 ppb; mean abs. bias: 16% vs. 17%). The urban + rural model offers slight improvement in performance for rural areas, but at the cost of overall model parsimony. Based on these results, I employ the traditional LUR as the base spatial model for the remainder of the analysis.

Figure 3.3 shows model performance (median and IQR R^2, absolute error, and absolute bias among n=500 Monte Carlo iterations per comparison) as a function of the number of monitor locations used in model-building. The final spatial LUR (derived from n=369 monitoring locations) is robust to large holdout evaluations; for example, median R^2 values for model-building vs holdout datasets are 0.79 vs 0.77 with 20% holdout (n=295 monitors in model-building), 0.79 vs 0.76 with 50% holdout (n=184 monitors in model-building). For cases with more than ~150-200 monitors in model-building, model-building R^2 is stable and is similar to the holdout R^2. This suggests that large-scale LUR may require more locations than the ~40-100 locations suggested for smaller-scale LUR[98–100] in order to obtain a robust model. The IQR of the holdout-R^2 is ~0.1 for holdout subsets of 10-20%, suggesting a need to use large holdout subsets (here, ~50%), systematic holdouts (e.g., 10-fold 10% holdout), or to conduct Monte Carlo approaches so model evaluation is not impacted by unusual holdout subsets.

3.4.2 Monthly NO_2 Surfaces

Based on EPA data for the 11 years, on average 370 (IQR: 362 – 381) monitors meet the reliability criteria each month. The average (IQR) monthly mean NO_2 concentration (units: ppb) during the 11 years is 12.4 (9.9-14.6), and decreased from 15.2 (13.1-17.6) in year 2000 to 9.3 (7.2-11.4) in year 2010; population-weighted values have a mean of 19.5 (IQR: 16.1-22.3) for the 11 years, reflecting a 42% decrease overall, from 23.2 (21.1-25.0) in year 2000 to 13.5 (10.6-16.3) in year 2010. Mean concentrations over the 11 years are higher for urban (16.2) and suburban (13.6) locations than for rural (6.0) monitors. NO_2 concentration decreases observed here (for unweighted concentrations: 0.59 ppb y^{-1}, ~4.7% y^{-1}; for population-weighted concentrations: 1.0 ppb y^{-1}, 5.2% y^{-1}) correspond to significant reductions in NO_x emissions throughout the United States.[130] The long-term temporal trend varies spatially (IQR: 29−42% [3.3–7.3 ppb] decrease in annual average NO_2 concentration), and includes increasing concentrations at a small number of rural locations (5% of monitors). These trends are consistent with findings from satellite-based measurements, and support the use of a spatially varying temporal scaling surface.[131] Tables 3.8-3.10 summarize monthly NO_2 surface estimates for the three temporal scaling techniques. All three methods perform similarly well, with the kriging method performing slightly better than IDW and NN. The resulting NO_2 surfaces (kriging, IDW, NN) predict, on population-weighted average, 82% (kriging), 79% (IDW), and 80% (NN) of the spatial-only variability; 76%, 73%, and 74% of the annual temporal-only variability; and 85%, 84%, and 84% of the combined spatiotemporal variability in U.S. EPA monitored NO_2 concentrations. (Unweighted R^2 values are 0.81, 0.78, 0.79 [spatial only]; 0.73, 0.69, and 0.70 [temporal only]; and 0.84, 0.81, and 0.82 [spatiotemporal].) From here forward, I will focus primarily on the monthly NO_2 estimates employing kriging temporal scaling. The model mean

bias and absolute error are low (21% and 2.4 ppb, respectively), and consistent with the previously published year-2006 spatial LUR model. For illustrative purposes, I apply the final national NO_2 surface estimates to a 100 m grid for two cities (Los Angeles, CA, and New York, NY; see Figure 3.4). This figure illustrates month-to-month variability in the modeled spatial patterns.

Table 3.8 and Figure 3.5 show model performance by distance to the nearest monitor. Model performance is generally better for locations within 10 km (mean spatial-R^2: 0.80, mean temporal-R^2: 0.72, spatiotemporal-R^2: 0.82; mean absolute error: 2.6 ppb, mean bias: 3%) and within 25 km (0.82, 0.73, 0.84, 2.5 ppb, 12%), than for locations between 25-50 km (0.70, 0.79, 0.77, 2.1 ppb, 23%) and further from (>50 km) nearby monitors (0.71, 0.69, 0.75, 2.2 ppb, 40%); differences among those four groups are greater for the mean bias than for the R^2 value. The mean absolute error is similar among the four location types. The spatial-only year-2006 LUR explains, on population-weighted average, 71% (unweighted: 72%) of the spatial variability in monthly-mean concentrations for years 2000-2010. Figure 3.6 exhibits spatial-only, temporal-only and spatiotemporal R^2 values for each year using monthly-mean concentrations for each monitor. Model performance is good, with R^2 values generally >0.70. The annual temporal-R^2 shown is typically greater than for the long-term (2000-2011) temporal performance (R^2: 0.72 [unweighted], 0.77 [weighted]). Monthly spatial-only correlation coefficients are given in Figure 3.7.

Figures 3.5-3.7 also show plots for urban, suburban, and rural monitor locations. Monitor performance is better for urban (mean spatial R^2 = 0.76, mean temporal R^2 = 0.76, mean

spatiotemporal R^2 = 0.80, mean absolute error: 2.6 ppb, mean bias: 1%) and suburban (0.76, 0.76, 0.81, 2.4 ppb, 6%) locations than for rural locations (0.63, 0.63, 0.69, 2.0 ppb, 78%). As above, differences in mean absolute error are small, differences in mean bias are larger. Urban and suburban locations typically outperform rural locations for each year (Figure 3.6), except for mean absolute error. Population-weighted performance metrics (Table 3.8) are similar to urban- and suburban-only metrics, in part because a minority (~19%) of the population lives in rural areas.[132] This fact emphasizes the potential utility of these models for estimating exposures. I found limited evidence of spatial autocorrelation in model residuals. For the months with significant values (102 of 132 months with $p < 0.05$), the Moran's *I* coefficients were negative and small (values range from -0.05 to -0.22).

I assess within-urban performance of the monthly NO_2 estimates by considering model performance separately in the ten urban areas (UAs) with the most available monitors. Model performance varies among UAs (Table 3.11), but generally suggests reasonable within-urban predictive power (spatial-R^2: 0.25 - 0.75; temporal-R^2: 0.52 - 0.90; spatiotemporal-R^2: 0.61 - 0.79), even when considering only one UA at a time, as in Table 3.11. For the three cities with an average of at least 10 monitors (Los Angeles, New York, Houston), within-urban model performance is similar to the nationwide model performance. Scatterplots in Figure 3.4 of predicted versus observed concentrations for LA and NYC show strong model-measurement agreement.

As a sensitivity analysis, and to compare to the temporal scaling approach developed here, for year 2006, I developed 12 monthly LURs (i.e., using the same LUR model building

procedure outlined above, but with monthly-mean NO_2 monitor concentrations as the dependent variable). Model performance for the monthly LUR models (and corresponding performance for spatial LUR + temporal scaling) are in Table 3.12. The base-case spatial LUR + temporal scaling approach exhibits better model performance than the individual monthly LUR models (spatial-R^2: 0.77 - 0.84 [LUR + temporal scaling] vs. 0.65 - 0.76 [monthly LUR]; mean bias: 14 - 26% vs. 19 - 32%; mean abs. error: 2.0 - 2.7 ppb vs. 2.3 - 3.4 ppb). This finding highlights the potential difficulty in fitting monthly LUR models, and the utility of the temporal scaling approach.

I also tested the value of the monthly scaling approach by comparing the monthly estimates against (1) straightforward satellite-only estimates of surface concentrations (DOMINO) and (2) standard IDW interpolation of monitoring-station-only data. Summary statistics are in Table 3.13 (DOMINO, 2005–2007) and Table 3.14 (IDW, 2000–2010). The core LUR + temporal scaling approach outperforms the two alternatives for predicting temporal variability (mean temporal R^2 = 0.73 [LUR + temporal scaling], 0.42, [DOMINO], 0.64 [IDW]), spatial variability (mean spatial R^2 = 0.81 vs 0.45 and 0.51), and spatiotemporal variability (R^2 = 0.84 vs 0.35 and 0.59). The mean bias is approximately 3 times lower for the LUR + temporal scaling than for IDW (21% vs 64%), and the mean absolute error is 1.7 times lower for the LUR + temporal scaling than for IDW (2.4 ppb vs 4.1 pbb). These findings illustrate the utility of the land-use information and LUR for predicting spatial variability, and the utility of the temporal scaling approach described here for predicting spatiotemporal variability.

3.5 Discussion

I created national-scale monthly NO_2 surfaces for the contiguous United States using fixed-site regulatory monitors, satellite-derived NO_2 estimates, and GIS-derived land-use data. The resulting surfaces exhibit good spatial, temporal, and spatiotemporal predictive performance (overall $R^2 = 0.84$), with spatial resolution typical of urban LUR models (~100 m). The large spatial and temporal coverage of this model is useful for national-scale longitudinal research on outdoor air pollution (e.g., population exposure assessment, epidemiology, environmental justice, surveillance, public policy) with excellent spatial resolution. For example, a cohort study of exposures during pregnancy could use NO_2 estimates provided here to explore impacts of exposure by pregnancy month or trimester. To facilitate future research, I estimated monthly NO_2 concentrations at the centroid locations for all ~8 million Census blocks in the contiguous United States (blocks are the smallest area enumerated by the U.S. Census); this data set is publicly and freely available online (see Appendix A).

With relative measures (% rather than ppb), the model exhibits the greatest predictive power in urban and suburban locations. This finding supports the use of the LUR + temporal scaling model for population-based research. (Most [~81%] of the U.S. population lives in urban or suburban areas.[132]) Rural monitors are, on average, further from nearby monitors (Table 3.8) and experience cleaner concentrations, and may suffer from greater relative error in estimating monthly scaling factors. In absolute terms (ppb rather than %), errors appear similar for urban, suburban, and rural areas. The correlation between NO_2 emissions (and concentrations) and GIS-derived land uses may be greater in urban areas than in suburban areas. Here, model performance generally is similar or better for population-weighted metrics than unweighted metrics. The three

methods of creating temporal scaling surfaces (kriging, IDW, NN) performed similarly well, suggesting that temporal scaling is relatively robust to the selection of interpolation technique. Moreover, this approach for temporal scaling (interpolating temporal trends from regulatory monitors) is straightforward and simple to implement. Alternative methods of temporal scaling (e.g., use of a CTM) may be more complex and require greater expert knowledge and computational resources to run. Satellite measurements offer another potential source of temporal scale factors; however, temporal scaling with that approach may be complicated by the need to combine data from several instruments with differing overpass times and retrieval algorithms.[133] Improved spatial and temporal resolution from future satellite measurements (e.g., Sentinel-5 Precursor, TEMPO) may improve the spatial performance of satellite-based LUR models and could provide an alternative temporal scaling approach.[134,135]

The model spatial-only performance (mean R^2 = 0.81) is consistent with that of other continental-scale NO_2 models (R^2 = 0.61–0.78)[32,34–36] and most urban- and national-scale LUR models for long-term average NO_2.[95] Spatiotemporal performance based on monthly mean estimates (R^2 = 0.84) is consistent with published monthly PM_{10} (R^2 = 0.76) and $PM_{2.5}$ (R^2 = 0.79–0.85) estimates in the United States.[33,113,114] Hart et al.[31] estimated annual average NO_2 concentrations for the years 1985–2000 in the United States with similar modeled spatiotemporal performance (R^2 = 0.88 vs 0.84 here, using annual mean concentrations). Kloog et al.[116,117] predicted daily mean $PM_{2.5}$ for the years 2000–2008 in New England and the Mid-Atlantic states with similar spatial R^2 (0.69–0.86) and spatiotemporal R^2 (0.73–0.90) and slightly better temporal R^2 (0.73–0.91). Lee et al.[119] predicted daily mean NO_2 for the years 2005–2010 in New England with similar spatiotemporal R^2 (0.79). These daily models, using a mixed effects

modeling approach, offer excellent temporal coverage; to my knowledge, they have not been applied on a national scale.

This work provides useful information for future continental LUR building. I found that model performance was relatively insensitive to the type of regional NO_2 covariate used (here, satellite-based ground level, satellite-based column total, DOMINO versus BEHR satellite data, 12 km CTM); the satellite column NO_2 slightly outperformed satellite-based surface estimates. These findings suggest that, for the purposes of LUR, it might be unnecessary to employ a CTM to convert satellite column measurements to surface estimates. Moreover, findings indicate that the number of monitors needed to build a robust continental LUR (>150–200) is greater than that for a smaller scale LUR, and that large holdout subsets, systematic holdout, or Monte Carlo approaches may be needed to adequately evaluate the model performance.

The model approach combines the spatial predictive power of LUR with the temporal coverage of the EPA monitoring network. The resulting model exhibits slightly better temporal predictive performance than IDW interpolation of monthly mean monitor values (on average, temporal-only R^2 = 0.73 [LUR + temporal scaling] vs 0.64 [IDW]), but with the greatly improved spatial performance (on average, spatial-only R^2 = 0.81 vs 0.51, spatiotemporal R^2 = 0.84 vs 0.59) typical of LUR.[94]

Table 3.1. Independent variables used for model building[†]

Parameter	Units	Spatial resolution	Buffer[‡] or point estimate
Impervious surface [a]	%	1,000 m	buffer
Tree canopy [b]	%	500 m	buffer
Population [c]	#	1 km	buffer
Major road length [d]	m	NA	buffer
Minor road length [d]	m	NA	buffer
Total road length [d]	m	NA	buffer
Elevation [e]	m	90 m	Point
Distance to coast [f]	m	NA	point
DOMINO NO_2 [g]	ppb	13 × 24 km^2 at nadir	point

[†]Data sources: a ([78]), b: ([79]), c: ([136]), d: (2009 US Census Tiger), e: ([137]), f: (ESRI ArcGIS), g: ([138]).

[‡]Buffers employed (m): 100; 200; 300; 400; 500; 600; 700; 800; 1000; 1200; 1500; 1800; 2000; 2500; 3000; 3500; 4000; 5000; 6000; 7000, 8000; 10000. (adapted from Novotny et al. 2011)

Table 3.2. Model performance for LUR models with various regional NO_2 covariates

Regional NO_2 covariate	***R^2***	**Adj-*R^2***	**Mean abs. err. (ppb)**	**Mean bias (%)**	**Mean abs. bias (%)**
Without regional NO_2	0.66	0.65	2.9	28	46
DOMINO column	0.79	0.79	2.3	22	38
DOMINO surface	0.77	0.76	2.5	20	39
BEHR column	0.78	0.78	2.4	22	39
BEHR surface	0.77	0.76	2.5	22	41
WRF-Chem	0.77	0.76	2.2	18	34
DOMINO + WRF-Chem	0.81	0.80	2.2	17	33
BEHR + WRF-Chem	0.80	0.80	2.3	17	34

Table 3.3. Final year-2006 model

Parameter	Units	β	Std. error	$p > \|t\|$	Partial R^2	IQR	$\beta \times$ IQR
Intercept	ppb	2.44	0.41	< 0.01			
DOMINO + WRF-Chem NO_2	unitless	0.72	0.036	< 0.01	0.62	6.3	6.0
Impervious (800 m)	%	0.085	0.0094	< 0.01	0.75	43	4.9
Elevation (truncated)	km	11.1	0.17	< 0.01	0.76	0.27	1.9
Major roads (800 m)	km	0.30	0.056	< 0.01	0.78	3.2	0.91
Residential roads (100 m)	km	2.82	1.04	0.01	0.78	0.27	0.77
Distance to coast	km	-1.2e-3	3.8e-4	<0.01	0.79	630	-0.72

Table 3.4. Model performance for final spatial LUR model

	R^2	Adj.-R^2	Mean err. (ppb)	Mean abs. err. (ppb)	Mean bias (%)	Mean abs. bias (%)
All	0.79	0.79	-0.30	2.3	18	34
Urban	0.76	0.76	-0.78	2.4	-1	18
Rural	0.50	0.49	0.39	2.4	57	75
Pop-wtd	0.81	0.81	-0.71	2.4	-1	17

Table 3.5. Alternative model using natural-logarithm of annual-mean NO_2

Parameter	Units	B	Std. error	$p > \|t\|$
Intercept	ln[ppb]	1.46	0.058	< 0.01
Impervious (3500 m)	%	0.015	0.002	< 0.01
DOMINO + WRF-Chem NO_2	unitless	0.056	0.006	< 0.01
Distance to coast	km	-2.8e-4	5.4e-5	< 0.01
Elevation (truncated)	km	0.75	0.24	< 0.01
Total roads (200 m)	km	0.13	0.041	< 0.01
Population (8000 m)	persons	-4.5e-5	1.7e-5	0.01

Table 3.6. Alternative model using 2-step urban + rural approach

Parameter	**Units**	***β***	**Std. error**	***p*** **> |*t*|**
Rural model				
Intercept	ppb	2.49	0.43	< 0.01
DOMINO + WRF-Chem NO_2	unitless	0.64	0.13	< 0.01
Major roads (1500 m)	km	0.31	0.097	< 0.01
Total roads (200 m)	km	1.6	0.69	0.02
Population (10000 m)	persons	4.1e-3	1.4e-3	< 0.01
Urban model				
Intercept	ppb	3.57	0.57	< 0.01
DOMINO + WRF-Chem NO_2	unitless	0.67	0.042	< 0.01
Impervious (1200 m)	%	0.076	0.017	< 0.01
Elevation (truncated)	km	15.6	1.9	< 0.01
Major roads (800 m)	km	0. 23	0.061	< 0.01
Residential roads (100 m)	km	2.46	1.14	0.03
Population (1200 m)	persons	2.2e-4	9.2e-5	0.02
Distance to coast	km	-1.3e-3	5.3e-4	0.01
Residential roads (7000 m)	km	-2.3e-3	9.0e-4	0,01
Major roads (7000 m)	km	5.4e-3	2.6e-3	0.04

Table 3.7. Model performance for traditional and alternative LUR models

	R^2	Adj.-R^2	Mean err. (ppb)	Mean abs. err. (ppb)	Mean bias (%)	Mean abs. bias (%)
Traditional model						
All	0.79	0.79	-0.30	2.34	18	34
Urban	0.76	0.76	-0.78	2.36	-1	18
Rural	0.50	0.49	0.39	2.40	57	75
Pop-wtd	0.81	0.81	-0.71	2.43	-1	17
Natural-logarithm of NO_2 model						
All	0.64	0.63	-0.29	3.16	11	37
Urban	0.57	0.56	0.06	3.86	2	25
Rural	0.48	0.47	-0.43	2.40	44	70
Pop-wtd	0.54	0.53	0.26	4.39	2	25
Urban + rural model						
All	0.80	0.79	-0.58	2.31	9	29
Urban	0.79	0.78	-1.05	2.33	-2	17
Rural	0.60	0.59	-0.33	2.00	28	53
Pop-wtd	0.83	0.82	-0.84	2.30	-2	16

Table 3.8. Summary of monthly mean NO_2 estimates using kriging temporal scaling[a] (2000 - 2010)

	Mean spatial R^2	Mean temporal R^2	Spatio-temporal R^2	Mean conc. (ppb)	Mean error (ppb)	Mean abs. error (ppb)	Mean bias (%)	Mean abs. bias (%)	Mean (IQR[b]) distance to nearest monitor (km)
All									
Population-weighted	0.82	0.76	0.85	19.6	-0.3	2.7	2	18	32
Unweighted	0.81	0.73	0.84	12.4	-0.05	2.4	21	38	48 (13 - 50)
Distance to nearest monitor									
< 10 km[b]	0.80	0.72	0.82	16.3	-0.5	2.6	3	22	6 (4 - 8)
< 25 km[b]	0.82	0.73	0.84	15.4	-0.1	2.5	12	28	13 (8 - 18)
25 - 50 km[b]	0.70	0.79	0.77	10.6	-0.06	2.1	23	40	36 (29 - 40)
> 50 km[b]	0.71	0.69	0.75	9.5	0.1	2.2	40	57	133 (65 - 158)
Urban classification									
Urban	0.76	0.76	0.80	16.2	-0.5	2.7	1	20	12 (7 - 16)
Suburban	0.76	0.76	0.81	13.6	-0.02	2.4	6	22	30 (21 - 38)
Rural	0.63	0.63	0.69	6.0	0.4	2.0	78	95	104 (36 - 136)

[a] All values except the first row are unweighted metrics. [b] IQR is interquartile range.

Table 3.9: Summary of monthly mean NO_2 estimates using IDW temporal scaling (2000 - 2010)

	Mean spatial R^2	Mean temporal R^2	Spatio-temporal R^2	Mean conc. (ppb)	Mean error (ppb)	Mean abs. error (ppb)	Mean bias (%)	Mean abs. bias (%)	Mean (IQR) distance to nearest monitor (km)
All									
Population-weighted	0.79	0.73	0.84	19.55	-0.10	2.81	2	19	32
Unweighted	0.78	0.69	0.81	12.44	0.13	2.56	23	40	48 (13 - 50)
Distance to nearest monitor									
< 10 km	0.78	0.70	0.80	16.33	0.02	2.68	6	23	6 (4 - 8)
< 25 km	0.79	0.71	0.82	15.42	0.15	2.70	13	29	13 (8 - 18)
25 - 50 km	0.65	0.75	0.73	10.56	0.07	2.36	23	42	36 (29 - 40)
> 50 km	0.63	0.62	0.69	9.47	0.17	2.47	42	61	133 (65 - 158)
Urban classification									
Urban	0.71	0.73	0.77	16.23	-0.13	2.91	3	22	12 (7 - 16)
Suburban	0.73	0.72	0.79	13.62	0.08	2.54	7	24	30 (21 - 38)
Rural	0.57	0.59	0.65	6.0	0.51	2.13	71	89	104 (36 - 136)

Table 3.10: Summary of monthly mean NO_2 estimates using NN temporal scaling (2000 - 2010)

	Mean spatial R^2	Mean temporal R^2	Spatio-temporal R^2	Mean conc. (ppb)	Mean error (ppb)	Mean abs. error (ppb)	Mean bias (%)	Mean abs. bias (%)	Mean (IQR) distance to nearest monitor (km)
All									
Population-weighted	0.80	0.74	0.84	19.55	-0.23	2.76	1	18	32
Unweighted	0.79	0.70	0.82	12.44	0.05	2.52	20	38	48 (13 - 50)
Distance to nearest monitor									
< 10 km	0.77	0.70	0.80	16.33	-0.10	2.72	5	23	6 (4 - 8)
< 25 km	0.80	0.72	0.83	15.42	0.14	2.66	11	27	13 (8 - 18)
25 - 50 km	0.66	0.75	0.74	10.56	-0.08	2.31	20	39	36 (29 - 40)
> 50 km	0.63	0.65	0.69	9.47	0.01	2.43	38	59	133 (65 - 158)
Urban classification									
Urban	0.73	0.74	0.78	16.23	-0.27	2.80	2	21	12 (7 - 16)
Suburban	0.74	0.74	0.79	13.62	0.05	2.52	6	23	30 (21 - 38)
Rural	0.53	0.59	0.61	6.0	0.42	2.09	65	84	104 (36 - 136)

Table 3.11. Summary of within-city monthly-mean LUR estimates (2000-2010) for the ten U.S. cities with the largest number of NO_2 monitors

City	Mean (range) number of monitors	Mean spatial R^2	Mean temporal R^2	Spatio-temporal R^2	Mean error (ppb)	Mean abs. error (ppb)	Mean bias (%)	Mean abs. bias (%)
Los Angeles	16 (11- 18)	0.59	0.80	0.77	0.4	3.6	10	20
New York City	12 (9 - 15)	0.75	0.73	0.79	0.6	3.2	8	19
Houston	10 (6 - 11)	0.61	0.86	0.78	0.2	1.8	7	18
D.C.	9 (6 - 10)	0.61	0.81	0.77	-0.6	2.4	0.2	17
Chicago	7 (6 - 10)	0.57	0.52	0.62	-0.7	3.6	-2	17
Philadelphia	7 (4 - 8)	0.66	0.76	0.73	0.4	2.2	5	14
St Louis	6 (1 - 9)	0.66	0.65	0.76	-0.1	1.9	3	15
San Diego	6 (5 - 8)	0.32	0.79	0.61	0.2	3.4	7	27
Pittsburgh	6 (4 - 6)	0.38	0.74	0.62	-0.7	2.5	-2	18
Phoenix	5 (1 - 7)	0.25	0.90	0.67	-0.01	3.4	4	16
MEDIAN	7	0.60	0.78	0.75	0.1	2.9	5	17

Table 3.12. Summary of year-2006 monthly performance for monthly LUR and the final spatial LUR + temporal scaling approach

	Monthly LUR					Spatial LUR + temporal scaling				
Month	**Mean spatial R^2**	**Mean error (ppb)**	**Mean abs. error (ppb)**	**Mean bias (%)**	**Mean abs. bias (%)**	**Mean spatial R^2**	**Mean error (ppb)**	**Mean abs. error (ppb)**	**Mean bias (%)**	**Mean abs. bias (%)**
Jan	0.70	0.15	3.0	19	35	0.82	0.10	2.5	18	34
Feb	0.73	0.14	3.3	19	36	0.84	0.04	2.6	13	29
Mar	0.75	0.17	2.4	24	40	0.81	-0.12	2.1	16	32
Apr	0.76	0.09	2.3	31	49	0.83	-0.16	2.0	22	40
May	0.73	0.08	2.4	32	51	0.77	-0.14	2.2	26	45
Jun	0.75	0.11	2.3	27	46	0.80	-0.14	2.1	24	42
Jul	0.72	0.11	2.3	30	48	0.82	-0.10	2.0	23	42
Aug	0.65	0.11	2.5	28	46	0.81	-0.09	2.0	22	39
Sep	0.71	0.08	2.7	28	46	0.83	-0.13	2.1	26	43
Oct	0.73	-0.04	2.9	23	42	0.82	-0.09	2.2	19	35
Nov	0.74	0.06	3.1	22	38	0.83	0.10	2.5	14	28
Dec	0.67	0.11	3.4	30	46	0.78	0.17	2.7	22	37

Table 3.13. Summary of satellite-based estimates of monthly-mean monitor values (2005 - 2007)

	Mean spatial R^2	**Mean temporal R^2**	**Spatio-temporal R^2**	**Mean conc. (ppb)**	**Mean error (ppb)**	**Mean abs. error (ppb)**	**Mean bias (%)**	**Mean abs. bias (%)**
All								
Population-weighted	0.53	0.45	0.38	17.89	-13.49	13.53	-78	78
Unweighted	0.45	0.42	0.35	11.96	-9.17	9.21	-76	77
Urban classification								
Urban	0.45	0.45	0.36	15.49	-12.25	12.27	-81	77
Suburban	0.42	0.43	0.32	12.95	-9.74	9.79	-67	73
Rural	0.37	0.37	0.31	6.10	-4.50	4.55	-78	78

Table 3.14. Summary of IDW interpolation of monthly-mean monitor values (2000 - 2010)

	Mean spatial R^2	Mean temporal R^2	Spatio-temporal R^2	Mean conc. (ppb)	Mean error (ppb)	Mean abs. error (ppb)	Mean bias (%)	Mean abs. bias (%)
All								
Population-weighted	0.60	0.70	0.67	19.54	-0.74	3.96	3	27
Unweighted	0.51	0.64	0.59	12.44	1.23	4.14	64	83
Distance to nearest monitor								
< 25 km	0.62	0.68	0.69	15.80	0.57	3.79	27	46
25 - 50 km	0.26	0.71	0.38	12.18	1.81	4.34	63	81
> 50 km	0.20	0.52	0.29	10.91	2.03	4.68	101	122
Urban classification								
Urban	0.51	0.65	0.61	16.23	-1.13	4.06	0.5	32
Suburban	0.56	0.68	0.65	13.62	1.38	3.69	23	39
Rural	0.25	0.52	0.34	5.99	3.99	4.94	205	216

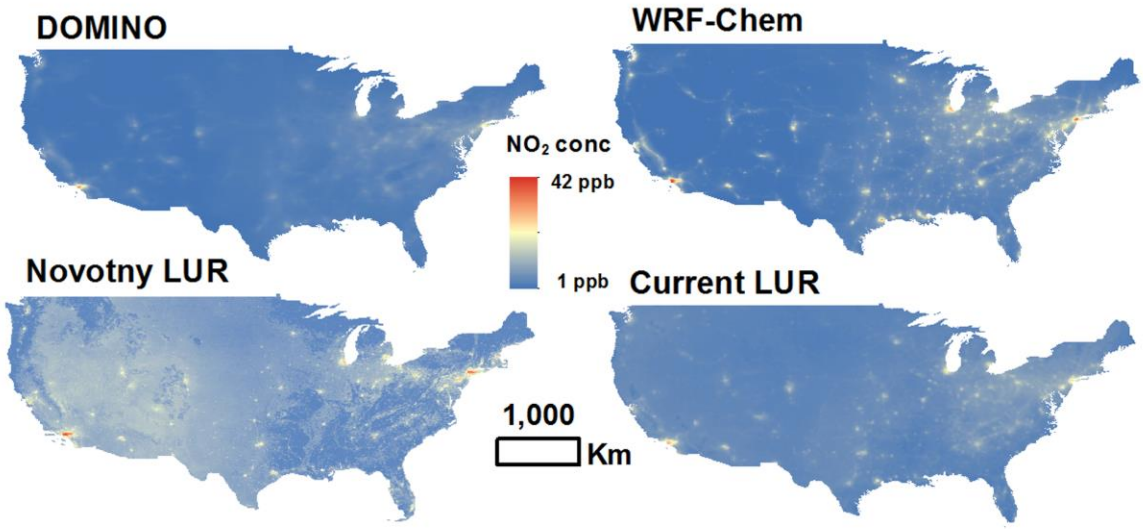

Figure 3.1. NO_2 surface estimates for the contiguous US. Panels show ground-level NO_2 concentrations for the continental U.S. from 0.1° DOMINO satellite-derived estimates (top left), 12 km WRF-Chem chemical transport model (top right), Novotny et al. LUR model (bottom left), and the final spatial-LUR model used here (bottom right).

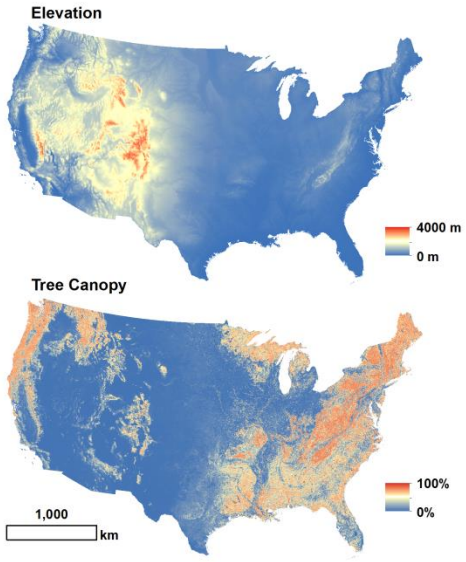

Figure 3.2. Elevation (top) and percent tree canopy (bottom) variables employed in the LUR model.

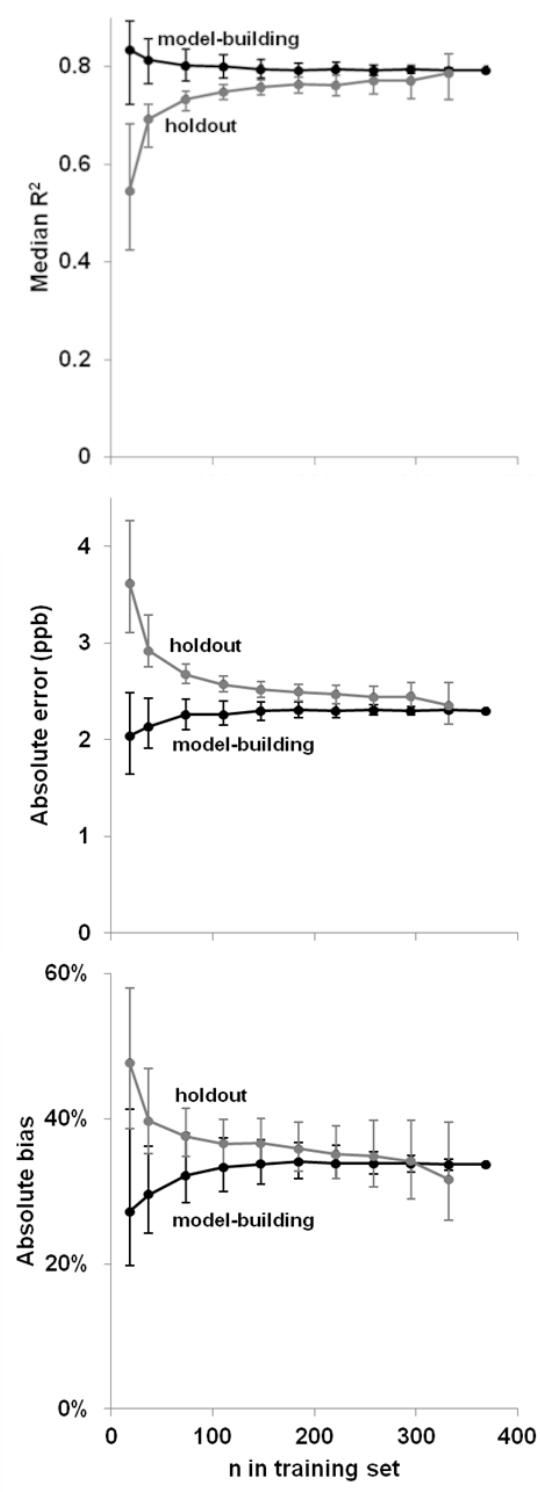

Figure 3.3. Median and inter-quartile range R^2 (top), absolute error (middle), and absolute bias (bottom) for Monte Carlo random sampling for n number of training monitors employed in model building out of 369 possible monitor locations. Model building (black) shows model evaluation against the monitors used in model building; holdout (grey) shows model evaluation against the monitors excluded from the training set in the model building stage.

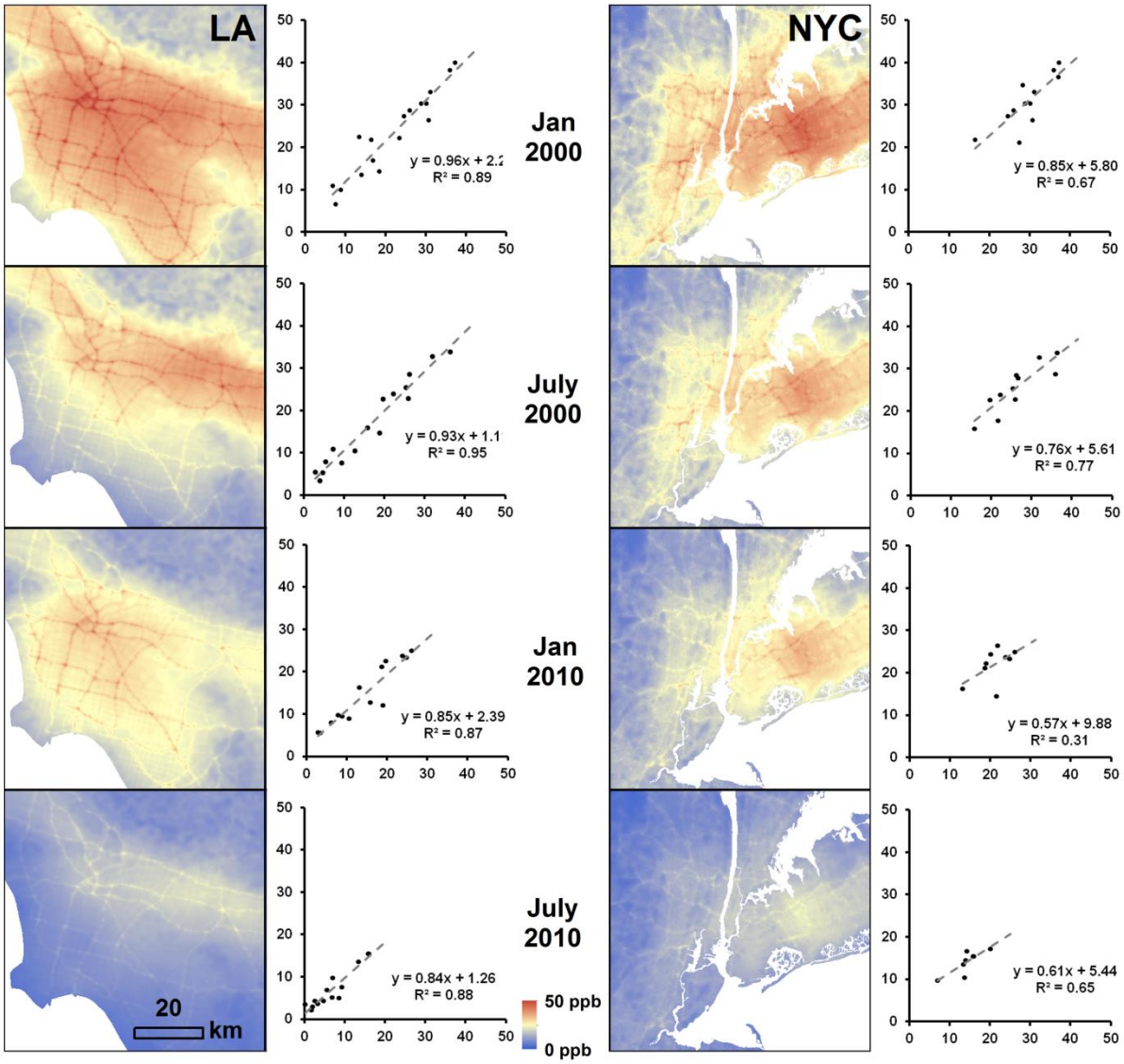

Figure 3.4. Modeled winter (January) and summer (July) ground-level monthly-mean NO_2 concentrations for Los Angeles (LA) and New York (NYC) employing a 100m grid for display purposes. Scatterplots show predicted (y-axis) vs. observed (x-axis) NO_2 concentrations for monitors within corresponding map panel.

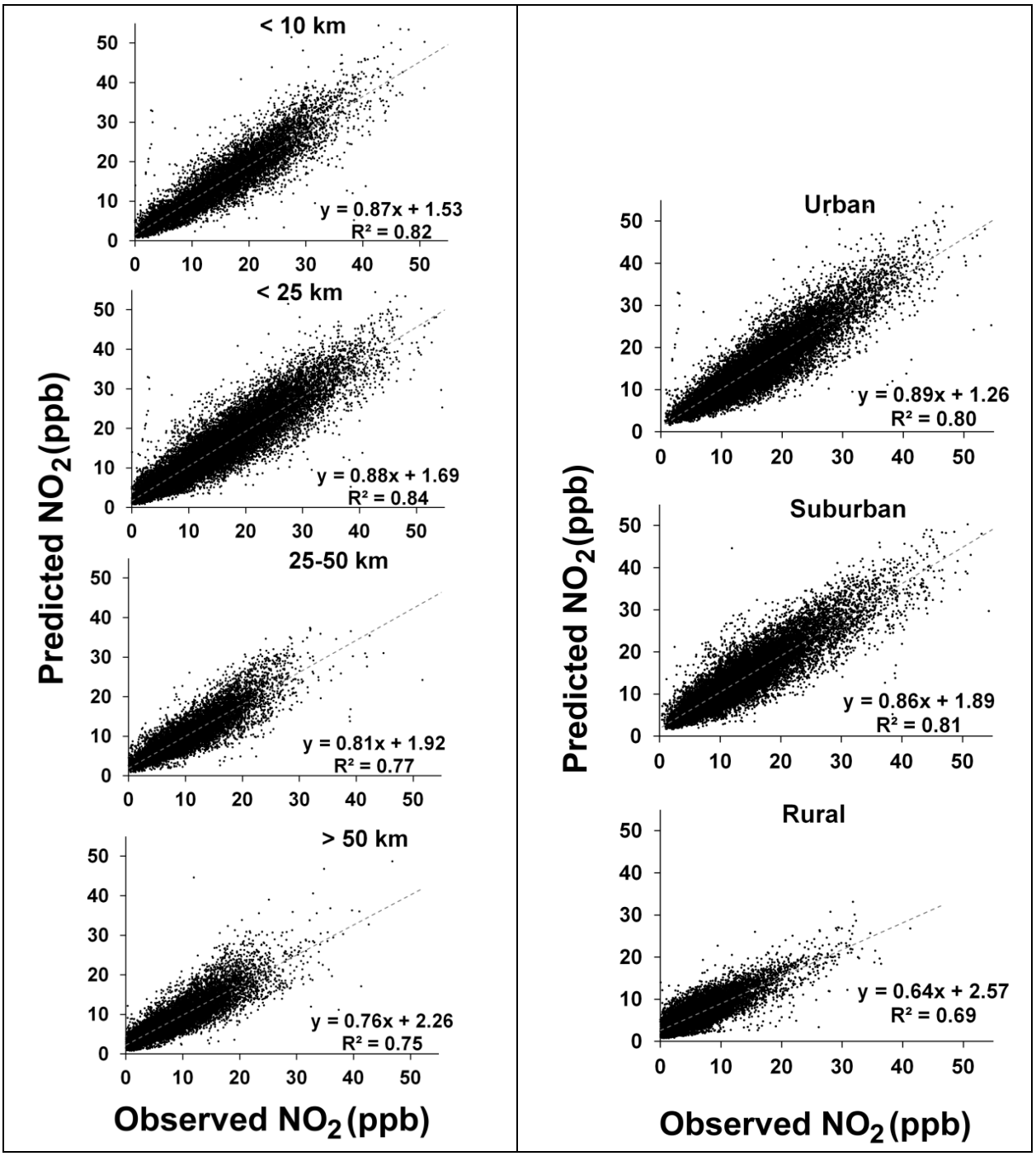

Figure 3.5. Predicted versus observed monthly mean monitor NO_2 values by distance to the nearest monitor (left) and by level of urbanization (right). Not shown are the 8 data points (0.02% of the data) with predicted or observed concentrations greater than 55 ppb.

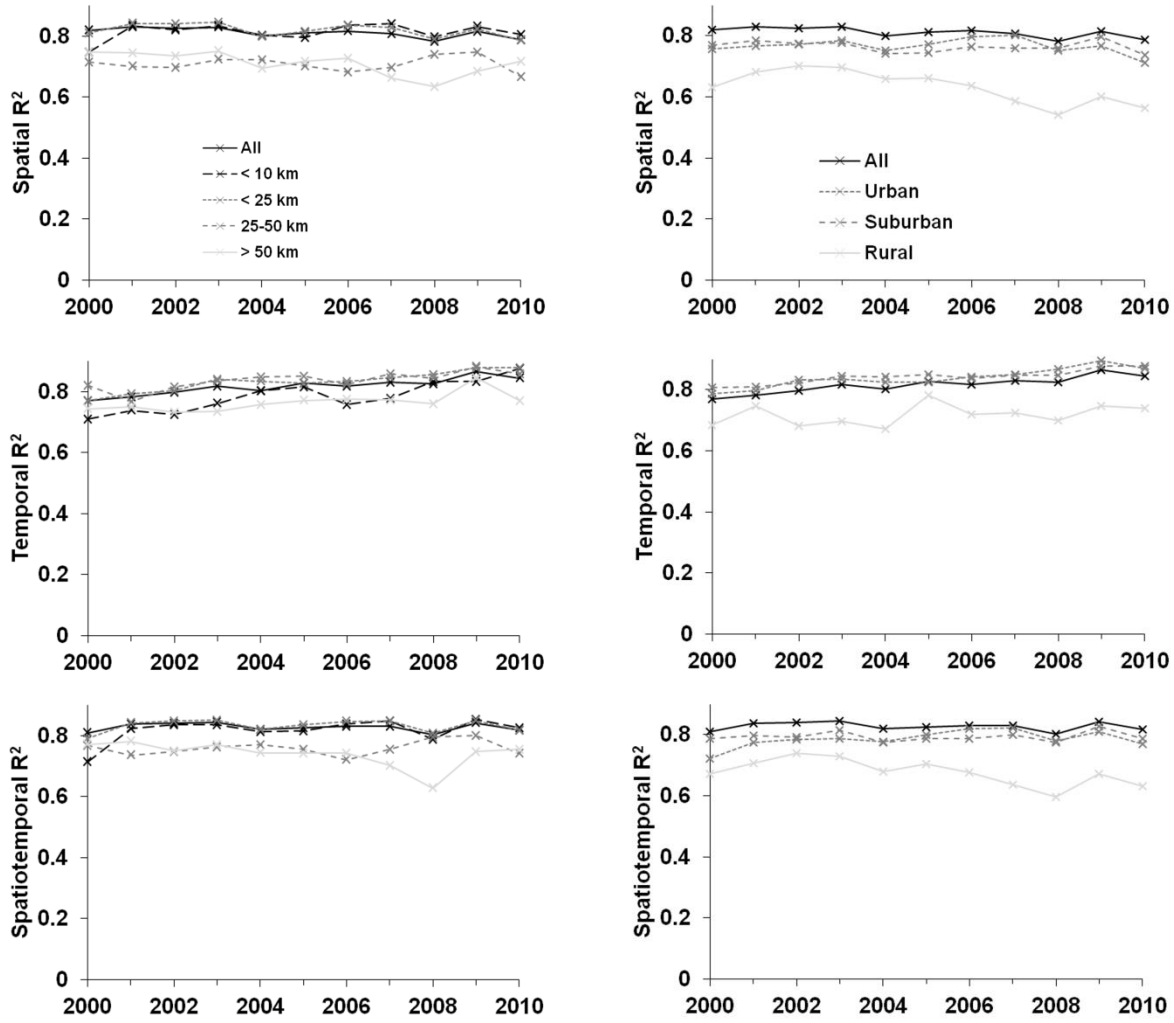

Figure 3.6. Spatial-, temporal-, and spatiotemporal-R^2 for each year using monthly-mean values for all monitors; by distance to the nearest monitor (left panels); and by level of urbanization (right panels). Spatial-R^2 reported is the median of monthly spatial-R^2, temporal-R^2 reported is the median of 12-month temporal-R^2 for monitors with 12 months of valid measurements.

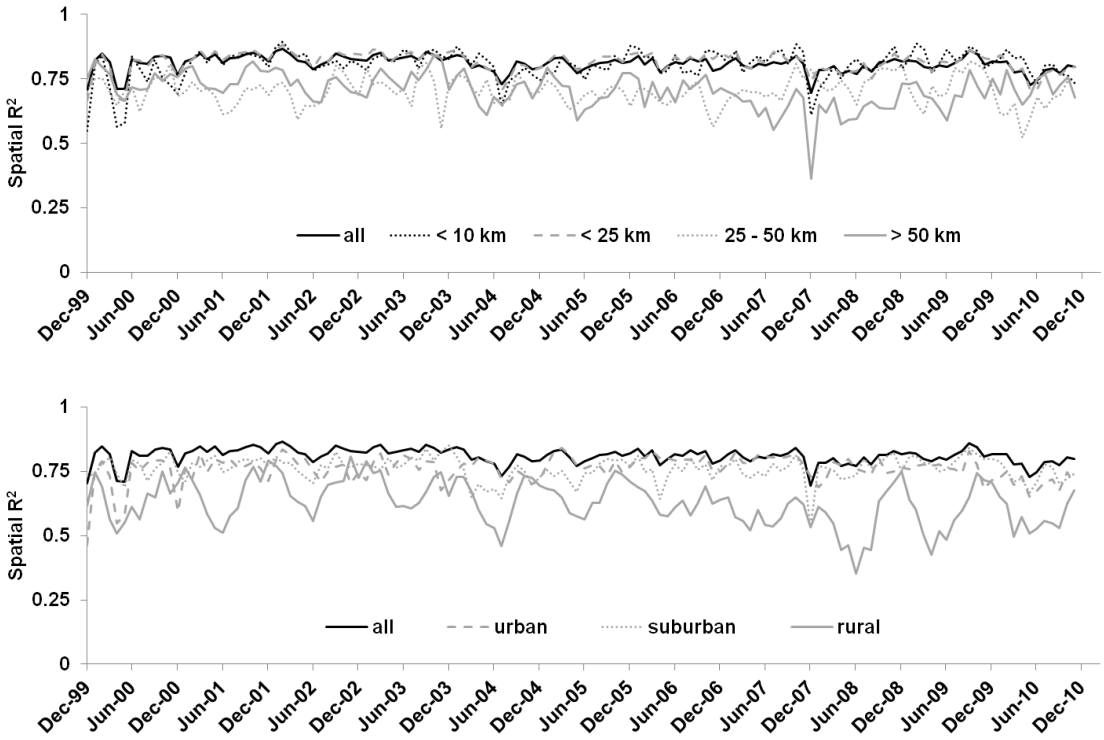

Figure 3.7. Spatial R^2 for each month by distance to the nearest monitor (top) and by level of urbanization (bottom). Solid black line shows spatial R^2 for all valid monitors for that month. Top plot: dotted, long-dash, short-dash, and grey lines show values for locations <10 km, < 25 km, locations between 25 - 50 km, and locations > 50 km from the nearest monitor. Bottom plot: long-dash, short-dash, and grey lines show urban, suburban, and rural monitor locations.

Chapter 4

NO_2 at public school locations in the contiguous US

4.1 Summary

Children are more vulnerable to air pollution than adults and have little agency over where they live and attend school. Therefore, schools may play an important role in children's air pollution exposure and disparities, yet (1) air quality at schools is not consistently tracked, and (2) regulations are few and limited to new schools. Here I employ satellite-based outdoor Nitrogen Dioxide (NO_2) estimates, administrative public-school data, and US Census data to characterize student's home and school location air quality and disparities by race/ethnicity (home and school) and income (school only, using lunch program eligibility as a proxy) in the contiguous US. On average, racial and ethnic minority students live and attend school in areas with higher NO_2 levels (population-weighted mean: 13.5 ppb and 13.4 ppb at home and school, respectively) than their non-Hispanic, white peers (8.7 and 9.8 ppb). Minority students are more likely than their white peers to live (5.5×) and attend school (8.0×) in areas above the World Health Organization's annual NO_2 guideline. Predominately minority schools (> 50% minority students) are 20× more likely than predominately white schools to be above the WHO guideline. In urban areas, on average, schools with more minority students and/or more impoverished students experience elevated NO_2 levels relative to less diverse and more well-off schools, yet the relative effect of income versus race and ethnicity is indistinguishable, except for large urban areas, where disparities by race persist when controlling for school-level income. This work

shows that disparities follow students from home to school and that school exposures may widen disparities.

4.2 Introduction

Children spend a large portion of their time in and around schools; consequently, exposure to air pollution at school locations may play an important role in children's total exposure. Moreover, children may be more susceptible to health effects from air pollution, owing to their developing biological systems, higher intake of air relative to body mass when compared to adults, and large amount of time spent outdoors.[43–45] Children's exposure to air pollution has been associated with the onset and exacerbation of asthma[139–142], decreased cognitive and neurological function[143–146], and higher rates of school absenteeism and poorer performance on standardized tests[147]. A study of U.S. students found that 12.5% (6.4 million students) attended school within 250m of a major roadway during the 2005-2006 school year.[148] Schools are a form of lasting infrastructure: a 2012-2013 survey found that the average age of public school buildings in the U.S. was 44 years.[149] The U.S. EPA provides voluntary guidance on school siting[150] and best practices for reducing near-roadway exposure in and near schools,[151] yet only 10 U.S. states have laws that prohibit siting new schools near environmental hazards and no legislation exists that provides a framework for assessing or mitigating hazards at existing schools[152]. In this context, quantifying outdoor air pollution levels at schools throughout the U.S. could provide insights into an important risk factor for school aged children and rationale for future legislation mitigating this risk.

Environmental injustice in residential air pollution exposure has been well documented in North America[3,153–155]. Despite decreasing concentrations in recent years, disparities have persisted[40,156,157]. Air pollution at school locations may play an important role in exposure disparities for children. Studies in a small number of U.S. cities have found that students of color are more likely to attend schools with elevated levels of hazardous air pollutants, near major roadways, and with elevated traffic-related air pollution (TRAP).[152,158–163] Studies of school location air pollution disparities over broader geographic regions have been limited. Mohai et al., (2011) found that black and Latino students were more likely to attend schools with the highest levels of industrial air pollution in Michigan, and that these schools had the highest levels of absenteeism and highest proportion of students failing to meet state testing standards, even when controlling for level of urbanization and other confounders.[147]

To my knowledge, only three studies in total, in the white and grey literature, have attempted to assess air pollution hazards at school locations for the contiguous U.S. (1) A 2008 USA Today report employed a 1km model, based on emissions from the Toxic Release Inventory, to estimate industrial air pollution outside public and private school locations during the 2005-2006 school year.[164] They found hundreds of schools across the U.S. with potentially toxic air, and provided a database that allowed readers to lookup toxicity estimates by school or see relative rankings nationally and by state. While this report provided information on an important source of air pollution (toxic industrial emissions), it ignored important emission sources (e.g., area and mobile sources) and did not explore exposure disparities.[164] (2) Kingsley et al. (2014) explored the proximity of public and private schools to major roadways during the 2005-2006 school year and found that black students were 7% more likely to attend a school

within 250 m of a major roadway than white non-Hispanic students, and predominately black schools (those with a majority of black students) were 18% more likely to be within 250 m of a major roadway than majority white schools.[148] Public schools with a majority of students eligible for free or reduced price lunch (heretofore referred to as impoverished students and impoverished schools) were 18% more likely to be within 250 m of a roadway than non-impoverished schools, and impoverished students were 17% more likely attend school within 250 m of a roadway than non-impoverished students.[148] This study highlights racial and economic disparities in exposure to a proxy for TRAP, however, it does not account for actual exposure to TRAP, nor exposure to air pollution sources other than major roadways. (3) Grineski and Collins (2018) investigated exposure to neurotoxicants, based on the US EPA's National Air Toxic Assessment (NATA), for all public schools in the contiguous US in 2011.[46] They found that students attending "high risk" schools (those in the top 10% for a summed metric of neurotoxicants) were more likely to be Hispanic, black, Asian/Pacific Islander, and impoverished.[46] This is an important study that highlights both racial/ethnic and economic disparities in children's exposure to key air pollutants related to their brain functioning at school. One limitation of this study is its reliance on NATA modeled concentrations, which have been shown to suffer from underestimation, particularly at high concentrations, owing in part to missing emission sources and uncertainty in the spatial allocation of emissions.[165,166] None of the three studies considered criteria air pollutants. Moreover, all three of these studies focus only on children's exposure to ambient air pollution at school. An important policy consideration is whether exposures and exposure disparities differ at home, versus at school.

Here I aim to assess exposure and exposure disparities to nitrogen dioxide (NO_2), a key marker of TRAP, for school-aged children at home and at public school locations in the contiguous U.S. using satellite-based estimates of NO_2 and administrative datasets of public school locations and student residential locations. This is, to my knowledge, the first study to characterize student exposure to a criteria pollutant for the contiguous U.S., and the first to compare home and school location exposures nationally to understand the impact school locations have on childhood NO_2 disparities.

4.3 Data and Methodology

School and Home Location Data Sets

School location data are from the National Center for Education Statistics School Universe Survey for school year 2005-2006, a comprehensive database of public elementary and secondary schools in the United States.[167] This database provides the name, location (both address and geographic coordinates), grade levels offered, enrollment, enrollment by race/ethnicity (i.e., American Indian/Alaska Native; Asian/Pacific Islander; Hispanic; black, non-Hispanic; white, non-Hispanic), number of students eligible for free or reduced price lunch (at or below 185% of the federal poverty level), and number of full-time-equivalent classroom teachers for ~100,000 public schools.[168] I exclude inactive schools (inactive schools remain in the database for one year), schools reporting zero student enrollment or zero full-time-equivalent classroom teachers, and schools with missing location information. The database contains online schools but does not have a formal classification of such schools; I attempt to exclude these schools using keyword searches of the school names (keywords: virtual, electronic, online, e-school).

I use demographic information for students by their residential block group location from the US Census 5-year American Community Survey for years 2005-2009. The data provide counts of the population 3 years old and over by enrollment status (nursery school, preschool, kindergarten; grades 1-8; grades 9-12; college or graduate school; not enrolled), by race (white alone; black or African American alone; American Indian and Alaska Native alone; Asian alone; Native Hawaiian and other Pacific Islander alone; some other race alone; and two or more races), and by ethnicity (white alone, not Hispanic or Latino; Hispanic or Latino).

I include only elementary and secondary students (enrolled in grades 1-12) and consider two race/ethnicity categories (non-Hispanic, white students; racial/ethnic minority students, considering all categories excluding non-Hispanic whites). More detailed racial/ethnic categories are not considered owing to discrepancies in categorization between the two data sets.

Level of Urbanization Data

I use year-2000 Decennial U.S. Census boundaries and population counts for urbanized areas (UAs; cities with 50,000 or more people) and urban clusters (UCs; cities with 2,500 to 49,999 people) to classify schools and residential block groups as urban or rural, and to assign the UA or UC name and population to schools within their corresponding boundaries. I also further classify UAs by size, determined by UA population tertile: large (9 cities; 3.9 million to 18 million residents; 10.1 million students), medium (41 cities; 720,000 to 3.8 million residents; 10.3 million students), and small (397 cities; 50,000 to 700,000 residents; 10.7 million students). To avoid potential issues with a small number of locations near urban/rural borders, a 1km buffer

is applied to all UAs and UCs. Locations that fall within this buffer are considered urban and assigned UA or UC characteristics.

Air Pollution Prediction Data

I estimate annual average, year-2006, outdoor NO_2 mixing ratios using a previously published satellite-based land use regression model for the contiguous U.S.[48] Model predictions are calculated (1) for the school location coordinates provided in the school database, and (2) as the population-weighted average of block centroid predictions within each block group for enrolled students home locations. I select NO_2 in part because of epidemiological evidence of health effects: A literature review of TRAP and childhood asthma found that NO_2 showed the most significant and consistent association with the onset and prevalence of childhood asthma.[142] NO_2 has also been found to be a marker for a toxic mix of pollutants associated with automobile and other combustion-related emissions.[9] The NO_2 model I employ has mean absolute error = 2.55 ppb (normalized to the mean: 21%) and R2 = 0.74 in 10-fold holdout cross-validation.

Statistical Analyses

For all public schools in the contiguous U.S., I assess student population-weighted distributions of NO_2 levels at school by the following attributes: school type (elementary, secondary), level of urbanization (rural, UCs, small UAs, medium UAs, large UAs), race/ethnicity (white, non-Hispanic versus racial/ethnic minority students), and by income (impoverished versus non-impoverished students). As a comparison, for all block groups in the contiguous U.S., I also assess student population-weighted distributions of NO_2 levels at home by level of urbanization and by race/ethnicity.

I estimate prevalence ratios to assess the likelihood of minority and impoverished students experiencing elevated outdoor NO_2 levels relative to their non-Hispanic, white and non-impoverished peers. I also estimate prevalence ratios with schools as the unit of analysis, to compare schools serving predominately minority or impoverished students (>50% of enrolled students) relative to schools serving predominately non-Hispanic, white and non-impoverished students. Here, I use the World Health Organization annual average outdoor NO_2 guideline of 40 $\mu g/m^3$ (~21.3 ppb) as the cutoff for elevated levels.[169] I do not use the U.S. EPA annual average standard of 53 ppb for several reasons: (1) no locations has modeled levels above this standard, (2) no area in the U.S. has been in nonattainment with this standard since 1998,[170] and (3) the annual mean standard has not changed since it was originally set in 1971.[171]

I also assess student population-weighted NO_2 levels by school-level percent of racial/ethnic minority students and percent of impoverished students. I perform two school-based analyses. (1) line plots with student population-weighted NO_2 levels for student percentile bins (bin size: 5%) of the school-level percentage of minority students and impoverished students (i.e., each bin corresponds to 5% of the students, centered on the median student percentile); and (2) a sensitivity analysis based on line plots with student population-weighted NO_2 levels for ten equally-spaced bins of the percentage of minority students and impoverished students (i.e., ten 10% bins corresponding to 0-100%). In multiple cases, I account for differences between urban and rural locations by summarizing each level of urbanization separately. To explore differences in the effect of race/ethnicity and income, when controlling for school-level race/ethnicity (i.e., binning by percent minority students), I consider the population-weighted NO_2 levels for

impoverished and non-impoverished students separately within each bin. Similarly, when controlling for school level income (i.e., binning by percent impoverished students), I consider the population-weighted levels for minority and non-Hispanic white students separately.

4.4 Results and Discussion

Within the contiguous U.S., 48 million students attending 89,420 public schools remained in my analysis after quality control screening. More enrolled students, 52 million, was reported in the Census ACS database of residential block group locations (n=207,225), owing largely to the inclusion of private school students, as well as differences in data collection and years covered. The student population-weighted average NO_2 level for all schools is 11.36 ppb. Owing to similar NO_2 levels for elementary and secondary schools nationally (11.41 vs 11.30 ppb, respectively) and by level of urbanization (see Figure 4.1), the remaining analysis includes both elementary and secondary schools together.

Figure 4.1 shows the distribution of annual outdoor NO2 levels at home and school locations for minorities and white students, as well as at school locations for impoverished and non-impoverished students. Racial/ethnic minority students, on average, attend schools with higher NO_2 levels (population-weighted mean: 13.4 ppb) than non-Hispanic white students (9.8 ppb). A similar disparity is observed at the home locations. (minority students: 13.5 ppb; white students: 8.7 ppb). Impoverished students, on average, attend schools with higher NO_2 (12.2 ppb) than non-impoverished students (10.8 ppb). Note that the average disparity by income (1.4 ppb) is several-fold smaller than the disparity by race/ethnicity (3.6 ppb).

Disparities exist too for the upper end of the distribution – i.e., when comparing the most-polluted school locations. For example, Figure 4.2 also shows that minority students and impoverished students are more likely to attend schools and to live in areas above the WHO guideline than their white and non-impoverished peers. Violin plots akin to Figure 4.2 but subdivided by level of urbanization (Figure 4.3) illustrate that (1) disparities are generally limited to urban locations, and (2) the distribution of NO_2 levels for minority students in large UAs is bimodal, with 38% above the WHO guideline. Indeed, minority students are 5.5× more likely than their white peers to live in neighborhoods above the WHO guideline, yet they are 8.0× more likely to attend school at locations above the guidelines, suggesting school locations could exacerbate disparities (see Tables 4.1 and 4.2). When considering only schools in urban locations, the gap between white students and racial/ethnic minorities, and between home and school locations, remains: at home minorities are 4.4× more likely than whites to have NO2 levels above the guideline; at school school, this same gap 7.0×. Predominately minority schools (> 50% minority students) are 20× more likely than predominately white schools to be in locations above the WHO guideline. This disparity persists when restricting to urban schools (15×), with higher prevalence ratios in medium UAs (31×) than large UAs (6.1×).

Impoverished students are 2.6× more likely than their less impoverished peers to attend school in a location above the WHO guideline. Unlike race/ethnicity, the likelihood of higher NO_2 levels for impoverished students is relatively unchanged when restricted to urban (2.6×), large UAs (2.3×) and medium UAs (3.0×). Predominately impoverished schools, those with > 50% impoverished students, are 4.0× more likely than predominately non-impoverished schools to be in locations above the WHO guideline; that result is relatively unchanged for urban (3.8×),

large UAs (3.1×), and medium UAs (5.1×). The likelihood of disparate elevated NO2 levels is higher for minority students and schools than for impoverished students and schools, suggesting race/ethnicity may play a larger role than income in elevated school location pollution levels and disparities.

Figure 4.4 shows student population-weighted average NO_2 levels as a function of the school-level proportion of racial/ethnic minority (left) and impoverished (right) students, by level of urbanization. Lines are based on 5 percentile bins (i.e., each bin contains 5 percent of the students) centered on the median school-level proportion of minority or impoverished students. Three aspects stand out: (1) For UAs (but not UC or rural areas), the lines' slopes are positive in both plots, NO_2 levels are comparatively higher for schools with a greater proportion of impoverished students and, independently, for schools with a greater proportion of minority students. (2) Consider Figure 4.4 as consisting of ten pairs of lines (i.e., five pairs per panel); for each pair, the two lines occupy an overlapping but distinct range of x-axis values (i.e., in each pair, one line is to the left or right of the other line). This emphasizes the intertwined nature of race and income, and more importantly that students of different demographic groups are attending fundamentally different schools: impoverished students generally attend schools with a larger percentage of racial/ethnic minorities (Figure 4.4 left plot) and minorities generally attend schools with a larger percentage of impoverished students (Figure 4.4 right plot), owing in part to a large portion of impoverished minority students, especially for urban areas. Minority students generally attend impoverished schools. White students almost exclusively attend non-impoverished schools (Figure 4.4 right). In urbanized areas non-impoverished students generally attend predominately white schools, while impoverished students generally attend predominately

minority schools (Figure 4.4 left). In UCs and rural areas, all students, regardless of income, generally attend predominately white schools. (3) Further considering each pair of lines, for many cases, the two lines touch (i.e., for the x-axis values that overlap between the two lines, the y-axis values are similar). This suggests that in most cases, race and income are intertwined; when controlling for school-level income, differences in NO_2 level by race are generally negligible, and when controlling for school-level race/ethnicity, differences by poverty are generally negligible. One exception is large urban areas: here, the two lines are overlapping in the left plot but in the right plot, one line (minorities) is higher than the other (whites). That suggests that for large UAs, race/ethnicity is a separate and distinct predictor of at-school NO_2 levels: for a given level of impoverishment at a school, students who are racial-ethnic minorities on average attend schools with higher NO_2 levels than do students who are white. As a sensitivity analysis, I plotted the same data as in Figure 4.4 but using 10 equally-spaced bins; the results reveal similar patterns (see Figure 4.5).

An important goal of this work was to explore the intersection of race/ethnicity and income. Recent work on outdoor air pollution disparities have found that disparities by race/ethnicity are typically larger than other factors such as income and education. Here I find evidence that this phenomenon exists for school-location exposures, but only in large UAs. This work advances understanding of school-aged children's total exposure by specifically comparing air pollution at school and home locations. I find that, on average, NO_2 levels and disparities between minority and white students are similar in school and home locations, however, minority students are more likely than their white peers to live in neighborhoods with NO_2 levels above the WHO standard and much more likely to attend schools with NO_2 levels above the

WHO standard. This finding, that public schools could possibly exacerbate disparities for minority students, has important implications for strategies to address these disparities among school-aged children.

Table 4.1. Prevalence ratios for likelihood of being above WHO guideline*

	All locations	UAs & UCs	Large UAs	Medium UAs
Minority students – home	5.22	4.28	2.80	2.46
Minority students – school	8.01	6.96	3.50	7.11
Impoverished students – school	2.59	2.60	2.26	2.97
Minority schools (> 50% minority students)	20.1	15.1	6.13	30.5
Impoverished schools (> 50% impoverished students)	3.97	3.83	3.09	5.08

*All school locations in rural areas, UCs and small UAs were found to be below the WHO guideline. Home locations: in rural areas were found to be below the WHO guideline, however, in small UAs (17.6) and UCs (12.2) minority students are much more likely than their non-Hispanic white peers to live in locations above the WHO guideline.

Table 4.2. Percentage of students and schools above the WHO guideline*

	All locations	UAs & UCs	Large UAs	Medium UAs
Minority students – home	16.2	17.8	40.5	6.66
White students - home	3.10	4.15	14.4	2.71
Minority students – school	14.3	15.1	38.2	2.98
White students – school	1.79	2.18	10.9	0.419
Impoverished students – school	11.2	12.8	40.5	2.84
Non-impoverished students – school	4.30	4.91	17.9	0.954
Majority minority schools (> 50% minority students)	13.8	15.0	40.2	3.28
Majority white schools (> 50% white students)	0.686	0.994	6.56	0.108
Impoverished schools (> 50% impoverished students)	9.27	11.8	42.8	3.15
Non-impoverished schools (> 50% non-impoverished students)	2.33	3.08	13.9	0.621

*All school locations in rural areas, UCs and small UAs were below the WHO guideline. All home locations in rural areas were below the WHO guideline, however, in small UAs 0.192% of minority students and 0.0109% of non-Hispanic white students live in locations above the guideline. Similarly, in UCs 0.0411% of minority students and 0.00337% of non-Hispanic white students live in locations above the guideline.

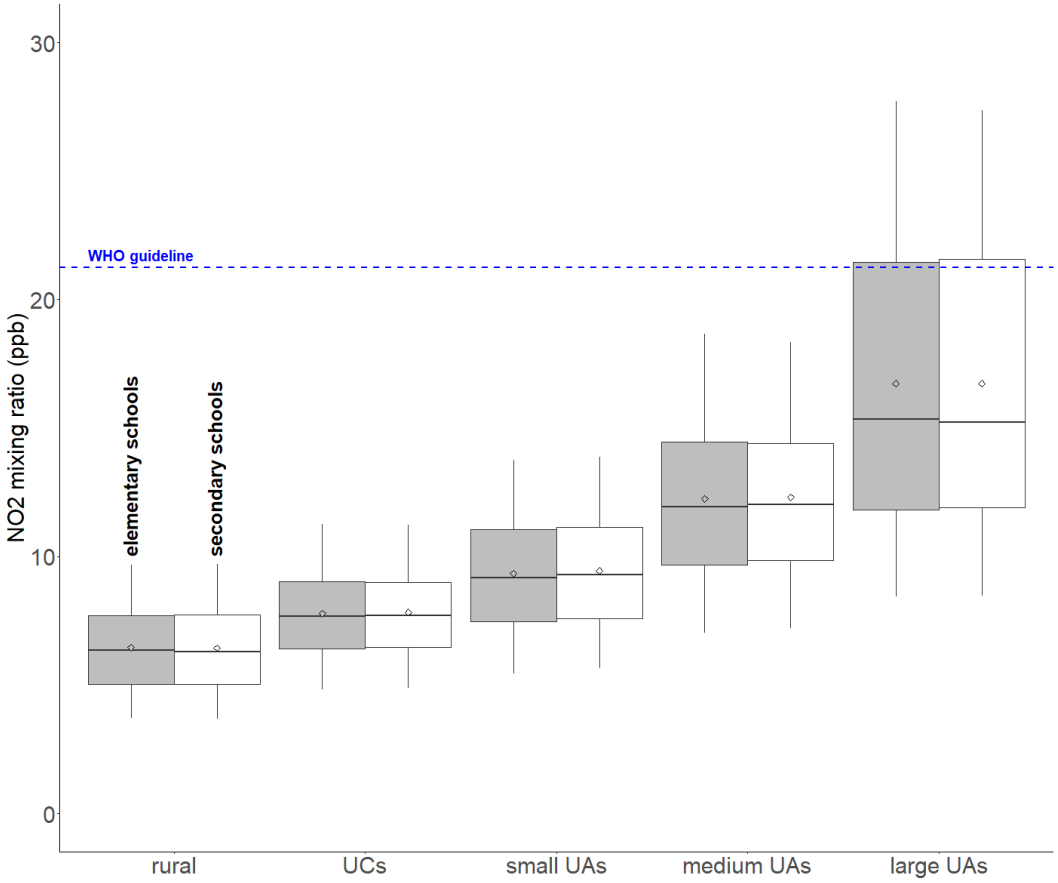

Figure 4.1. Summary of school-location NO_2 mixing ratio by school type and level of urbanization. Horizontal bars show the median value, boxes show the interquartile range, vertical lines show the 5th and 95th percentile, diamond shape shows mean values. The dashed blue horizontal line shows the World Health Organization (WHO) annual NO_2 guideline ~21 ppb) for reference.

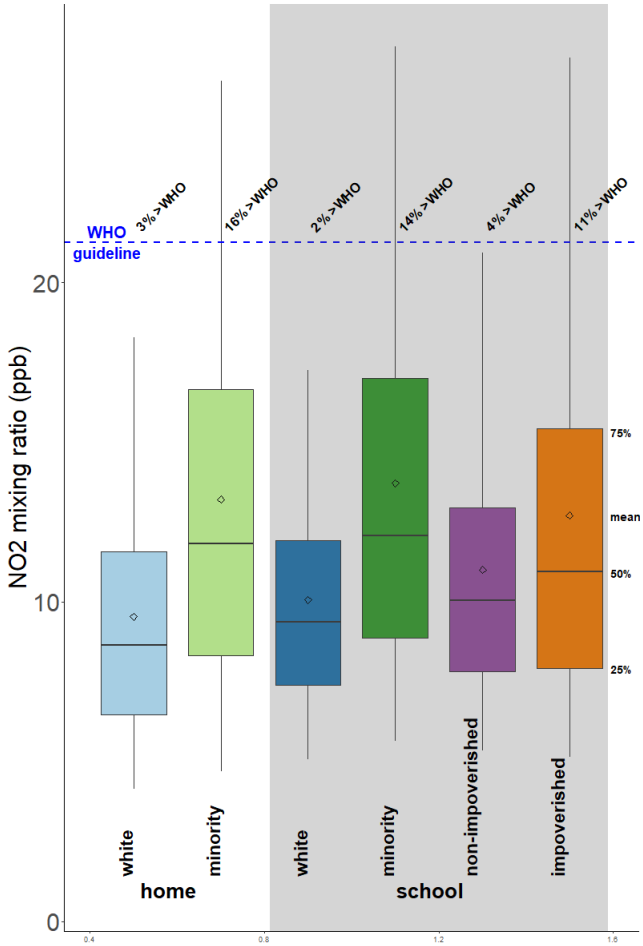

Figure 4.2. Summary of home location (left) and school location (right; shaded gray) NO_2 mixing ratio for non-Hispanic white students (blue), minority students (green), non-impoverished (purple) and impoverished (orange) students. Horizontal bars show the median value, boxes show the interquartile range, vertical lines show the 5th and 95th percentile, diamond shape shows mean values. The dashed blue horizontal line shows the World Health Organization (WHO) annual NO_2 guideline ~21 ppb) for reference. Numeric values listed near the WHO annual guideline indicate the percentage of students attending schools with NO2 levels above the guideline.

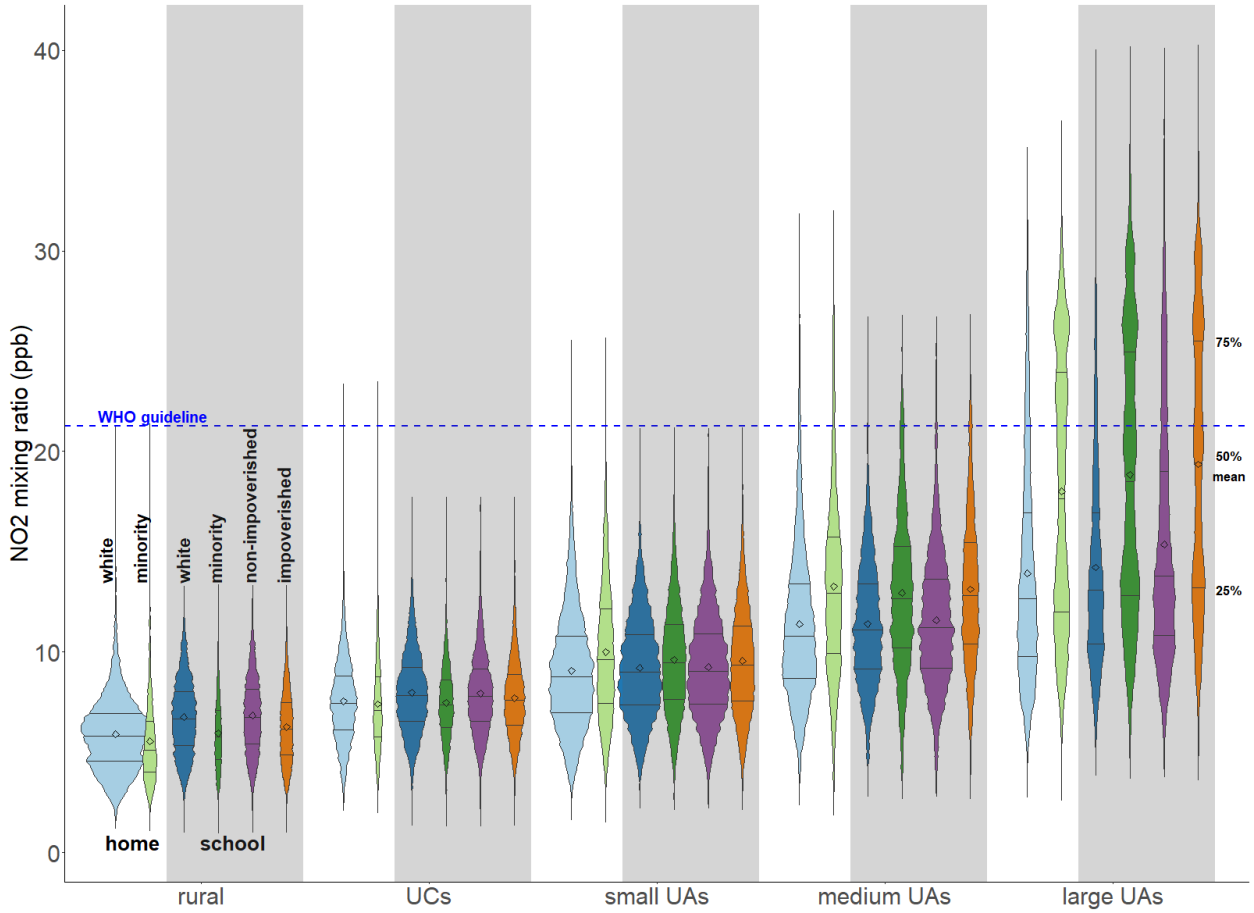

Figure 4.3. Summary of NO_2 mixing ratio at home location for non-Hispanic white students (light blue) and minority students (light green) and at school location for non-Hispanic white students (dark blue), minority students (dark blue), non-impoverished (purple), and impoverished students (orange) by level of urbanization (rural, urban clusters, small UAs, medium UAs, and large UAs). For clarity, school locations are shaded in grey. Violin plots show distribution of student NO_2 levels along the y-axis, horizontal bars show the median (50th percentile) and interquartile range (25^{th} and 75^{th} percentile), circle shows mean values. The dashed blue horizontal line shows the WHO annual NO_2 guideline for reference. The width of each plot is proportional to the number of students.

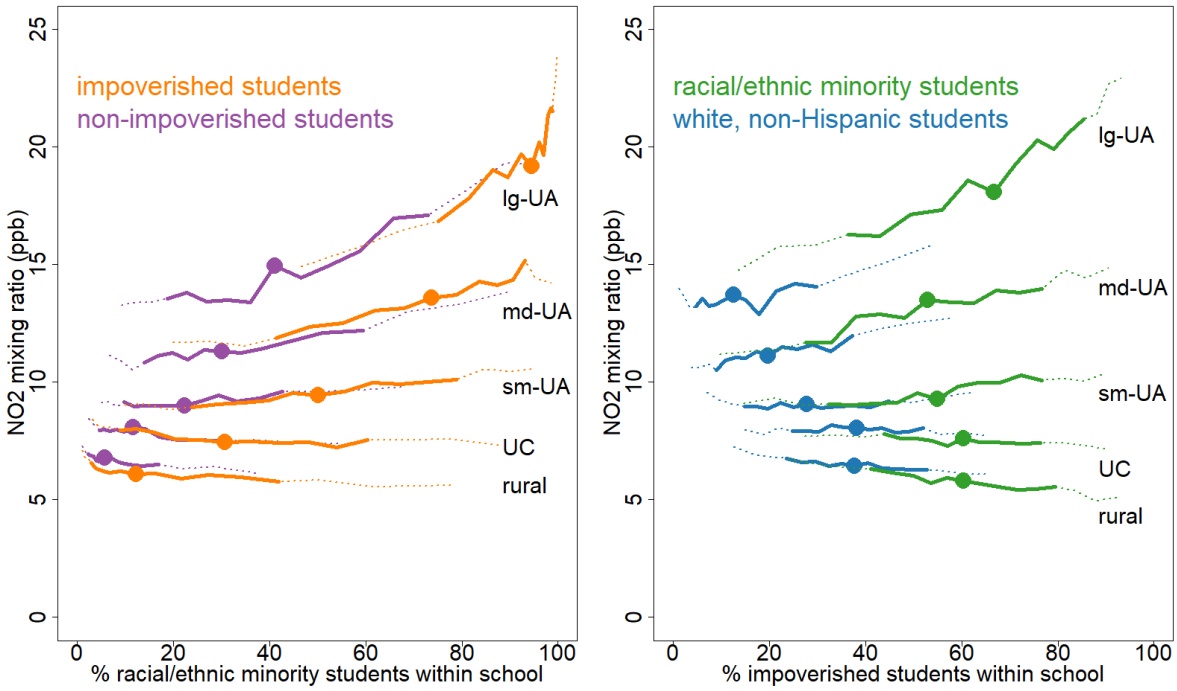

Figure 4.4. School location student population-weighted NO_2 mixing ratio by school proportion of minority students (left) and impoverished students (right) attending. Lines are comprised of points corresponding to the student population-weighted mean for students within a 5 percentile bin, centered on the 50th percentile of school-level proportion of minority students (left) or impoverished students (right) for the specified level of urbanization (large-UA, medium-UA, small-UA, UCs, and rural) and student sub-population (impoverished and non-impoverished students at left; minority and non-Hispanic, white students at right). Circles indicate the student population-weighted mean for the 5% of students centered along the 50th percentile (i.e., 47.5-52.5 percentile) for the school-level demographics. The bold lines indicate student population-weighted means for the 5 percentile bins approximating the interquartile range (22.5-77.5 percentile). The thin dashed lines indicate student population-weighted means for the 5 percentile bins approximating the 10th and 90th percentile (7.5-92.5 percentile).

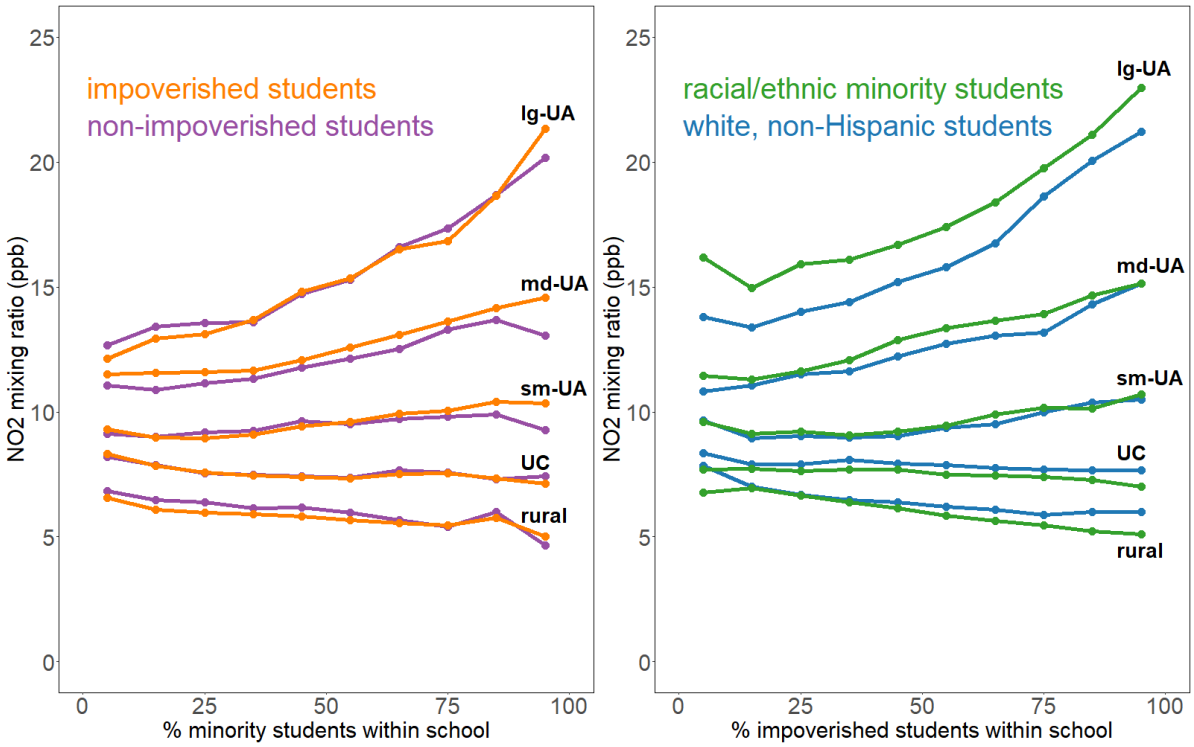

Figure 4.5. School location student population-weighted NO_2 mixing ratio by school proportion of minority students (left) and impoverished students (right) attending. Each line is comprised of points corresponding to the student population-weighted mean for students within 10 equally-spaced bins of school-level proportion (i.e., 10% incremental bins) of minority students (left) or impoverished students (right) for the specified level of urbanization (large-UA, medium-UA, small-UA, urban clusters, and rural) and student sub-population (impoverished and non-impoverished students at left; minority and white students at right). Circles indicate the student population-weighted mean for the bin, x-axis value is the midpoint of the bin.

Chapter 5

Conclusions

This dissertation demonstrates the utility of satellite-based remote sensing of air pollution, capable of exploring global aspects of urban air pollution, and when combined with additional data in an empirical model at the neighborhood level within the US. Satellite air pollution measurements allow for the exploration of previously unmonitored or insufficiently monitored locations with globally consistent methodology, enabling analyses over broad geographic areas and across administrative boundaries. I have shown that, globally, the urban form of a city may significantly impact its air quality, suggesting that strategic urban-planning could be part of comprehensive policies to improve urban air quality globally. Moreover, this work found that urban form may have a greater impact on urban air pollution in small cities, an important finding since most of the world's population lives in small cities and most future growth is projected to occur in small cities.[23] This work also shows that country-level economic conditions and environmental policy may impact air pollution – urban form relationships, highlighting a need for more multinational studies to explore these relationships further. A major limitation of this work is the spatial resolution of the satellite data employed here, which is capable of city-wide averages but not spatially precise enough to estimate local exposure. Therefore, I am unable to explore issues such as the potential emission-dilution tradeoff of compact development (i.e., people and emissions closer together) and within-urban disparities.

Empirical models incorporating satellite air pollution measurements have shown they can combine the broad geographic coverage of satellite measurements with much greater spatial

precision (1 km or less). In this dissertation, I extend the temporal coverage of a year-2006 annual average model of NO_2 for the contiguous US, resulting in 132 monthly mean predictions (2000-2010) with predictive power similar to the original model. To my knowledge, this is the first effort to evaluate an ex post facto temporal scaling of a national empirical air pollution prediction model to extend temporal coverage. While similar approaches have been successfully applied to prediction models at the urban scale[120–122], it was uncertain whether this methodology would provide robust results over a broad geographic region with a sparse monitoring network. Since publication, this ex post facto scaling approach has been cited and used by several epidemiological studies to extend temporal coverage of existing prediction surfaces.[172–177] I have also made monthly NO_2 estimates at the centroid locations for all ~8 million Census blocks in the contiguous US publicly and freely available online (see Appendix A). These estimates have since been used in several studies, including epidemiological studies on the health effects of air pollution[178–180] and green space[181,182], studies quantifying the disease burden of air pollution[42,183], and a national environmental justice analysis exploring changes in residential exposure disparities over time.[40]

Concurrent with this dissertation work, and informed by it, I have also collaborated on the development of national and continental scale satellite-based empirical air pollution prediction models throughout the world.[36,115,184–188] An important contribution of this work has been a better understanding of the role of satellite-based air pollution measurements as a geographic variable, particularly in models that account for spatial autocorrelation using universal kriging. Universal kriging combines an LUR-type mean model with a spatial smoothing component based on the covariance between monitoring locations, leveraging

correlation in the LUR residuals to improve predictions. The spatial smoothing from kriging can account for regional spatial patterns in concentrations, potentially providing similar information to prediction as satellite-based air pollution measurements. However, since kriging relies on nearby monitoring data, it likely provides less predictive performance in locations far from monitors. LUR models are often evaluated using 10-fold cross-validation: randomly dividing the observations into ten groups, and for each group, using the remaining groups to make an approximate out-of-sample prediction for that group. To assess performance at locations far from monitors, an alternative validation approach was developed: instead of randomly dividing the observations into groups, a spatially clustered grouping approach can assess model performance at locations far from monitors. [186] This work shows that satellite air pollution measurements and kriging are complementary, models with both satellite data and kriging performed best for both validation approaches, however, the value of satellite measurements in a model with kriging is masked when considering only conventional (rather than spatially-clustered) 10-fold cross validation.[186–188]

Satellite-based empirical prediction models allow for the exploration of local exposure disparities over broad geographic areas. In this dissertation I use the satellite-based NO_2 prediction model described in Chapter 2 to evaluate student air pollution levels at home and public school locations in the contiguous US. This work advances scientific understanding by providing the first quantification of school-location exposure to a criteria pollutant, NO_2, on a national scale. The results indicate that minority students and impoverished students experience, on average, higher levels of NO_2 than their white and non-impoverished peers. Disparities in student NO_2 levels are largely driven by disparities in the 50 largest US cities. Future work

exploring all or a subset of these cities could explore city-level or school-district level modifiable factors associated with student air pollution disparities. For example, whether cities or school districts with policies meant to desegregate schools (e.g., school busing, open enrollment) exhibit less disparities in NO_2 levels at schools than locations without these policies. This dissertation has also shown that for large urban areas, even when controlling for school level income, school NO_2 levels are higher for students who are racial-ethnic minorities than for their white peers. This phenomena, that race/ethnicity may play a larger role than income in exposure disparities, is consistent with disparities at residential locations, however, for residential locations it is exhibited across all levels of urbanization.[40,153] Future studies could explore the intersection of income and race/ethnicity in more detail by looking at a smaller subset of schools and considering additional school-level indicators of income and socioeconomic status. A key finding from this work is that, when considering the highest NO_2 levels, public schools exacerbate exposure disparities for racial-ethnic minority students. Since children have little agency over where they attend school, this finding has important implications for strategies to address exposure disparities for children. Strategies to improve or mitigate NO_2 levels at the most polluted school locations could have a profound effect on childhood exposure disparities. Moreover, nearly one third of all public schools need updates to their heating and ventilation systems, yet most states do not conduct regular assessments and often leave this to local school districts.[189] Policies that require regular assessments of school building conditions and nearby air pollution sources to identify problem areas and funding to address these issues could help to reduce disparities. The results from this work will be relevant to policy makers, non-profit organizations working on myriad issues (e.g., environmental justice, children's health, education), school districts, and education boards hoping to better understand and reduce air

pollution disparities among students. A limitation of this work was that it was for a single school year; future work could explore how air quality at public school locations has changed over time and whether new schools are sited in more or less polluted areas than nearby older schools. Another area of possible future research would be to explore the effect of state, city, and school district level school segregation on the disparities seen here. This knowledge would help to inform policy interventions for addressing school air quality disparities.

Current racial segregation patterns are linked to many factors, including the historical policy of redlining, a racist mortgage appraisal policy from the 1930s whereby the federal government (via the Home Owners' Loan Corporation) graded residential neighborhoods by their investment risk in a color-coded manner, denoting majority non-white neighborhoods as risky investments.[190] The practice started with the passing of the New Deal's Home Owners' Loan Act in 1933 to provide government subsidized mortgages for homeowners in default or foreclosure, however, the investment risk maps created from this process affected decades of federal, state, and local housing decisions.[190] Researchers have digitized these historical mortgage appraisal maps,[191] paving the way for studies exploring the impact of these redlined neighborhoods on myriad of factors, including exposure to extreme heat[192] and access to green space[193]. Nardone et al. (2020) find that for eight Californian cities, redlined neighborhoods have higher levels of air pollution and higher rates of emergency department visits due to asthma.[194] Tessum et al. (2021) use a reduced form model based on a chemical transport model to show that, for areas covered by the HOLC maps, redlined neighborhoods in the contiguous US experience elevated air pollution levels.[195] This dissertation suggests that satellite-based air pollution estimates would be ideal for future empirical explorations of the impact of redlined

neighborhoods on air pollution exposures at residential and school locations, as well as how exposures are changing over time in these neighborhoods relative to other locations.

The next generation of satellites will provide even greater opportunities for exploring air pollution globally. The TROPOMI sensor, onboard the Sentinel 5 Precursor satellite, launched in 2018 and provides daily global coverage with nadir spatial resolution less than 10 km.[196] Measurements from this instrument have been shown to capture disparities in NO_2 levels within the greater Houston area by exploiting overlapping measurements and temporal oversampling to create ~1 km maps of NO_2.[197] A constellation of three geostationary air quality sensors will be launched in the early 2020s providing daytime hourly measurements over North America, Europe, and Asia with spatial resolution less than 10 km.[198] However, it is worth noting that Africa and South America will not be covered by this constellation of sensors, mirroring current disparities in ground-based monitoring networks.[6] Nevertheless, the improved spatial resolution of TROPOMI and the improved spatial and temporal resolution of the geostationary sensors will allow for better characterization of local emission sources and improve satellite-based empirical modeling. In the future, satellite-based air pollution measurements could be employed to continuously monitor and track air quality (e.g., at schools, by neighborhood) and provide information on potential hotspots and problem areas to the public, regulatory bodies, and policy makers.

References

1. Cohen, A. J. *et al.* Estimates and 25-year trends of the global burden of disease attributable to ambient air pollution: an analysis of data from the Global Burden of Diseases Study 2015. *The Lancet* **389**, 1907–1918 (2017).
2. Schraufnagel, D. E. *et al.* Air Pollution and Noncommunicable Diseases: A Review by the Forum of International Respiratory Societies' Environmental Committee, Part 2: Air Pollution and Organ Systems. *Chest* vol. 155 417–426 (2019).
3. Hajat, A., Hsia, C. & O'Neill, M. S. Socioeconomic Disparities and Air Pollution Exposure: a Global Review. *Current Environmental Health Reports* **2**, 440–450 (2015).
4. Martin, R. V. Satellite remote sensing of surface air quality. *Atmospheric Environment* **42**, 7823–7843 (2008).
5. Duncan, B. N. *et al.* Satellite data of atmospheric pollution for U.S. air quality applications: Examples of applications, summary of data end-user resources, answers to FAQs, and common mistakes to avoid. *Atmospheric Environment* vol. 94 647–662 (2014).
6. Pinder, R. W. *et al.* Opportunities and challenges for filling the air quality data gap in low- and middle-income countries. *Atmospheric Environment* **215**, 116794 (2019).
7. McLinden, C. A. *et al.* Air quality over the Canadian oil sands: A first assessment using satellite observations. *Geophysical Research Letters* vol. 39 (2012).
8. Lelieveld, J., Beirle, S., Hörmann, C., Stenchikov, G. & Wagner, T. Abrupt recent trend changes in atmospheric nitrogen dioxide over the Middle East. *Science Advances* **1**, e1500498 (2015).
9. Brook, J. R. *et al.* Further interpretation of the acute effect of nitrogen dioxide observed in Canadian time-series studies. *Journal of Exposure Science & Environmental Epidemiology* **17 Suppl 2**, S36-44 (2007).
10. US Environmental Protection Agency. *Integrated Science Assessment (ISA) for Oxides of Nitrogen – Health Criteria (Final Report, Jan 2016)*. (2016).
11. Braun-Fahrlander, C. *et al.* Air Pollution and Respiratory Symptoms in Preschool Children. *AM REV RESPIR DIS* **145**, 42–47 (1992).
12. Ponka, A. & Virtanen, M. Chronic Bronchitis, Emphysema, and Low-Level Air Pollution in Helsinki, 1987-1989. *Environmental Research* **65**, 207–217 (1994).
13. Bates, D. V. & Sizto, R. Air pollution and hospital admissions in Southern Ontario: The acid summer haze effect. *Environmental Research* **43**, 317–331 (1987).
14. Gauderman, W. J. *et al.* Childhood asthma and exposure to traffic and nitrogen dioxide. *Epidemiology (Cambridge, Mass.)* **16**, 737–743 (2005).
15. Burnett, R. T. *et al.* Associations between short-term changes in nitrogen dioxide and mortality in Canadian cities. *Archives of Environmental Health* **59**, 228–36 (2004).

16. Crouse, D. L. *et al.* Within- and between-city contrasts in nitrogen dioxide and mortality in 10 Canadian cities; a subset of the Canadian Census Health and Environment Cohort (CanCHEC). *Journal of Exposure Science and Environmental Epidemiology* **25**, 482–489 (2015).
17. Hoek, G. *et al.* Long-term air pollution exposure and cardio- respiratory mortality: a review. *Environmental Health* **12**, 43 (2013).
18. Nafstad, P. *et al.* Lung cancer and air pollution: a 27 year follow up of 16,209 Norwegian men. *Thorax* **58**, 1071–6 (2003).
19. Filleul, L. *et al.* Twenty five year mortality and air pollution: results from the French PAARC survey. *Occupational and environmental medicine* **62**, 453–460 (2005).
20. Perez, L. *et al.* Near-roadway pollution and childhood asthma: implications for developing "win-win" compact urban development and clean vehicle strategies. *Environmental health perspectives* **120**, 1619–26 (2012).
21. PLoS Medicine Editors. The air that we breathe: addressing the risks of global urbanization on health. *PLoS medicine* **9**, e1001301 (2012).
22. Parrish, D. D. & Zhu, T. Clean air for megacities. *Science* **326**, 674–675 (2009).
23. United Nations Department of Economic and Social Affairs, P. D. *World Urbanization Prospects: The 2014 Revision*. (2015).
24. Stone, B. Urban sprawl and air quality in large US cities. *Journal of environmental management* **86**, 688–98 (2008).
25. Schweitzer, L. & Zhou, J. Neighborhood air quality, respiratory health, and vulnerable populations in compact and sprawled regions. *Journal of the American Planning Association* **76**, 363–371 (2010).
26. Bechle, M. J., Millet, D. B. & Marshall, J. D. Effects of income and urban form on urban NO2 : global evidence from satellites. *Environmental Science & Technology* **45**, 4914–4919 (2011).
27. Clark, L. P., Millet, D. B. & Marshall, J. D. Air quality and urban form in U.S. urban areas: evidence from regulatory monitors. *Environmental science & technology* **45**, 7028–35 (2011).
28. Bereitschaft, B. & Debbage, K. Urban form, air pollution, and CO2 emissions in large U.S. metropolitan areas. *The Professional Geographer* **65**, 612–635 (2013).
29. McCarty, J. & Kaza, N. Urban form and air quality in the United States. *Landscape and Urban Planning* **139**, 168–179 (2015).
30. Larkin, A., van Donkelaar, A., Geddes, J. A., Martin, R. V. & Hystad, P. Relationships between changes in urban characteristics and air quality in East Asia from 2000 to 2010. *Environmental Science & Technology* **50**, 9142–9149 (2016).
31. Hart, J. E. *et al.* Spatial modeling of PM10 and NO2 in the continental United States, 1985-2000. *Environmental Health Perspectives* **117**, 1690–6 (2009).
32. Novotny, E. V, Bechle, M. J., Millet, D. B. & Marshall, J. D. National satellite-based land-use regression: NO2 in the United States. *Environmental Science & Technology* **45**, 4407–14 (2011).

33. Beckerman, B. S. *et al.* A hybrid approach to estimating national scale spatiotemporal variability of PM2.5 in the contiguous United States. *Environmental science & technology* **47**, 7233–41 (2013).
34. Hystad, P. *et al.* Creating national air pollution models for population exposure assessment in Canada. *Environmental Health Perspectives* **119**, 1123–9 (2011).
35. Beelen, R. *et al.* Mapping of background air pollution at a fine spatial scale across the European Union. *The Science of the Total Environment* **407**, 1852–67 (2009).
36. Vienneau, D. *et al.* Western European land use regression incorporating satellite- and ground-based measurements of NO2 and PM10. *Environmental Science & Technology* **47**, 13555–13564 (2013).
37. Knibbs, L. D., Hewson, M. G., Bechle, M. J., Marshall, J. D. & Barnett, A. G. A national satellite-based land-use regression model for air pollution exposure assessment in Australia. *Environmental Research* **135**, 204–211 (2014).
38. He, Q. & Huang, B. Satellite-based mapping of daily high-resolution ground PM2.5 in China via space-time regression modeling. *Remote Sensing of Environment* **206**, 72–83 (2018).
39. Zhan, Y. *et al.* Satellite-Based Estimates of Daily NO2 Exposure in China Using Hybrid Random Forest and Spatiotemporal Kriging Model. *Environmental Science and Technology* **52**, 4180–4189 (2018).
40. Clark, L. P., Millet, D. B. & Marshall, J. D. Changes in Transportation-Related Air Pollution Exposures by Race-Ethnicity and Socioeconomic Status: Outdoor Nitrogen Dioxide in the United States in 2000 and 2010. *Environmental Health Perspectives* **125**, (2017).
41. Kaufman, J. D. *et al.* Association between air pollution and coronary artery calcification within six metropolitan areas in the USA (the Multi-Ethnic Study of Atherosclerosis and Air Pollution): a longitudinal cohort study. *The Lancet* **388**, 696–704 (2016).
42. Alotaibi, R. *et al.* Traffic related air pollution and the burden of childhood asthma in the contiguous United States in 2000 and 2010. *Environment International* **127**, 858–867 (2019).
43. Schwartz, J. Air pollution and children's health. *Pediatrics* **113**, 1037–43 (2004).
44. Bearer, C. F. How are children different from adults? *Environmental health perspectives* **103 Suppl 6**, 7–12 (1995).
45. Brumberg, H. L. & Karr, C. J. Ambient Air Pollution: Health Hazards to Children. *Pediatrics* e2021051484 (2021) doi:10.1542/peds.2021-051484.
46. Grineski, S. E. & Collins, T. W. Geographic and social disparities in exposure to air neurotoxicants at U.S. public schools. *Environmental Research* **161**, 580–587 (2018).
47. Bechle, M. J., Millet, D. B. & Marshall, J. D. Does urban form affect urban NO2? Satellite-based evidence for more than 1200 cities. *Environmental Science and Technology* **51**, (2017).

48. Bechle, M. J., Millet, D. B. & Marshall, J. D. National spatiotemporal exposure surface for NO2: monthly scaling of a satellite-derived land-use regression, 2000-2010. *Environmental Science and Technology* **49**, (2015).
49. Lim, S. S. *et al.* A comparative risk assessment of burden of disease and injury attributable to 67 risk factors and risk factor clusters in 21 regions, 1990-2010: a systematic analysis for the Global Burden of Disease Study 2010. *Lancet* **380**, 2224–60 (2013).
50. Straif, K., Cohen, A. & Samet, J. *Air Pollution and Cancer (IARC Scientific Publication No. 161)*. (2013).
51. Geddes, J. A., Martin, R. V., Boys, B. L. & van Donkelaar, A. Long-term trends worldwide in ambient NO_2 concentrations inferred from satellite observations. *Environmental Health Perspectives* **124**, 281–289 (2015).
52. Schneider, P., Lahoz, W. A. & Van Der A, R. Recent satellite-based trends of tropospheric nitrogen dioxide over large urban agglomerations worldwide. *Atmos. Chem. Phys* **15**, 1205–1220 (2015).
53. van Donkelaar, A., Martin, R. V., Brauer, M. & Boys, B. L. Use of satellite observations for long-term exposure assessment of global concentrations of fine particulate matter. *Environmental Health Perspectives* **123**, 135–143 (2015).
54. Duncan, B. N. *et al.* A space-based, high-resolution view of notable changes in urban NO_x pollution around the world (2005-2014). *Journal of Geophysical Research: Atmospheres* **121**, 976–996 (2016).
55. Krzyzanowski, M., Kuna-Dibbert, B. & Schneider, J. *Health Effects of Transport-Related Air Pollution*. (2005).
56. Dora, C., Hosking, J., Mudu, P. & Fletcher, E. R. *Sustainable Transport: A Sourcebook for Policy-Makers in Developing Cities*. (2011).
57. Karagulian, F. *et al.* Contributions to cities' ambient particulate matter (PM): A systematic review of local source contributions at global level. *Atmospheric Environment* **120**, 475–483 (2015).
58. Bento, A. M. *et al.* The effects of urban spatial structure on travel demand in the United States. *Review of Economics and Statistics* **87**, 466–478 (2005).
59. Cervero, R. & Radisch, C. Travel choices in pedestrian versus automobile oriented neighborhoods. *Transport Policy* **3**, 127–141 (1996).
60. Cervero, R. Built environments and mode choice: toward a normative framework. *Transportation Research Part D: Transport and Environment* **7**, 265–284 (2002).
61. Handy, S., Cao, X. & Mokhtarian, P. Correlation or causality between the built environment and travel behavior? Evidence from Northern California. *Transportation Research Part D: Transport and Environment* **10**, 427–444 (2005).
62. Ewing, R. & Cervero, R. Travel and the built environment. *Journal of the American Planning Association* **76**, 265–294 (2010).
63. Hankey, S. & Marshall, J. D. Impacts of urban form on future US passenger-vehicle greenhouse gas emissions 2.
64. Marshall, J. D. Energy-efficient urban form. *Environmental science & technology* **42**, 3133–3137 (2008).

65. Stone Jr., B., Mednick, A. C., Holloway, T. & Spak, S. N. Is compact growth good for air quality? *JOURNAL OF THE AMERICAN PLANNING ASSOCIATION* **73**, 404–418 (2007).
66. Mansfield, T. J. & Gibson, J. M. Estimating Active Transportation Behaviors to Support Health Impact Assessment in the United States. *Frontiers in Public Health* **4**, 63 (2016).
67. Bartholomew, K. & Ewing, R. Hedonic Price Effects of Pedestrian- and Transit-Oriented Development. *Journal of Planning Literature* **26**, 18–34 (2011).
68. Ahlfeldt, G. M. If we build it, will they pay? Predicting property price effects of transport innovations. *Environment and Planning A* **45**, 1977–1994 (2013).
69. Kasraian, D., Maat, K., Stead, D. & Wee, B. van. Long-term impacts of transport infrastructure networks on land-use change: an international review of empirical studies. *Transport Reviews* **36**, 772–792 (2016).
70. Angel, S., Parent, J., Civco, D., Blei, A. & Potere, D. *A Planet of Cities: Urban Land Cover Estimates and Projections for All Countries, 2000-2050*. (2010).
71. Bechle, M. J., Millet, D. B. & Marshall, J. D. Remote sensing of exposure to NO2: satellite versus ground-based measurement in a large urban area. *Atmospheric Environment* **69**, 345–353 (2013).
72. Lamsal, L. N., Martin, R. V, Parrish, D. D. & Krotkov, N. A. Scaling relationship for NO2 pollution and urban population size: a satellite perspective. *Environmental science & technology* **47**, 7855–61 (2013).
73. Angel, S. *et al. The Dynamics of Global Urban Expansion*. (2005).
74. Angel, S., Parent, J., Civco, D. L. & Blei, A. M. *Atlas of Urban Expansion*. (2010).
75. Schneider, A., Friedl, M. A. & Potere, D. A new map of global urban extent from MODIS satellite data. *Environmental Research Letters* **4**, 044003 (2009).
76. Potere, D., Schneider, A., Angel, S. & Civco, D. L. Mapping urban areas on a global scale: which of the eight maps now available is more accurate? *International Journal of Remote Sensing* **30**, 6531–6558 (2009).
77. Angel, S., Parent, J. & Civco, D. L. Ten compactness properties of circles: measuring shape in geography. *The Canadian Geographer* **54**, 441–461 (2010).
78. Elvidge, C. D. *et al.* Global distribution and density of constructed impervious surfaces. *Sensors* **7**, 1962–1979 (2007).
79. DeFries, R. S., Hansen, M. C., Townshend, J. R. G., Janetos, a C. & Loveland, T. R. A new global 1 km dataset of percentage tree cover derived from remote sensing. *Global Change Biology* **6**, 247–254 (2000).
80. Mellander, C., Lobo, J., Stolarick, K. & Matheson, Z. Night-Time Light Data: A Good Proxy Measure for Economic Activity? *PloS one* **10**, e0139779 (2015).
81. Yuan, F. & Bauer, M. E. Comparison of impervious surface area and normalized difference vegetation index as indicators of surface urban heat island effects in Landsat imagery. *Remote Sensing of Environment* **106**, 375–386 (2007).
82. The World Bank. World Development Indicators. http://data.worldbank.org/data-catalog/world-development-indicators.

83. Rienecker, M. M. *et al.* MERRA: NASA's Modern-Era Retrospective Analysis for Research and Applications. *Journal of Climate* **24**, 3624–3648 (2011).
84. NASA Earth Observations. Solar Insolation (1 month) | NASA. https://neo.sci.gsfc.nasa.gov/view.php?datasetId=CERES_INSOL_M (2016).
85. Mollner, A. K. *et al.* Rate of gas phase association of hydroxyl radical and nitrogen dioxide. *Science (New York, N.Y.)* **330**, 646–9 (2010).
86. Donahue, N. M. Atmospheric chemistry: The reaction that wouldn't quit. *Nature Chemistry* **3**, 98–99 (2011).
87. Harris, I., Jones, P. D., Osborn, T. J. & Lister, D. H. Updated high-resolution grids of monthly climatic observations - the CRU TS3.10 Dataset. *International Journal of Climatology* **34**, 623–642 (2014).
88. Esty, D. C. *et al. 2008 Environmental Performance Index*. (2008).
89. Ponce de Leon Barido, D. & Marshall, J. D. Relationship between urbanization and CO2 emissions depends on income level and policy. *Environmental Science & Technology* **48**, 3632–3639 (2014).
90. Lin, M., Lucas Jr, H. C. & Shmueli, G. Too big to fail: large samples and the p-value problem. *Information Systems Research* **24**, 906–917 (2013).
91. Beirle, S., Boersma, K. F., Platt, U., Lawrence, M. G. & Wagner, T. Megacity emissions and lifetimes of nitrogen oxides probed from space. *Science* **333**, 1737–1739 (2011).
92. Spicer, C. W. Nitrogen oxide reactions in the urban plume of Boston. *Science* **215**, 1095–1097 (1982).
93. Mansfield, T. J., Rodriguez, D. A., Huegy, J. & MacDonald Gibson, J. The Effects of Urban Form on Ambient Air Pollution and Public Health Risk: A Case Study in Raleigh, North Carolina. *Risk Analysis* **35**, 901–918 (2015).
94. Marshall, J. D., Nethery, E. & Brauer, M. Within-urban variability in ambient air pollution: comparison of estimation methods. *Atmospheric Environment* **42**, 1359–1369 (2008).
95. Hoek, G. *et al.* A review of land-use regression models to assess spatial variation of outdoor air pollution. *Atmospheric Environment* **42**, 7561–7578 (2008).
96. Jerrett, M. *et al.* A review and evaluation of intraurban air pollution exposure models. *Journal of Exposure Analysis and Environmental Epidemiology* **15**, 185–204 (2005).
97. Ross, Z., Jerrett, M., Ito, K., Tempalski, B. & Thurston, G. A land use regression for predicting fine particulate matter concentrations in the New York City region. *Atmospheric Environment* **41**, 2255–2269 (2007).
98. Basagaña, X. *et al.* Effect of the number of measurement sites on land use regression models in estimating local air pollution. *Atmospheric Environment* **54**, 634–642 (2012).
99. Wang, M. *et al.* Systematic evaluation of land use regression models for NO2. *Environmental Science & Technology* **46**, 4481–9 (2012).

100. Johnson, M., Isakov, V., Touma, J. S., Mukerjee, S. & Özkaynak, H. Evaluation of land-use regression models used to predict air quality concentrations in an urban area. *Atmospheric Environment* **44**, 3660–3668 (2010).
101. Chen, H. *et al.* Back-extrapolation of estimates of exposure from current land-use regression models. *Atmospheric Environment* **44**, 4346–4354 (2010).
102. Eeftens, M. *et al.* Stability of measured and modelled spatial contrasts in NO_2 over time. *Occupational and Environmental Medicine* **68**, 765–70 (2011).
103. Fang, T. B. & Lu, Y. Constructing a Near Real-time Space-time Cube to Depict Urban Ambient Air Pollution Scenario. *Transactions in GIS* **15**, 635–649 (2011).
104. Mölter, A., Lindley, S., de Vocht, F., Simpson, A. & Agius, R. Modelling air pollution for epidemiologic research--part II: predicting temporal variation through land use regression. *The Science of the Total Environment* **409**, 211–7 (2010).
105. Rose, N., Cowie, C., Gillett, R. & Marks, G. B. Validation of a spatiotemporal land use regression model incorporating fixed site monitors. *Environmental Science & Technology* **45**, 294–9 (2011).
106. Sampson, P. D., Szpiro, A. A., Sheppard, L., Lindström, J. & Kaufman, J. D. Pragmatic estimation of a spatio-temporal air quality model with irregular monitoring data. *Atmospheric Environment* **45**, 6593–6606 (2011).
107. Su, J. G. *et al.* An innovative land use regression model incorporating meteorology for exposure analysis. *The Science of the Total Environment* **390**, 520–9 (2008).
108. Maynard, D., Coull, B. A., Gryparis, A. & Schwartz, J. Mortality risk associated with short-term exposure to traffic particles and sulfates. *Environmental Health Perspectives* **115**, 751–5 (2007).
109. Dons, E., Van Poppel, M., Kochan, B., Wets, G. & Int Panis, L. Modeling temporal and spatial variability of traffic-related air pollution: Hourly land use regression models for black carbon. *Atmospheric Environment* **74**, 237–246 (2013).
110. Gulliver, J. *et al.* Land use regression modeling to estimate historic (1962-1991) concentrations of black smoke and sulfur dioxide for Great Britain. *Environmental Science & Technology* **45**, 3526–32 (2011).
111. Gulliver, J., de Hoogh, K., Hansell, A. & Vienneau, D. Development and back-extrapolation of NO2 land use regression models for historic exposure assessment in Great Britain. *Environmental Science & Technology* **47**, 7804–11 (2013).
112. Mao, L., Qiu, Y., Kusano, C. & Xu, X. Predicting regional space-time variation of PM2.5 with land-use regression model and MODIS data. *Environmental Science and Pollution Research International* **19**, 128–38 (2012).
113. Yanosky, J. D. *et al.* Spatio-temporal modeling of chronic PM10 exposure for the Nurses' Health Study. *Atmospheric Environment* **42**, 4047–4062 (2008).
114. Yanosky, J. D., Paciorek, C. J. & Suh, H. H. Predicting chronic fine and coarse particulate exposures using spatiotemporal models for the Northeastern and Midwestern United States. *Environmental Health Perspectives* **117**, 522–9 (2009).
115. Knibbs, L. D., Hewson, M. G., Bechle, M. J., Marshall, J. D. & Barnett, A. G. A national satellite-based land-use regression model for air pollution exposure assessment in Australia. *Environmental Research* **135**, (2014).

116. Kloog, I., Koutrakis, P., Coull, B. A., Lee, H. J. & Schwartz, J. Assessing temporally and spatially resolved PM2.5 exposures for epidemiological studies using satellite aerosol optical depth measurements. *Atmospheric Environment* **45**, 6267–6275 (2011).
117. Kloog, I., Nordio, F., Coull, B. A. & Schwartz, J. Incorporating local land use regression and satellite aerosol optical depth in a hybrid model of spatiotemporal $PM_{2.5}$ exposures in the Mid-Atlantic states. *Environmental Science & Technology* **46**, 11913–21 (2012).
118. Cohen, M. A. *et al.* Approach to Estimating Participant Pollutant Exposures in the Multi-Ethnic Study of Atherosclerosis and Air Pollution (MESA Air). *Environmental Science & Technology* **43**, 4687–4693 (2009).
119. Lee, H. J. & Koutrakis, P. Daily Ambient NO2 Concentration Predictions Using Satellite Ozone Monitoring Instrument NO2 Data and Land Use Regression. *Environmental Science & Technology* **48**, 2305–2311 (2014).
120. Gan, W. Q. *et al.* Long-term exposure to traffic-related air pollution and the risk of coronary heart disease hospitalization and mortality. *Environmental Health Perspectives* **119**, 501–7 (2011).
121. Slama, R. *et al.* Traffic-related atmospheric pollutants levels during pregnancy and offspring's term birth weight: a study relying on a land-use regression exposure model. *Environmental Health Perspectives* **115**, 1283–92 (2007).
122. Nethery, E., Teschke, K. & Brauer, M. Predicting personal exposure of pregnant women to traffic-related air pollutants. *The Science of the Total Environmentnment* **395**, 11–22 (2008).
123. Hystad, P. *et al.* Spatiotemporal air pollution exposure assessment for a Canadian population-based lung cancer case-control study. *Environmental Health* **11**, 22 (2012).
124. Su, J. G., Jerrett, M. & Beckerman, B. A distance-decay variable selection strategy for land use regression modeling of ambient air pollution exposures. *Science of the Total Environment* **407**, 3890–3898 (2009).
125. Russell, a. R. *et al.* A high spatial resolution retrieval of NO_2 column densities from OMI: method and evaluation. *Atmospheric Chemistry and Physics* **11**, 8543–8554 (2011).
126. Tessum, C. W., Hill, J. D. & Marshall, J. D. Twelve-month, 12 km resolution North American WRF-Chem v3.4 air quality simulation: performance evaluation. *Geoscientific Model Development* **8**, 957–973 (2015).
127. Grundström, M. & Pleijel, H. Limited effect of urban tree vegetation on NO2 and O3 concentrations near a traffic route. *Environmental Pollution* **189**, 73–76 (2014).
128. Pataki, D. E. *et al.* Coupling biogeochemical cycles in urban environments: ecosystem services, green solutions, and misconceptions. *Frontiers in Ecology and the Environment* **9**, 27–36 (2011).
129. U.S. Enivironmental Protection Agency. Air Quality System Data Mart. http://www.epa.gov/ttn/airs/aqsdatamart/ (2011).

130. U.S. Enivironmental Protection Agency. *Our Nation's Air: Status and Trends Through 2010*. (2012).
131. Russell, A. R., Valin, L. C. & Cohen, R. C. Trends in OMI NO2 observations over the United States: effects of emission control technology and the economic recession. *Atmospheric Chemistry and Physics* **12**, 12197–12209 (2012).
132. U.S. Census Bureau. 2010 Urban Area Facts. http://www.census.gov/geo/www/ua/uafacts.html (2012).
133. Kharol, S. K. *et al.* Assessment of the Magnitude and Recent Trends in Satellite-Derived Ground-Level Nitrogen Dioxide over North America. *Atmospheric Environment* **118**, 236–245 (2015).
134. NASA. Missions: TEMPO. http://science.nasa.gov/missions/tempo/ (2013).
135. ESA. sentinel-5 precursor. http://esamultimedia.esa.int/docs/S5-prec_Data_Sheet.pdf (2013).
136. Center for International Earth Science Information Network (CIESIN); Gridded Population of the World Version 3 (GPWv3): Population Density Grids. (2005).
137. Jarvis, A., Reuter, H. I. & Nelson, E. G. SRTM 90m Digital Elevation. (2008).
138. Bechle, M. J., Millet, D. B. & Marshall, J. D. Remote sensing of exposure to NO2: satellite versus ground-based measurement in a large urban area. *Atmospheric Environment* **69**, 345–353 (2013).
139. Gauderman, W. J. *et al.* Childhood asthma and exposure to traffic and nitrogen dioxide. *Epidemiology (Cambridge, Mass.)* **16**, 737–43 (2005).
140. McConnell, R. *et al.* Traffic, Susceptibility, and Childhood Asthma. *Environmental Health Perspectives* **114**, 766–772 (2006).
141. Jerrett, M. *et al.* Traffic-Related Air Pollution and Asthma Onset in Children: A Prospective Cohort Study with Individual Exposure Measurement. *Environmental Health Perspectives* **116**, 1433–1438 (2008).
142. Jadaan, K., Khreis, H. & Török, Á. Exposure to Traffic-related Air Pollution and the Onset of Childhood Asthma: A Review of the Literature and the Assement Methods Used. *Periodica Polytechnica Transportation Engineering* (2017) doi:10.3311/PPtr.10113.
143. Sunyer, J. The neurological effects of air pollution in children. *The European respiratory journal* **32**, 535–7 (2008).
144. Wang, S. *et al.* Association of Traffic-Related Air Pollution with Children's Neurobehavioral Functions in Quanzhou, China. *Environmental Health Perspectives* **117**, 1612–1618 (2009).
145. Sunyer, J. *et al.* Association between Traffic-Related Air Pollution in Schools and Cognitive Development in Primary School Children: A Prospective Cohort Study. *PLoS Medicine* **12**, (2015).
146. Annavarapu, R. N. & Kathi, S. Cognitive disorders in children associated with urban vehicular emissions. *Environmental Pollution* **208**, 74–78 (2016).
147. Mohai, P., Kweon, B.-S., Lee, S. & Ard, K. Air pollution around schools is linked to poorer student health and academic performance. *Health affairs (Project Hope)* **30**, 852–62 (2011).

148. Kingsley, S. L. *et al.* Proximity of US Schools to Major Roadways: a Nationwide Assessment. *Journal of Exposure Science and Environmental Epidemiology* **24**, 253–259 (2014).
149. Alexander, D. & Lewis, L. *Condition of America's Public School Facilities: 2012-13 First Look*.
150. U.S. Environmental Protection Agency. *School Siting Guidelines*. (2011).
151. U.S. Environmental Protection Agency. *Best Practices for Reducing Near-Road Pollution Exposure at Schools*. (2015).
152. Gaffron, P. & Niemeier, D. School locations and traffic emissions—environmental (in)justice findings using a new screening method. *International journal of environmental research and public health* **12**, 2009–25 (2015).
153. Clark, L. P., Millet, D. B. & Marshall, J. D. National Patterns in Environmental Injustice and Inequality: Outdoor NO2 Air Pollution in the United States. *PLoS ONE* **9**, e94431 (2014).
154. Zwickl, K., Ash, M. & Boyce, J. K. Regional variation in environmental inequality: Industrial air toxics exposure in U.S. cities. *Ecological Economics* **107**, 494–509 (2014).
155. Martenies, S., Milando, C., Williams, G. & Batterman, S. Disease and Health Inequalities Attributable to Air Pollutant Exposure in Detroit, Michigan. *International Journal of Environmental Research and Public Health* **14**, 1243 (2017).
156. Ard, K. Trends in exposure to industrial air toxins for different racial and socioeconomic groups: A spatial and temporal examination of environmental inequality in the U.S. from 1995 to 2004. *Social Science Research* **53**, 375–390 (2015).
157. Rosofsky, A., Levy, J. I., Zanobetti, A., Janulewicz, P. & Fabian, M. P. Temporal trends in air pollution exposure inequality in Massachusetts. *Environmental Research* **161**, 76–86 (2018).
158. Green, R. S., Smorodinsky, S., Kim, J. J., McLaughlin, R. & Ostro, B. Proximity of California public schools to busy roads. *Environmental health perspectives* **112**, (2004).
159. Pastor, Jr., M., Sadd, J. L. & Morello-Frosch, R. Who's Minding the Kids? Pollution, Public Schools, and Environmental Justice in Los Angeles. *Social Science Quarterly* **83**, 263–280 (2002).
160. Pastor, M., Sadd, J. L. & Morello-Frosch, R. Reading, Writing, and Toxics: Children's Health, Academic Performance, and Environmental Justice in Los Angeles. *Environment and Planning C: Government and Policy* **22**, 271–290 (2004).
161. Morello-Frosch, R., Pastor, M. & Sadd, J. Integrating Environmental Justice and the Precautionary Principle in Research and Policy Making: The Case of Ambient Air Toxics Exposures and Health Risks among Schoolchildren in Los Angeles. *The ANNALS of the American Academy of Political and Social Science* **584**, 47–68 (2002).

162. Stuart, A. L. & Zeager, M. An inequality study of ambient nitrogen dioxide and traffic levels near elementary schools in the Tampa area. *Journal of Environmental Management* **92**, 1923–1930 (2011).
163. Grineski, S. E., Clark-Reyna, S. E. & Collins, T. W. School-based exposure to hazardous air pollutants and grade point average: A multi-level study. *Environmental Research* **147**, 164–171 (2016).
164. The Smokestack Effect: Toxic Air and America's Schools. *USA Today* http://content.usatoday.com/news/nation/environment/smokestack/index (2008).
165. Xue, Z. & Jia, C. A model-to-monitor evaluation of 2011 National-Scale Air Toxics Assessment (NATA). *Toxics* **7**, (2019).
166. U.S. Environmental Protection Agency. *EPA's 2011 National-scale Air Toxics Assesment Technical Support Document*. (2015).
167. Common Core of Data. Public Elementary/Secondary School Universe Survey Data. https://nces.ed.gov/ccd/pubschuniv.asp.
168. Sable, J., Gaviola, N. & Garofano, A. *Documentation to the NCES Common Core of Data Public Elementary/Secondary School Universe Survey: School Year 2005–06 (NCES 2007-365)*. (2007).
169. World Health Organization. *Air Quality Guidelines: Global Update 2005*. (2006).
170. U.S. Environmental Protection Agency. Green Book Nitrogen Dioxide (1971) Area Information. https://www.epa.gov/green-book/green-book-nitrogen-dioxide-1971-area-information (2016).
171. U.S. Environmental Protection Agency. Table of Historical NO2 NAAQS. https://www3.epa.gov/ttn/naaqs/standards/nox/s_nox_history.html (2016).
172. Ashley-Martin, J. *et al.* Air Pollution During Pregnancy and Cord Blood Immune System Biomarkers. *Journal of Occupational and Environmental Medicine* **58**, 979–986 (2016).
173. Lavigne, E. *et al.* Ambient air pollution and adverse birth outcomes: Differences by maternal comorbidities. *Environmental Research* **148**, 457–466 (2016).
174. Lavigne, É. *et al.* Maternal exposure to ambient air pollution and risk of early childhood cancers: A population-based study in Ontario, Canada. *Environment International* **100**, 139–147 (2017).
175. Lavigne, É. *et al.* Effect modification of perinatal exposure to air pollution and childhood asthma incidence. *European Respiratory Journal* **51**, (2018).
176. Elten, M. *et al.* Ambient air pollution and incidence of early-onset paediatric type 1 diabetes: A retrospective population-based cohort study. *Environmental Research* **184**, 109291 (2020).
177. Elten, M. *et al.* Ambient air pollution and the risk of pediatric-onset inflammatory bowel disease: A population-based cohort study. *Environment International* **138**, 105676 (2020).
178. Coogan, P. F. *et al.* Long-Term Exposure to NO2 and Ozone and Hypertension Incidence in the Black Women's Health Study. *American Journal of Hypertension* **30**, 367–372 (2017).

179. Lim, C. C. *et al.* Association between long-term exposure to ambient air pollution and diabetes mortality in the US. *Environmental Research* **165**, 330–336 (2018).
180. Kazemiparkouhi, F., Eum, K. Do, Wang, B., Manjourides, J. & Suh, H. H. Long-term ozone exposures and cause-specific mortality in a US Medicare cohort. *Journal of Exposure Science and Environmental Epidemiology* 1–9 (2019) doi:10.1038/s41370-019-0135-4.
181. Cusack, L., Larkin, A., Carozza, S. E. & Hystad, P. Associations between multiple green space measures and birth weight across two US cities. *Health and Place* **47**, 36–43 (2017).
182. Cusack, L., Larkin, A., Carozza, S. & Hystad, P. Associations between residential greenness and birth outcomes across Texas. *Environmental Research* **152**, 88–95 (2017).
183. Sohrabi, S., Zietsman, J. & Khreis, H. Burden of Disease Assessment of Ambient Air Pollution and Premature Mortality in Urban Areas: The Role of Socioeconomic Status and Transportation. *International Journal of Environmental Research and Public Health* **17**, 1166 (2020).
184. Knibbs, L. D. *et al.* Long-term nitrogen dioxide exposure assessment using back-extrapolation of satellite-based land-use regression models for Australia. *Environmental Research* **163**, (2018).
185. de Hoogh, K. *et al.* Development of West-European PM2.5 and NO2 land use regression models incorporating satellite-derived and chemical transport modelling data. *Environmental Research* **151**, 1–10 (2016).
186. Young, M. T. *et al.* Satellite-Based NO2 and Model Validation in a National Prediction Model Based on Universal Kriging and Land-Use Regression. *Environmental Science and Technology* **50**, (2016).
187. Kim, S.-Y. *et al.* Concentrations of criteria pollutants in the contiguous U.S., 1979 – 2015: Role of prediction model parsimony in integrated empirical geographic regression. *PLOS ONE* **15**, e0228535 (2020).
188. Xu, H. *et al.* National PM2.5 and NO2 exposure models for China based on land use regression, satellite measurements, and universal kriging. *Science of The Total Environment* **655**, 423–433 (2019).
189. US Government Accountability Office. *K-12 EDUCATION School Districts Frequently Identified Multiple Building Systems Needing Updates or Replacement Report to Congressional Addressees United States Government Accountability Office*. (2020).
190. Mitchell, B. & Franco, J. *HOLC "REDLINING" MAPS: The persistent structure of segregation and economic inequality*. (2018).
191. Nelson, R. K., Winling, L., Marciano, R. & Connoly, N. Mapping Inequality. https://dsl.richmond.edu/panorama/redlining/.
192. Hoffman, J. S., Shandas, V. & Pendleton, N. The effects of historical housing policies on resident exposure to intra-urban heat: A study of 108 US urban areas. *Climate* **8**, 12 (2020).

193. Nardone, A., Rudolph, K. E., Morello-Frosch, R. & Casey, J. A. Redlines and greenspace: The relationship between historical redlining and 2010 greenspace across the United States. *Environmental Health Perspectives* **129**, 1–9 (2021).
194. Nardone, A. *et al.* Associations between historical residential redlining and current age-adjusted rates of emergency department visits due to asthma across eight cities in California: an ecological study. *The Lancet Planetary Health* **4**, e24–e31 (2020).
195. Tessum, C. W. *et al.* $PM_{2.5}$ polluters disproportionately and systemically affect people of color in the United States. *Science Advances* **7**, eabf4491 (2021).
196. Veefkind, J. P. *et al.* TROPOMI on the ESA Sentinel-5 Precursor: A GMES mission for global observations of the atmospheric composition for climate, air quality and ozone layer applications. *Remote Sensing of Environment* **120**, 70–83 (2012).
197. Demetillo, M. A. G. *et al.* Observing nitrogen dioxide air pollution inequality using high-spatial-resolution remote sensing measurements in Houston, Texas. *Environmental Science and Technology* **54**, 9882–9895 (2020).
198. Kim, J. *et al.* New era of air quality monitoring from space: Geostationary environment monitoring spectrometer (GEMS). *Bulletin of the American Meteorological Society* **101**, E1–E22 (2020).

Appendix A

Supplemental information for Chapter 3

Three data files provide LUR-derived NO_2 concentration estimates (ppb): one file ("Read me") describes the data, another file ("Preview") illustrates the semicolon-separated format for the database by providing data for the first 100 Census Blocks in the database, and the last file ("NO2_ByCensusBlock_2000_2010") provides estimates for all Census blocks in the contiguous United States. All files can be downloaded here: http://spatialmodel.com